Studies of Stimulated Brillouin Scattering in Optical Fibers and Applications

by

Stephen Paul Smith

S.B., 1986, S.M., 1988, E.E., 1989
Massachusetts Institute of Technology

Submitted to the Department of
Electrical Engineering and Computer Science
in Partial Fulfillment of the Requirements
for the Degree of

Doctor of Science

at the

Massachusetts Institute of Technology

September 29, 1993

Author _____
Department of Electrical Engineering and Computer Science
September 29, 1993

Certified by _____
Shaoul Ezekiel, Thesis Supervisor
Professor of Electrical Engineering and Computer Science
and Professor of Aeronautics and Astronautics

Accepted by _____
Frederic R. Morgenthaler
Chairman, Committee on Graduate Students

Studies of
Stimulated Brillouin Scattering
in
Optical Fibers and Applications

by

Stephen Paul Smith

Submitted to
the Department of Electrical Engineering and Computer Science
on September 29, 1993 in Partial Fulfillment of the Requirements
for the Degree of Doctor of Science in Electrical Engineering

Abstract

The properties of a laser based on stimulated Brillouin scattering (SBS) in optical fibers were studied and a number of applications were explored, particularly the creation of an SBS fiber ring laser gyroscope.

The study of solitary SBS laser properties resulted in the demonstration of a narrow 2 kHz laser linewidth, determined primarily by external environmental perturbations. SBS lasing thresholds as low as 35 μW were observed, along with slope efficiencies of up to 88%. Higher order SBS lasers, up to third order, were also demonstrated, and a number of SBS laser problems, including spontaneous modelocking and backscatter-induced threshold variations, were investigated.

The unique properties of common cavity SBS lasers, i.e., SBS lasers generated in the same fiber cavity using independent pumps, were demonstrated. The beat between two such lasers was shown to be as small as 2 Hz, limited by thermally-driven backscatter-induced dispersion effects. In addition, common cavity SBS lasers were also demonstrated with frequency separations up to 550 MHz. A number of applications for such lasers were proposed, including the generation of microwave or even millimeter wave sources, high resolution two-photon spectroscopy, atomic clocks, and high precision magnetic field sensors.

Finally, the first solid-state fiber ring laser gyroscope (RLG) was demonstrated using SBS as the gain medium. The SBS fiber RLG relies on the Sagnac effect for the measurement of inertial rotation in a fiber ring cavity. The directionality of the SBS gain medium prevents the gain competition that is normally observed in a conventional solid-state gain medium when generating simultaneous, counterpropagating lasers in the same ring cavity. Optical techniques for the elimination of the backscatter-induced lock-in effect, common to all RLGs, were demonstrated. The fundamental bias variation caused by the optical Kerr effect was also measured and a method for eliminating it proposed.

Thesis Supervisor: Dr. Shaoul Ezekiel
Title: Professor of Electrical Engineering,
and Aeronautics and Astronautics

Acknowledgments

My deepest thanks go to Professor Ezekiel, for letting his enthusiasm for this work spill into my life, for encouraging independent thinking while always having the time to look at new data and ask the right questions. Ziggy, thank you for teaching me so many things, not the least of which is "where the light goes".

I would also like to thank Prof. Weiss and Prof. Ippen for their helpful questions and comments.

My friends and former graduate students, Farhad "Z" Zarinetchi, Mara Prentiss, Bob Barat, Selim Shahriar, Phil Hemmer, and Bruce Bernacki all provided welcome suggestions and encouragement. In addition, I would like to thank John Kierstead and Margaret McCabe for their good humor and help over the years.

A special thanks to the past members of all the various **Vhat da Schmidt** teams, Jerry Shapiro, Joel Villaseñor, Greg Wornell, and Rick Stoner to name a few, who provided much needed fun and relaxation, helping me stay sane. There will always be a spot on my team for all of you.

I would especially like to thank my parents, Clair and Lyle Smith, my brother, Mike, his wife Nancy and their family, and also my parents-in-law, June and Otto Rosenau, and my sisters-in-law, Sherri, Anna, Susan, and Judi, for their constant support and *encouragement* over my numerous years as a "gradual" student.

Finally, a special thanks to my wife Karen, who put up with endless hours in the lab, who always knew that 15 more minutes meant an hour, who put up with many late nights, even though I don't procrastinate, and who was always there when I needed her. In addition, I especially want to thank her for drawing and revising and re-revising the figures in this thesis.

This work was supported in part by the Charles Stark Draper Laboratories, Cambridge, MA, the Joint Services Electronics Program at the MIT Research Laboratory for Electronics, and the U.S. Air Force Office of Scientific Research.

This thesis is dedicated to my wife,

and my best friend, Karen.

Table of Contents

Chapter One

Introduction

Stimulated Brillouin scattering is a nonlinear optical process in which an intense beam of light generates gain for a counterpropagating, frequency downshifted beam. Stimulated Brillouin scattering (SBS) was first predicted by L. Brillouin in 1922,[1] however, it was not experimentally observed until 1964 when Chiao, Townes and Stoicheff generated SBS in a solid using a pulsed ruby laser focused to a small spot inside a quartz or sapphire sample.[2]

Optical fibers, however, can greatly reduce the power required to generate nonlinear optical effects such as SBS. The tight transverse mode confinement in a single mode optical fiber creates very high pump intensities even for modest pump powers, and the low loss of the fiber makes very long interaction lengths possible. SBS was first observed in optical fibers in 1972 by Ippen and Stolen using a pulsed xenon laser.[3]

One important use of SBS in optical fibers is as the gain medium for fiber ring lasers. The first continuous SBS fiber laser was demonstrated by Hill, Kawasaki and Johnson in 1976 using a hybrid cavity made from both fiber-optic and bulk-optic components.[4] The SBS laser was pumped using an argon laser and had a linewidth of about 20 MHz and a 250 mW threshold. A more careful study of the properties of the SBS laser was then made by

Ponikvar and Ezekiel in 1981 by actively stabilizing the hybrid cavity.[5] In this way, an SBS laser linewidth of less than 100 kHz was achieved with a 77 mW SBS lasing threshold using an argon pump laser. In addition, they demonstrated the homogeneous-like behavior of the SBS gain medium. The advent of high finesse all-fiber cavities dramatically reduced the pump threshold for SBS to 0.5 mW as achieved by Stokes, Chodorow and Shaw in 1982,[6] using a low power He-Ne pump laser.

In addition to the creation of SBS fiber lasers, SBS in optical fibers has also been exploited for a number of applications, such as short pulse generation,[7] optical amplification,[8,9] distributed temperature sensing,[10] non-destructive measurement of fiber properties,[11,12] Brillouin enhanced four-wave mixing,[13,14] and microwave generation.[15]

In our laboratory, we have been exploring optical inertial rotation sensors, i.e., gyroscopes, including fiber interferometers,[16] and passive resonator gyroscopes using bulk-optic and fiber cavities.[17,18,19] One particularly important application of SBS lasers is for the development of a solid-state analog of the bulk-optic He-Ne ring laser gyroscope.[20] The availability of high finesse all-fiber cavities renewed interest in the SBS-based, ring laser gyroscope,[21,22] after many unsuccessful attempts with hybrid cavities.[20]

In 1989, we succeeded in demonstrating the first solid-state, SBS fiber ring laser gyroscope using a low power He-Ne pump laser.[23,24] In addition, we demonstrated a number of applications of solitary SBS lasers and common cavity SBS lasers, i.e., two or more SBS lasers sharing the same cavity.[25] The lowest SBS lasing threshold we observed was 35 μW. Since that time, a number of other groups have also begun active research on the SBS RLG.[26,27,28]

1.1 Overview

In this thesis, the properties and applications of SBS fiber ring lasers will be studied. In Chapter 2, the unique properties of solitary SBS lasers will be

examined, such as the directionality, tunability, and linewidth of the laser. Applications, based on the unique properties of such lasers, are then presented, and some of the potential problems with the laser are discussed. Chapter 3 examines the generation of multiple SBS lasers in the same ring cavity, i.e., common cavity SBS lasers. The properties of such lasers are explored, and some applications suggested.

In Chapter 4, the first solid-state ring laser gyroscope is demonstrated, and the problems for the gyroscope are examined. Further, two methods for eliminating an important problem in the gyroscope, the lock-in effect, are demonstrated. Chapter 5 presents a summary of the thesis, and Chapter 6 suggests several extensions of this work.

Chapter Two

Solitary Fiber-Optic SBS Lasers

In this chapter, stimulated Brillouin scattering (SBS) for the generation of optical gain in a fiber will be explained using a simplified physical model, and also using a more exact nonlinear optics treatment. The operation of a fiber ring laser based on SBS will then be demonstrated and the properties of this laser, including pump power threshold, broadening, linewidth, and efficiency will be examined. Applications for SBS lasers will then be proposed and demonstrated. Finally, some of the important experimental considerations in the development of SBS fiber lasers will be discussed, as well as their problems and limitations.

2.1 Stimulated Brillouin Scattering

Stimulated Brillouin scattering in a dielectric medium is a nonlinear optical process in which an intense beam of light, the pump, generates optical gain for a counterpropagating, frequency downshifted optical beam, the Brillouin beam.

2.1.1 Simplified Physical Model for SBS Gain

In a simplified explanation of SBS, the pump beam is initially scattered by thermally generated acoustic waves in the dielectric medium, in this case, the core of an optical fiber. Forward scattering from these acoustic waves does not change the frequency of the pump and hence, is of no interest here. Backward scattering, as shown in Fig. 2.1, results in a Doppler shift of the frequency of the backscattered beam, f_b, with respect to the pump given by,

$$\Delta f = f_p - f_b = f_p - \left(1 - \frac{-2v_a}{c}\right) \cdot f_p = \frac{-2v_a}{c} f_p \tag{2.1}$$

where v_a is the speed of sound in the medium, c is the speed of light in the medium, and f_p is the pump frequency. Of interest here is the backscattering from copropagating acoustic waves, which will be downshifted in frequency.

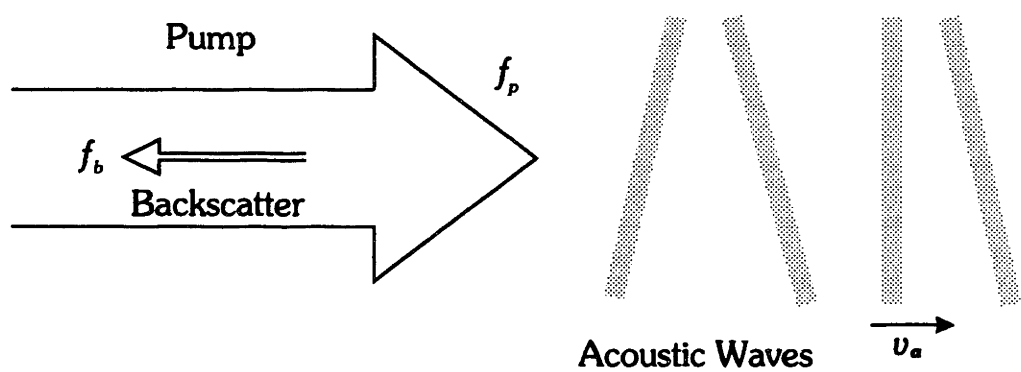

Figure 2.1 Scattering from thermal acoustic waves in the medium generates backscattering that is Doppler-shifted down in frequency.

The strongest backscattering, i.e., Brillouin scattering, will be from acoustic waves which satisfy the Bragg condition, i.e.,

$$2\lambda_a \approx \lambda_p \tag{2.2}$$

where λ_a and λ_p are the acoustic and pump wavelengths, respectively. The frequency of such acoustic waves, $f_a = v_a/\lambda_a$, can be rewritten using Eq. (2.2),

$$f_a = \frac{v_a}{\lambda_a} = \frac{2v_a}{\lambda_p} = \frac{2v_a}{c} f_p \tag{2.3}$$

which is the same as the frequency downshift of the Brillouin scattering from the pump beam in Eq. (2.1).

The pump and the Brillouin beams interfere to produce a weak intensity grating with a period of approximately $2\lambda_p \approx \lambda_a$, shown schematically in Fig. 2.2. Due to the frequency difference between the beams, this grating copropagates with the pump at velocity v_g given by,

$$v_g = \frac{f_p - f_b}{f_p + f_b} c \approx \frac{(2v_a/c)f_p}{2f_p} c = v_a \tag{2.4}$$

which is the same as the speed of sound in the fiber. Through the electrostriction effect in the medium, this intensity grating drives the λ_a acoustic wave, thus increasing the amount of Brillouin scattering. Hence, the initial backscattering from the λ_a acoustic wave is amplified, much like spontaneous emission is amplified in a conventional gain medium.

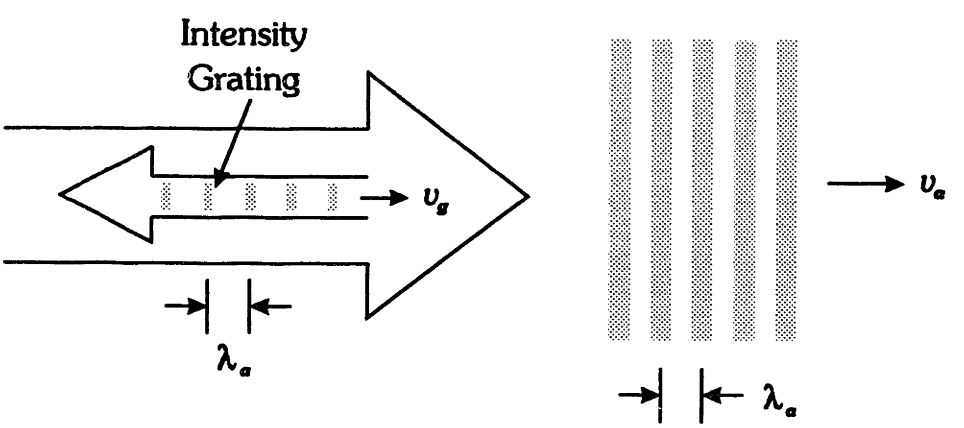

Figure 2.2 A weak intensity grating, formed by the Doppler-shifted backscattering and the pump, drives the acoustic wave through the electrostriction effect in the fiber.

Two important characteristics of SBS gain are its directionality and tunability, which serve as the basis for many of the applications of SBS ring lasers. In contrast to a conventional gain medium, the SBS gain is only along a direction opposite to that of the pump. Further, the center of the SBS gain is tied to the frequency of the pump, thus, the tunability of the SBS gain medium is determined by the tunability of the pump laser.

2.1.2 Classical Derivation of SBS Gain

While the simplified model for SBS scattering in the previous section gives good physical insight into SBS, it does not allow a quantitative evaluation of the SBS gain coefficient. In order to calculate the SBS gain coefficient, a classical nonlinear optics treatment of SBS will be presented.[29]

Since energy and momentum must be conserved by SBS, we can write a conservation of energy equation and a conservation of momentum equation. The conservation of energy equation can be written as,

$$\omega_p = \omega_s + \omega_a \tag{2.5}$$

where ω_p, ω_s and ω_a are the pump, SBS and acoustic frequencies, respectively. Conservation of momentum is given by,

$$\mathbf{k}_p = \mathbf{k}_s + \mathbf{k}_a \tag{2.6}$$

where $\mathbf{k}_p$, $\mathbf{k}_s$, and $\mathbf{k}_a$ are the pump, SBS and acoustic wave-vectors, respectively. Equation (2.6) implies that,

$$\begin{aligned} k_a^2 &= k_p^2 + k_s^2 - 2\,\mathbf{k}_p \cdot \mathbf{k}_s \\ &\approx k_p^2(1 + 1 - 2\cos\theta) \\ &= 4k_p^2 \sin^2\left(\frac{\theta}{2}\right) \end{aligned} \tag{2.7}$$

where θ is the angle between $\mathbf{k}_p$ and $\mathbf{k}_s$, i.e., the scattering angle, and using $k_p \approx k_s$. For maximum interaction length, $\mathbf{k}_p$ and $\mathbf{k}_s$ must be collinear, so θ must be equal to 0 or π. However, $\theta = 0$ corresponds to forward scattering and yields $\mathbf{k}_a = 0$, and hence, is of no interest. On the other hand, $\theta = \pi$, corresponds to backscattering and yields $k_a \approx 2k_p$, which is equivalent to Eq. (2.2).

In order to derive an expression for the gain experienced by the SBS beam, we will start with the equations for both the optical and the acoustic waves. Recall that in a nonlinear lossless medium, the optical wave equation is given by:

$$\nabla^2\mathbf{E} - \mu_\circ\epsilon\frac{\partial^2\mathbf{E}}{\partial t^2} = \frac{\partial^2}{\partial t^2}\mu_\circ\mathbf{P}_{NL} \tag{2.8}$$

where $\mathbf{E}$ is the electric field vector, $\mathbf{P}_{NL}$ is the nonlinear polarization, $\mu_\circ$ is the permeability of free space and ϵ is the permittivity of the medium. Similarly, the equation for the acoustic wave in a lossy medium is given by:

$$v_a^2\nabla^2\rho + \eta\nabla^2\frac{\partial\rho}{\partial t} - \frac{\partial^2\rho}{\partial t^2} = \nabla^2\rho_{NL} \tag{2.9}$$

where ρ is the mass density of the medium, v_a is the acoustic velocity, η is the viscosity coefficient, and $\nabla^2\rho_{NL}$ is the nonlinear optical driving term.

The equations for the two optical beams, the pump and SBS, and the acoustic beam are coupled through $\mathbf{P}_{NL}$, which is the nonlinear polarization caused by the variation in ρ, and through ρ_{NL}, which is the electrostrictive pressure caused by the intensity, $|\mathbf{E}|^2$.

The nonlinear polarizability, $\mathbf{P}_{NL}$, can be written as a change in $\epsilon\mathbf{E}$ as a function of density variation, i.e.,

$$\mathbf{P}_{NL} = \rho\frac{\partial\epsilon}{\partial\rho}\mathbf{E} \tag{2.10}$$

and in a similar fashion, ρ_{NL} can be written as a pressure variation due to the electric field intensity $\epsilon|\mathbf{E}|^2$ given by:

$$\rho_{NL} = \frac{\rho_\circ}{2}\frac{\partial}{\partial\rho}\epsilon\mathbf{E}^2 \tag{2.11}$$

where $\rho_\circ$ is the average density.

We assume solutions for the forward propagating pump field, $\mathbf{E}_p$, the backward propagating SBS field, $\mathbf{E}_s$, and the forward propagating acoustic wave ρ_a are of the form,

$$\mathbf{E}_p = E_p e^{j(k_p z - \omega_p t)} \tag{2.12}$$

$$\mathbf{E}_s = E_s e^{j(-k_s z - \omega_s t)} \tag{2.13}$$

$$\rho = \rho_a e^{j(k_a z - \omega_a t)} \tag{2.14}$$

where E_p and E_s are the complex field amplitudes, k_p and k_s the wave numbers, and ω_p and ω_s the frequencies of the pump and SBS respectively. Also, ρ_a is the complex field amplitude, k_a is the wavenumber, and ω_a is the frequency of the density wave. In addition, we will assume that all three waves are linearly polarized in the same direction.

Substituting Eq. (2.12) and (2.13) into Eq. (2.8) yields,

$$(\nabla^2 + \omega_p^2\mu_\circ\epsilon)\mathbf{E}_p = \mu_\circ\frac{\partial^2}{\partial t^2}\mathbf{P}_{NL}(\omega_p) \tag{2.15}$$

$$(\nabla^2 + \omega_s^2\mu_\circ\epsilon)\mathbf{E}_s = \mu_\circ\frac{\partial^2}{\partial t^2}\mathbf{P}_{NL}(\omega_s) \tag{2.16}$$

and substituting Eq. (2.14) into Eq. (2.9) yields,

$$(v_a^2\nabla^2 + \eta k_a^2\omega_a + \omega_a^2)\rho = \nabla^2\rho_{NL} \tag{2.17}$$

The optical wave equations, Eq. (2.15) and (2.16), can be further simplified by substituting Eq. (2.10) into each of the equations, yielding,

$$(\nabla^2 + \omega_p^2 \mu_o \epsilon)\mathbf{E}_p = \frac{\mu_o \gamma_e^2}{\rho_o} \frac{\partial^2}{\partial t^2}(\rho \mathbf{E}_s) \tag{2.18}$$

and,

$$(\nabla^2 + \omega_s^2 \mu_o \epsilon)\mathbf{E}_s = \frac{\mu_o \gamma_e^2}{\rho_o} \frac{\partial^2}{\partial t^2}(\rho \mathbf{E}_p) \tag{2.19}$$

where $\gamma_e = \rho_o \partial\epsilon/\partial\rho$ is the electrostriction coefficient.

In order to solve for E_p and E_s, we will first solve for ρ, and then substitute into the above equations. To solve for ρ, first we will find an expression for $\nabla^2 E^2$. Expanding E^2, and ignoring terms on the order of $2\omega_p$ gives,

$$\begin{aligned} E^2 &= EE^* \\ &= \frac{1}{2}\left(|E_p|^2 + |E_s|^2 + E_p E_s^* e^{i(\omega_a t - k_a z)} + E_p E_s^* e^{i(-\omega_a t + k_a z)}\right) \end{aligned} \tag{2.20}$$

where $\omega_a = \omega_p - \omega_s$ from Eq. (2.5), and $k_a = k_p + k_s$ from Eq. (2.6). Thus,

$$\nabla^2 E^2 = \frac{1}{2}[-k_a^2 E_p E_s^* e^{i(\omega_a t - k_a z)} - k_a^2 E_p^* E_s e^{i(-\omega_a t + k_a z)}] \tag{2.21}$$

which can be combined with the acoustic wave equation, Eq. (2.17), to find an expression for ρ_a, which after simplifying is given by,

$$\rho_a = \frac{k_a^2 \gamma_e E_p E_s^*}{2(k_a^2 v_a^2 - \omega_a^2 - i2\Gamma_B \omega_a)} \tag{2.22}$$

where $\Gamma_B = k_a^2 \eta/2$ is the half width of the SBS gain curve.

This solution for ρ can then be used to solve for E_p and E_s by substituting into Equations (2.18) and (2.19), and using the assumption that E_p and E_s are slowly varying, to give,

$$(-k_p^2 - 2ik_p \frac{\partial}{\partial z} + \mu_o \epsilon \omega_p^2)E_p = \frac{\mu_o \gamma_e \omega_p^2}{\rho_o} \rho_a E_s \tag{2.23}$$

$$(-k_s^2 - 2ik_s\frac{\partial}{\partial z} + \mu_o\epsilon\omega_s^2)E_s = \frac{\mu_o\gamma_e\omega_s^2}{\rho_o}\rho_a E_p \tag{2.24}$$

which can be simplified to a pair of coupled wave equations,

$$\frac{\partial E_p}{\partial z} = -K|E_s|^2 E_p \tag{2.25}$$

and,

$$\frac{\partial E_s}{\partial z} = -K|E_p|^2 E_s \tag{2.26}$$

with

$$K = \frac{-i\omega_p c_o \mu_o \gamma_e^2 k_a^2}{8n\rho_o\,(k_a^2 v_a^2 - (\omega_p - \omega_s)^2 - i2\Gamma_B(\omega_p - \omega_s))} \tag{2.27}$$

Evaluating K exactly on resonance and simplifying using $k_a v_a = 2\omega_s v_a n/c_o$, we get,

$$K = \frac{\omega_p^2 \mu_o \gamma_e^2}{8\rho_o v_a \Gamma_B} \tag{2.28}$$

Hence, the pump, E_p, traveling in the $+z$ direction experiences attenuation and the SBS beam, E_s, in the $-z$ direction experiences gain.

Thus, the equation for the intensity of the SBS beam, I_s, after propagating some distance L, assuming negligible pump depletion, can be written as,

$$I_s = I_o e^{gL} \approx I_o(1 + gL) \tag{2.29}$$

for $gL < 1$, where I_o is the initial SBS intensity, and g, the small signal intensity gain with $\omega_p - \omega_s = \omega_a$, is given by,

$$g = g_b I_p = \frac{\pi^2 \gamma_e^2}{2n\rho_o v_a c_o \Gamma_b \lambda_p^2} I_p \tag{2.30}$$

where λ_p is the free space wavelength of the pump.

For example, with a pump at 632 nm in an optical fiber having $v_a = 6 \times 10^3$ m/s, $\rho_o = 2.2 \times 10^3$ kg/m^3, $n = 1.48$, $c_o = 3 \times 10^8$ m/s, $\Gamma_b =$

$(2\pi)5 \times 10^7$ radians/s and an electrostriction coefficient of $\gamma_e = 0.3\epsilon_o$, yields $g_b \approx 5 \times 10^{-11}$ m/W.[30] Thus for a 1 mW laser in a single-mode optical fiber with an effective core diameter of 5 μm, the SBS gain is approximately 2.5×10^{-3}/m.

The half width of the SBS gain curve, Γ_b, is primarily determined by the acoustic damping in the material and has been observed to vary with the inverse of the square of the pump wavelength.[31] At 632.8 nm, the width of the gain curve in bulk silica is approximately 100 MHz, and at 1.3 μm, approximately 25 MHz. This linewidth narrowing offsets the explicit λ^{-2} dependence of the SBS gain in Eq. (2.30), causing the SBS gain to be almost constant with respect to wavelength.[30]

At a given a wavelength, the net gain due to SBS, Eq. (2.29), can be increased by increasing the pump intensity or increasing the interaction length. The small core of optical fibers creates very high pump intensities for modest input pump powers, while their low loss allows very long interaction lengths.

2.2 Properties of SBS Fiber Ring Lasers

In this section the SBS gain will be used to generate a fiber ring laser. First, the requirements for SBS lasing will be reviewed, and an expression for the minimum pump power required for lasing will be derived. Second, fiber-optic cavities, which provide the optical feedback for the laser, will be described, and third, an SBS fiber ring laser and its various properties will be demonstrated.

2.2.1 SBS Laser Threshold Pump Power

There are two basic requirements for generating a laser: a source of optical feedback, in this case an optical resonator, and optical gain sufficient to overcome the losses in the resonator. In this section, the pump power requirements for SBS lasing will be examined.

In addition to providing the optical feedback for the SBS laser, the optical cavity also greatly reduces the pump power requirements for SBS lasing. With the pump tuned near the center of a cavity resonance, the pump power inside the cavity is resonantly enhanced. This enhanced pump generates an SBS gain curve inside the resonator in a direction opposite to that of the pump, as shown in Fig. 2.3. As seen in the figure, several cavity resonances may fall under the SBS gain curve, and the round trip gain for one of these resonances must exceed the round trip losses to achieve lasing.

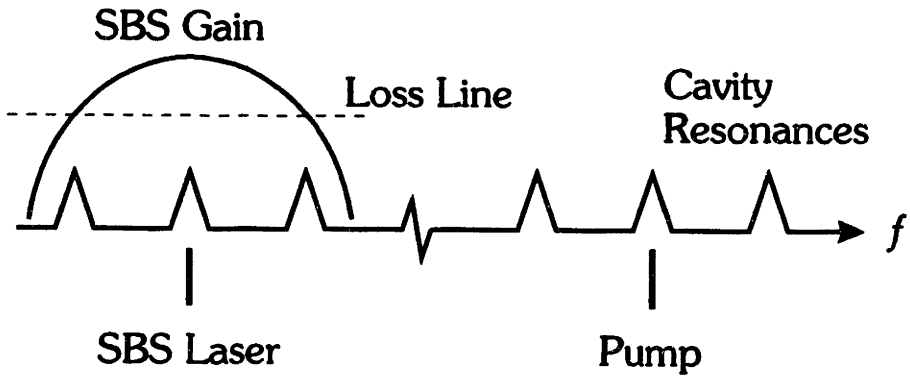

Figure 2.3 Illustration of the pump and SBS gain inside the fiber resonator.

Thus, the threshold gain for lasing is simply equal to the round trip loss in the cavity. For a matched cavity, i.e., a cavity where the internal losses are equal to the coupling loss, the round trip loss is equal to π/F, where F is the cavity finesse. Further, for such a cavity on resonance, the pump power inside the cavity is enhanced by F/π. Thus, using the gain expression from Eq. (2.29), and setting the gain equal to the loss we get,

$$\left(\frac{P_{th}}{A}\right) gL \left(\frac{F}{\pi}\right) = \left(\frac{\pi}{F}\right) \tag{2.31}$$

where P_{th} is the pump threshold power. Solving for the threshold power yields,

$$P_{th} = \frac{A\pi^2}{F^2 g L} \tag{2.32}$$

where L is the round trip length of the cavity. Thus, for low threshold SBS lasers, long, high finesse resonators are required. For example, at 632.8 nm with $L = 20$ m, $A = \pi\,(2.5 \times 10^{-6}\ \text{m})^2$, $F = 70$ and $g \approx 5 \times 10^{-11}$ m/W, $P_{th} = 40\ \mu$W, which can easily be achieved using a low power He-Ne laser.

2.2.2 Fiber Ring Cavities

The fiber ring cavities are constructed from a continuous loop of single-mode optical fiber and a polished, evanescent wave coupler,[22] as shown in Fig. 2.4. In this configuration, no splice is required in the cavity, but the coupler must strongly couple the light between the two fibers. For example, to achieve a finesse of 300, 99% of the power entering the coupler in one fiber must be coupled into the other fiber.

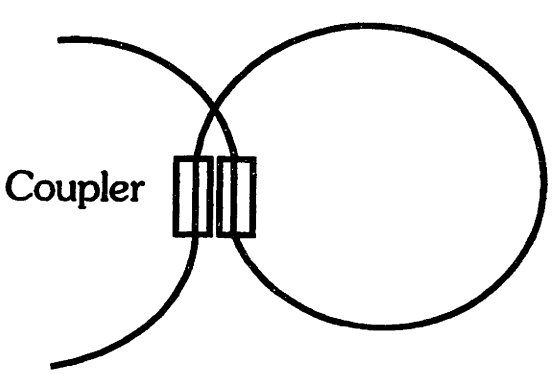

Figure 2.4 Schematic diagram of a continuous loop, fiber ring cavity using an evanescent wave coupler.

Several fiber cavities at 633 nm, 1150 nm, and 1300 nm were used throughout this research. The cavities ranged in length from 20 m to 2 m, with finesses ranging from 400 to 25. Table 2.1 lists the cavities along with some of their important characteristics.

Fiber Cavity Summary					
Label	λ (μm)	L (m)	F	FSR (MHz)	P_{th} (μW)
A	0.63	5	160	41	340
B	0.63	20	70	9.6	120
C	0.63	20	70	9.6	120
D	0.63	2	170	100	~ 225
E	0.63	3	200	65	~ 120
F	0.63	20	25	10	N/A
G	1.15/1.3	20	250	10	60
H	1.15/1.3	10	500	22	~ 50

Table 2.1

All cavities were used as multi-turn resonators, with most of the fiber wound in a coil, approximately 10 cm in diameter. In order to reduce the temperature perturbations to the cavity and protect it from physical damage, the cavity was kept inside a covered box, from which only the fiber arms and electrical connections emerged. This box, along with the fiber coupling stages, was then enclosed in a larger box, to further thermally and acoustically isolate the cavity. More details on the physical layout of the cavity can be found in Section 2.4.1.

The operation of a fiber resonator can be demonstrated using the setup shown in Fig. 2.5. In the simplified schematic diagram, a laser, in the direction labeled **P**, is coupled into a 20 m long fiber ring cavity, cavity **F** in Table 2.1. The cavity is viewed in reflection using detector **D**. As the laser frequency is scanned over a complete free spectral range (FSR) of the fiber cavity, the corresponding output of the cavity, as measured by detector **D**,

is shown in Fig. 2.6(a). With the laser well off resonance, the full intensity of the laser is observed, while with the laser on resonance, an intensity minimum is observed. A close-up of the resonance is shown in Fig. 2.6(b), with a linewidth of 400 kHz for a cavity finesse of 25.

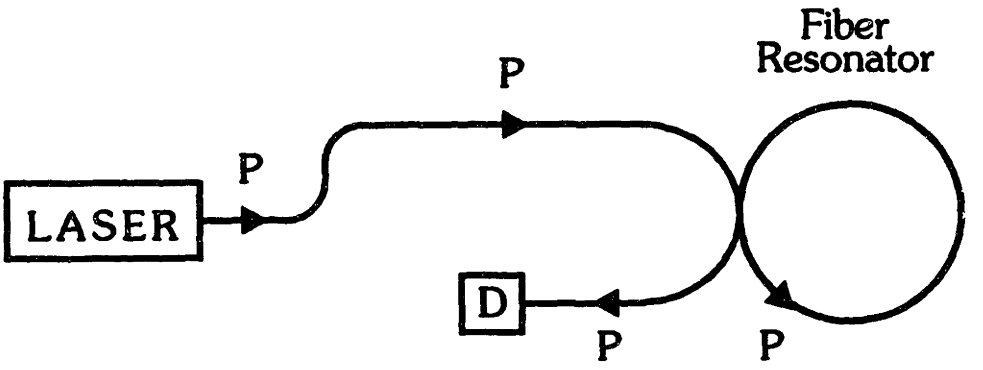

Figure 2.5 Simplified schematic diagram for a fiber ring cavity observed in reflection.

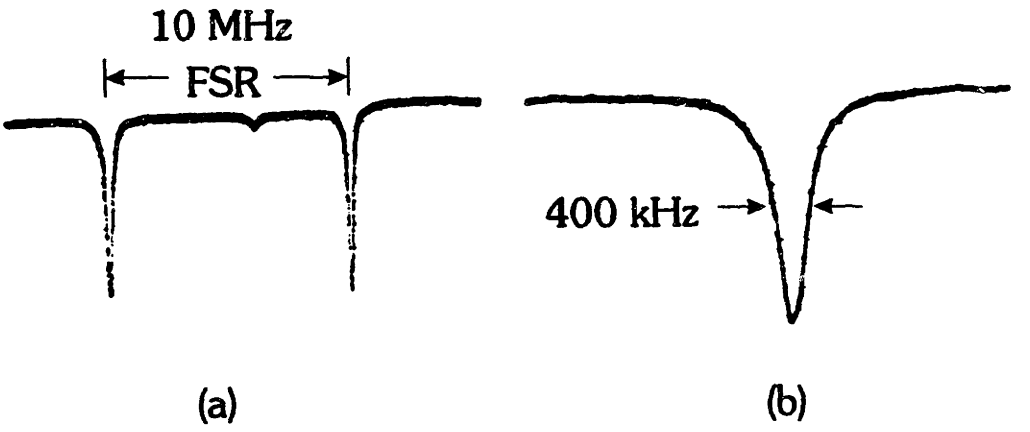

Figure 2.6 Fiber ring cavity observed in reflection as the pump laser frequency is tuned, showing (a) an entire cavity FSR, and (b) a close-up of a cavity resonance. Cavity F.

2.2.3 Demonstration of SBS Lasing

Figure 2.7 shows a simplified schematic diagram for an SBS laser. The pump laser, in the direction labeled **P**, first passes through directional coupler **C2** and then is coupled into the fiber cavity via coupler **C1**, and the reflected pump from the cavity falls on detector **D1**. With sufficient pump power inside the resonator, an SBS laser, in the direction labeled **B**, is generated and coupled out of the cavity by **C1**. In order to monitor the SBS, directional coupler **C2** is used to couple a fraction of the SBS output onto detector **D2**.

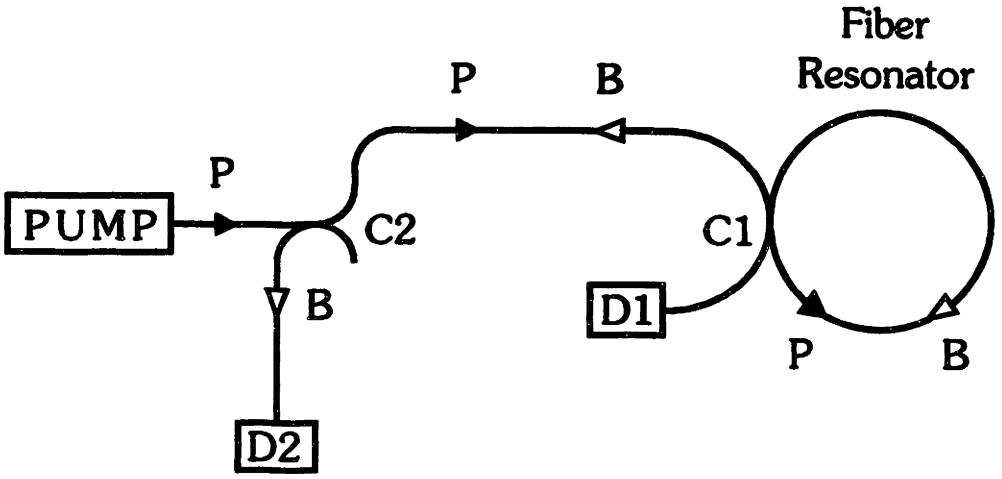

Figure 2.7 Simplified schematic diagram for an SBS laser.

In this case, the pump is a single longitudinal mode obtained from a randomly polarized, two-mode, 3 mW He-Ne laser at 632.8 nm. Since the longitudinal modes of this laser are orthogonally polarized, a single mode of the laser is selected using a simple polarizer. This pump laser was also frequency stabilized to its gain curve, as described in Section 2.4.3. The fiber cavity used to demonstrate SBS lasing, cavity **D** in Table 2.1, is 2 m

long with a finesse of 170, a linewidth of 600 kHz, and is constructed from nonpolarization preserving, single mode fiber.

In Fig. 2.8, the pump laser is scanned over a cavity resonance while simultaneously monitoring the outputs of detectors **D1** (top) and **D2** (bottom) on an oscilloscope. Figure 2.8(a) shows a cavity resonance in reflection, as measured by detector **D1**, but only a small signal, due to stray reflections external to the cavity, from detector **D2**. If the pump power is increased slightly above the 225 μW SBS threshold for this cavity, a dramatic increase in backscattering, shown in Fig. 2.8(b), is observed when the pump is very close to the center of the resonance, i.e., when the pump power inside the cavity is close to its maximum value. Finally, with the pump well above threshold, as in Fig. 2.8(c), very strong backscattering which follows the pump power inside the cavity, is observed.

It should be noted that the stable, unidirectional lasing observed here is in marked contrast to the behavior of a typical solid-state gain medium using a ring cavity. In a conventional solid-state ring laser, mode competition between lasers in the opposite directions of the cavity leads to unstable lasing in either direction. In contrast, the SBS laser demonstrates stable lasing in only one predictable direction of the cavity, without the use of any unidirectional devices inside the cavity.

In order to generate a continuous SBS laser, the pump laser must be held near the center of a cavity resonance using a servo loop. Although a simple DC servo can be used to lock the pump laser to the side of a cavity resonance, for maximum SBS power, the pump must be locked to the center of a cavity resonance using an AC servo, described in Section 2.4.2. In addition to locking the pump to the center of a cavity resonance, to achieve maximum pump power inside the resonator, the polarization of the pump must be matched to one of the two eigenpolarizations of the cavity, which are, in general, elliptical states of polarization.

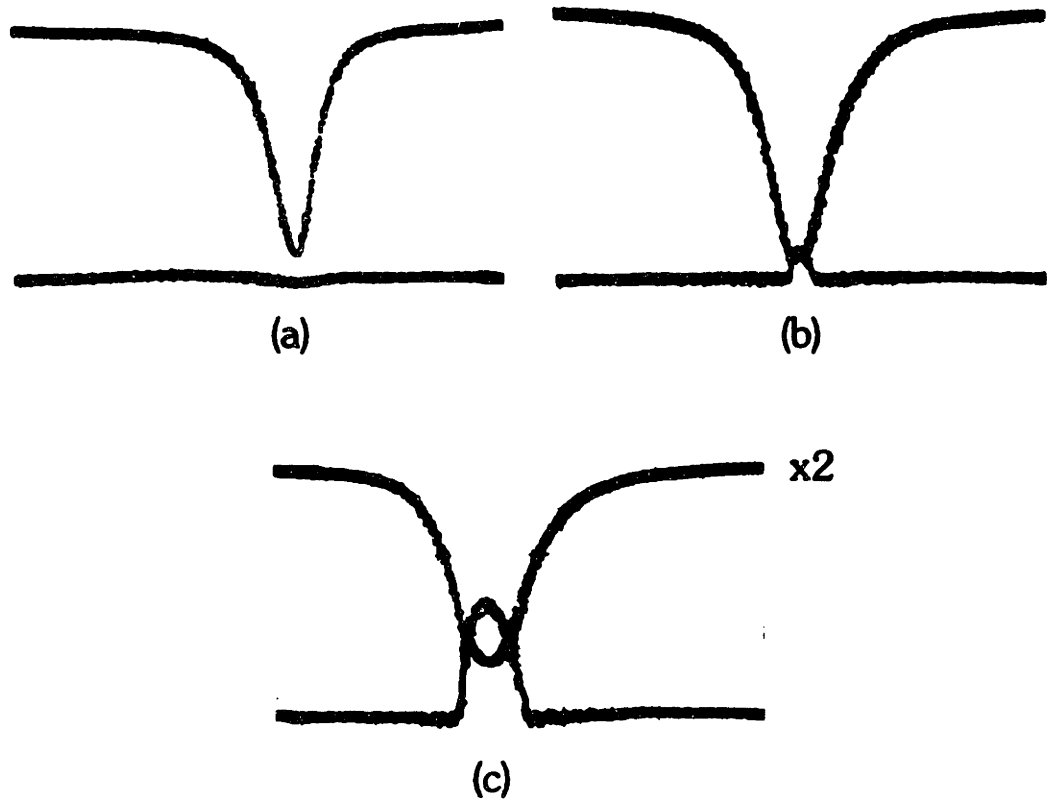

Figure 2.8 Simultaneous monitoring of the pump (top) and the SBS (bottom) with the pump power (a) below, (b) slightly above, and (c) well above SBS threshold. Cavity D.

2.2.4 SBS Laser Frequency

With the pump locked to the center of a cavity resonance, a more detailed study of the SBS laser can be performed. As seen in Fig. 2.9, a short, plane-parallel, scanning Fabry-Perot with a 70 GHz FSR is inserted at the SBS laser output. Though the Fabry-Perot in the figure is schematically shown with a fiber input and output, in practice, the light was coupled out of the fiber and collimated before passing through the Fabry-Perot and falling onto detector **D2**. Scanning of the Fabry-Perot was accomplished by mounting

one of its mirrors on a cylindrical piezoelectric transducer (PZT). When a high voltage is applied to the PZT, its length changes, thus changing the length of the Fabry-Perot by a few wavelengths. Hence, for scanning, a high voltage triangle wave was applied to the PZT, as shown in the figure.

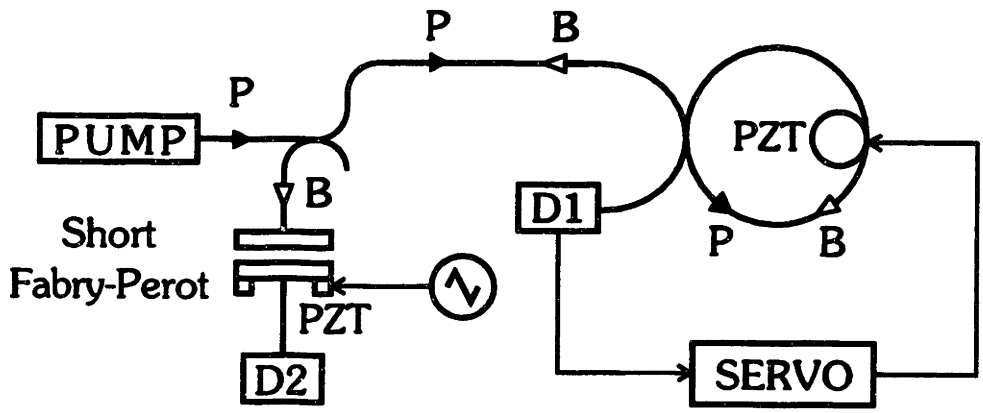

Figure 2.9 Setup for analyzing the SBS laser using a 70 GHz plane-parallel, scanning Fabry-Perot.

With the pump laser well below the SBS laser threshold, only a single peak is observed in the output of the Fabry-Perot, shown in Fig. 2.10(a), which is due to back reflections of the pump and is used here as a frequency marker. However, with the pump above SBS threshold, in Fig. 2.10(b), a second peak, due to the SBS laser, is seen downshifted by approximately 30 GHz from the pump. This is in good agreement with the expected frequency shift at this wavelength, and confirms that the observed backscattering was in fact SBS.

2.2.5 SBS Laser Longitudinal Modes

Further study of SBS laser behavior is possible by replacing the short, low resolution Fabry-Perot with a longer, confocal Fabry-Perot with an effective

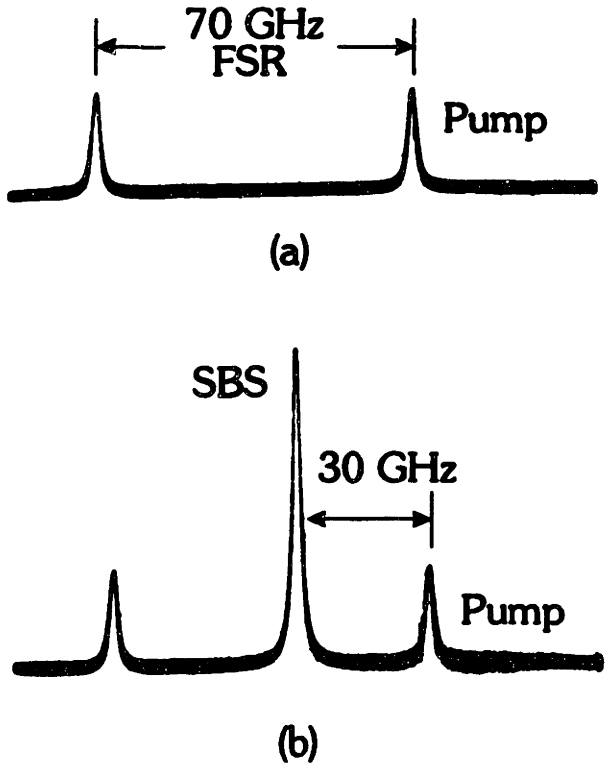

Figure 2.10 Scans of the SBS laser output on a 70 GHz FSR Fabry-Perot with the pump (a) below threshold, and (b) above threshold. Cavity B.

FSR of 250 MHz and a linewidth of 7 MHz, as shown in Fig. 2.11. With the pump laser well above threshold, two peaks are again observed, as shown in Fig. 2.12(a), a small peak due to pump back reflections, labeled **P**, and a much larger peak due to the SBS laser, labeled **B**.

Closer examination of the SBS peak in Fig. 2.12(b), shows that the SBS laser is only oscillating in a single longitudinal mode of its 10 MHz FSR cavity, despite the fact that the SBS gain is approximately 100 MHz wide and several longitudinal modes should be above the loss line. Thus, the SBS gain is behaving like a homogeneously broadened gain medium, confirming the earlier observations carried out in our laboratory.[5] It is also important to recognize that the observed linewidth of the SBS laser in Fig. 2.12(b)

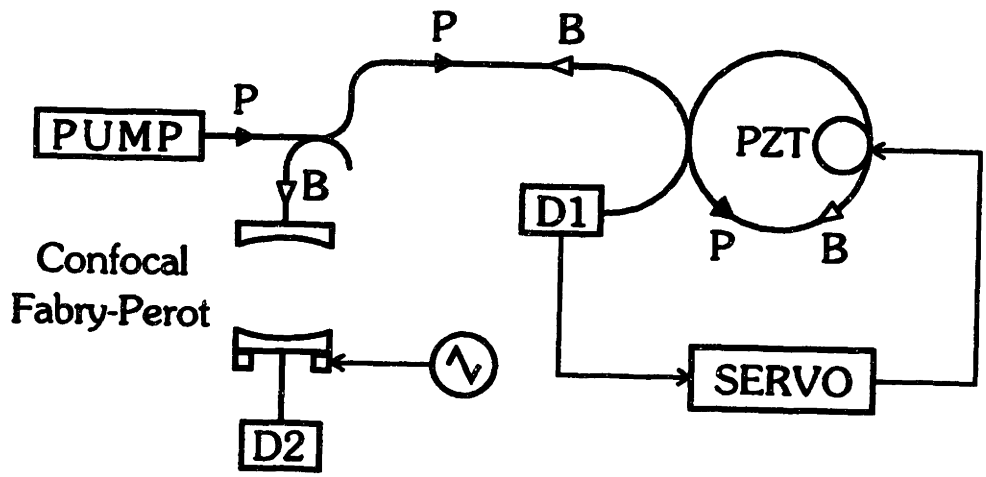

Figure 2.11 Setup for analyzing the SBS laser output using a 250 MHz FSR, confocal Fabry-Perot.

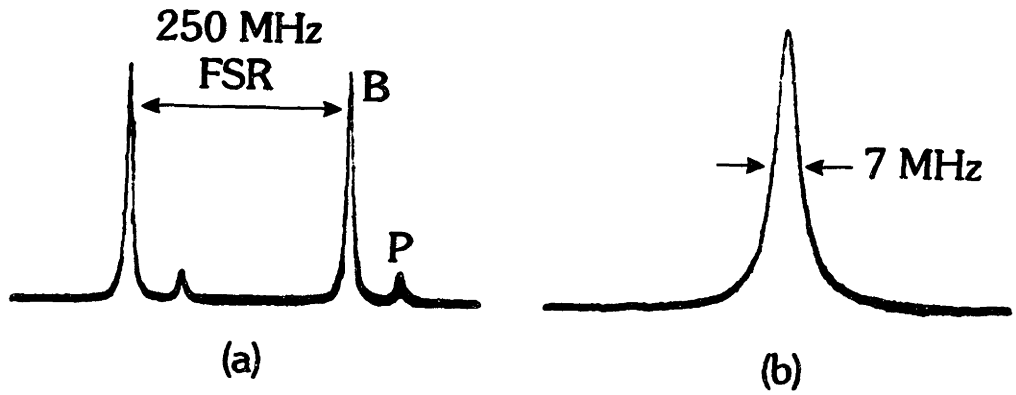

Figure 2.12 Scans of the output of the SBS laser on a 250 MHz FSR confocal Fabry-Perot showing (a) a complete FSR of the cavity with **P** and **B** marking the pump and SBS resonances respectively, and (b) a close-up of the SBS resonance. Cavity B.

is limited by the instrumental linewidth of the Fabry-Perot, and not the intrinsic linewidth of the SBS laser.

2.2.6 SBS Laser Linewidth

Better estimates of the actual linewidth of the SBS laser can be made by using a higher resolution Fabry-Perot. The low loss of optical fibers allows very long, narrow linewidth fiber cavities to be constructed, even though such cavities have relatively low finesses.

For example, when the confocal resonator shown in Fig. 2.11 is replaced with a higher resolution fiber cavity (Cavity **F**), which has a linewidth of only 400 kHz, a narrower linewidth for the SBS laser is obtained. Figure 2.13(a) shows a scan of a complete FSR of the fiber cavity. The larger peak, **B**, is due to the SBS lasing and the much smaller peak, **P**, is due to pump backscattering. Figure 2.13(b) shows a close-up of the SBS resonance and demonstrates, by the lack of noise on the side of the resonance, that the linewidth of the SBS laser is much narrower than the 400 kHz linewidth of the analyzer.

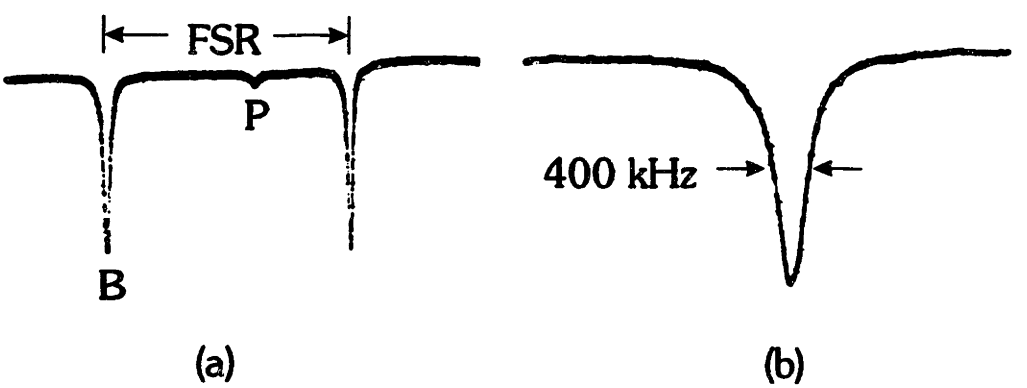

Figure 2.13 Scans of the SBS laser on a high resolution fiber cavity, which has a linewidth of 400 kHz, showing (a) a complete FSR of the cavity, and (b) a close-up of the SBS resonance. The SBS laser uses cavity B, and the passive cavity is cavity F.

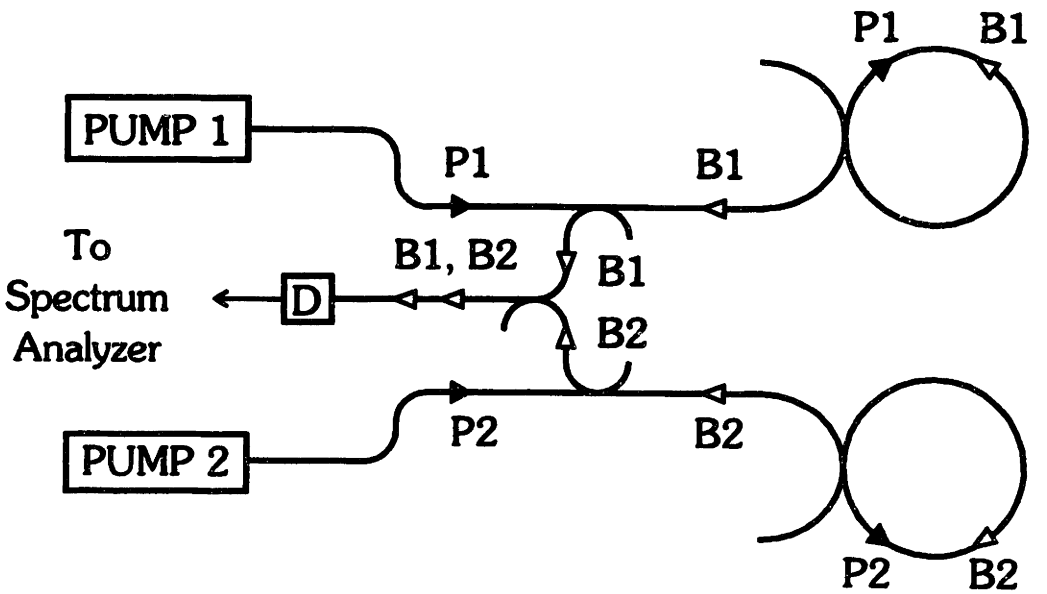

Figure 2.14 Setup for the measurement of the width of the beat between independent SBS lasers.

Due to the extremely narrow linewidth of the SBS laser, it is difficult to construct a Fabry-Perot which has a sufficiently narrow linewidth and is stable enough to directly measure the laser's linewidth. Instead, the SBS laser linewidth can be more easily measured by interfering the outputs of two independent SBS lasers, and then measuring the width of the resulting beatnote, using the setup shown in Fig. 2.14. In this figure, separate pump lasers, **P1** and **P2**, are each locked to their respective cavities using servos (not shown in the figure) and generate two independent SBS lasers, **B1** and **B2**, respectively. These SBS lasers are combined using a directional coupler and fall on detector **D**, whose output is fed to a spectrum analyzer.

Figure 2.15(a) shows a 3 kHz wide beatnote between the independent SBS lasers, centered on 101 MHz. This narrow beatnote, implies that the short-term linewidth of each laser is less than 2 kHz. It is important to note that this 2 kHz linewidth is not the result of using narrow linewidth pump lasers. In fact, the beat between the intentionally jittered pump lasers,

shown in 2.15(b), is more than an order of magnitude broader than the SBS laser beat.

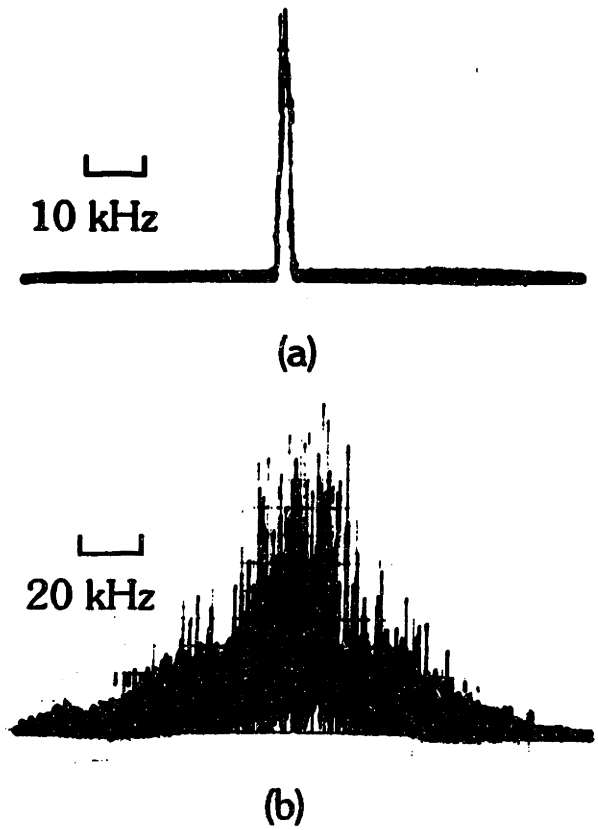

Figure 2.15 Spectrum of (a) the beat between two independent SBS lasers, and (b) the beat between the corresponding pump lasers which were intentionally jittered, both centered on 101 MHz. Cavities B and C.

This insensitivity of the SBS laser linewidth to pump frequency jitter is due to the bandwidth of the SBS gain being much greater than the fiber cavity linewidth, so that the frequency of the SBS laser is primarily determined by the cavity resonance. However, if the pump laser linewidth is larger than the cavity linewidth, the amplitude of the SBS gain will be modulated, thus broadening the spectrum of the SBS laser.[32]

The 2 kHz SBS laser linewidth in Fig. 2.15(a) is determined primarily by the residual acoustic and thermal drifts of the fiber cavities, and does not represent the intrinsic linewidth of the laser. For example, a relative change in average cavity temperature of only 10^{-6} degrees Celsius results in a 10 kHz change in the beat frequency. Clearly, further reduction to this free-running laser linewidth would require extremely precise control of the laser's environment.

2.2.7 SBS Laser Threshold and Efficiency

The generation efficiency of the SBS laser is measured by monitoring the SBS laser power at the output of the cavity as a function of the pump laser power. The SBS threshold can then be found by extrapolating the measured SBS power curve to zero.

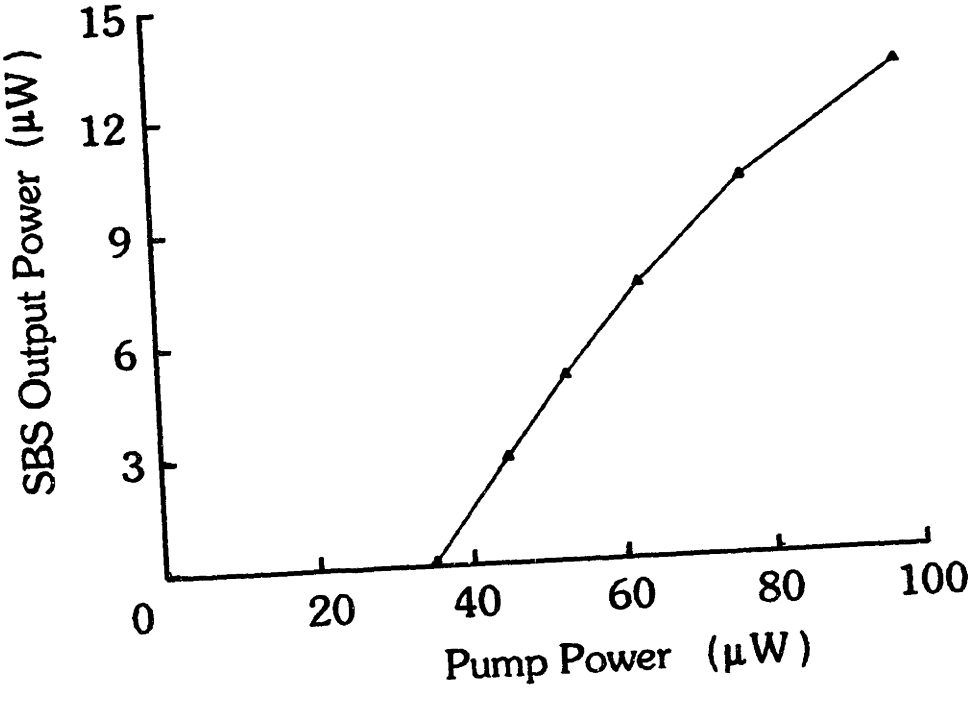

Figure 2.16 SBS laser power versus pump power demonstrating very low lasing threshold. Cavity G.

Figure 2.16 shows the SBS power versus pump power for a low threshold SBS cavity. In this case, the threshold is only 35 μW, and the slope efficiency of the laser is approximately 25%.

In addition, by using a cavity with an adjustable coupler, it is also possible to measure the efficiency as a function of output coupling. Figure 2.17 shows the SBS power versus pump power for several settings of the fiber coupler. At setting (a), the coupler was adjusted so that the cavity was well matched, i.e., the resonance depth was close to 100%, with the pump laser below SBS threshold. In this case, the SBS laser slope efficiency was measured at 28%. At setting (b), the output coupling of the cavity was increased, which lowered the cavity finesse, increased the SBS threshold and increased the slope efficiency to 55%. Finally, in (c), the output coupling was further increased, so that the cavity was well matched with the pump laser near its maximum value. The slope efficiency in this case increased to 88%.

Qualitatively, by increasing the output coupling of the cavity, the ratio of power coupled out of the cavity to power dissipated internally in the cavity increases, which increases the slope efficiency. In addition, if at low pump powers the cavity is undercoupled, i.e., the internal losses are less than the output coupling, then the resonance depth of the cavity is much less than 100%, and the power coupling into the cavity is poor. However, for larger pump powers, the additional internal loss due to SBS will increase the resonance depth and the power coupling into the cavity. Thus, for severely undercoupled cavities, low internal losses combined with increasing resonance depths can lead to slope efficiencies for the SBS laser in excess of 100%.

2.2.8 SBS Gain Thermal Tuning

Since both the speed of sound and the index of refraction of the fiber are temperature dependent, the frequency shift of the SBS gain curve is also temperature dependent. In addition, the difference in the thermal expansion

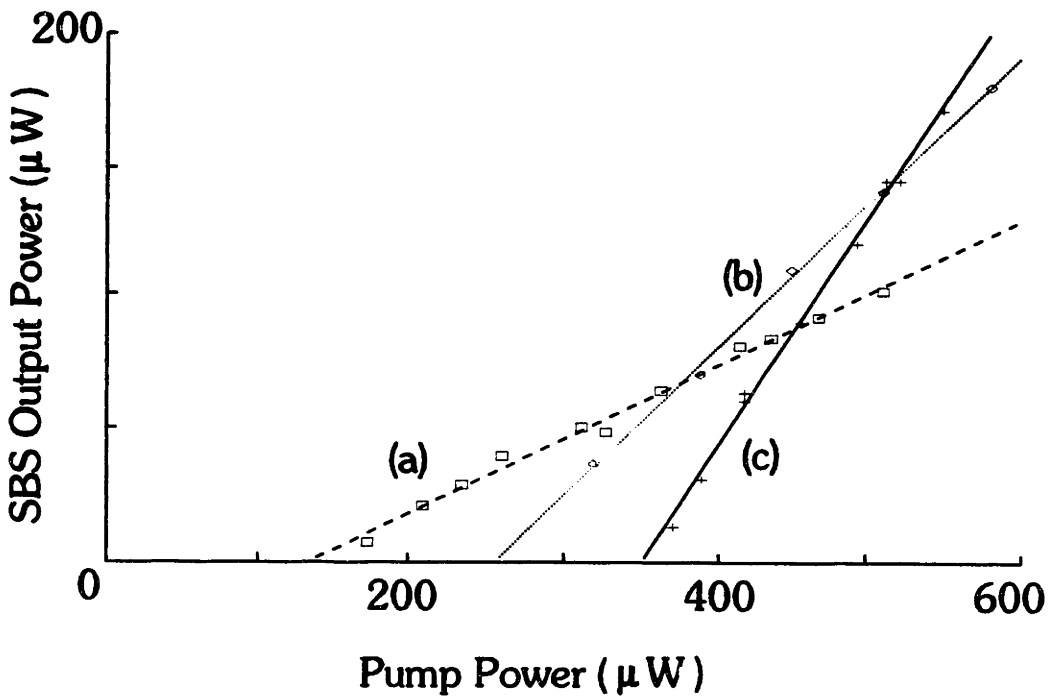

Figure 2.17 SBS laser power as a function of pump power for several cavity coupler settings. Cavity D.

coefficients between the optical fiber and its protective jacket can cause stress in the fiber, enhancing the apparent thermal coefficient of the SBS gain curve.[33]

The temperature dependence of the SBS gain curve can be found by measuring the frequency separation between the SBS laser and the pump as a function of cavity temperature. However, in order to accurately measure the thermal tuning of the SBS gain, the applied temperature perturbation must be large enough so that the center of the SBS gain is shifted by several cavity FSRs, since the SBS laser does not tune continuously with the center of the SBS gain.

In this case, changes in the frequency separation of the pump and the SBS laser were measured using a confocal Fabry-Perot with an effective FSR

of 250 MHz, in a setup similar to that previously shown in Fig. 2.11. With the pump laser locked to a fiber cavity resonance, the fiber cavity was slowly heated by several degrees Celsius, and the resulting change in the frequency separation of the pump and the SBS laser was measured using the confocal Fabry-Perot. In this way, the tuning of the SBS gain was measured to be 7 MHz/°C using a pump at 633 nm. Due to the size of the thermal perturbation, the thermal tuning of the fiber cavity greatly exceeded the tuning range of the pump laser, which required the pump to be periodically re-locked throughout the course of the measurement.

Since the FSR of the Fabry-Perot, 250 MHz, is small compared to the frequency separation of the pump and the SBS, 30 GHz, the longitudinal mode number, i.e., the q, of the pump and SBS Fabry-Perot resonances differed by over 100. Thus, changes in the FSR of the Fabry-Perot would also lead to an apparent change in the frequency separation between the pump and the SBS. However, the frequency "hops" of the SBS laser as it changed longitudinal modes were easily observed, and the drift of the Fabry-Perot was negligible over the time span of the thermal perturbation.

Further, the thermal perturbation of the fiber cavity also changed the fiber cavity FSR, thus changing the frequency separation between the pump and SBS laser's cavity modes. This tuning, however, was only about 600 kHz per degree Celsius, which was much smaller than the observed SBS gain tuning.

2.3 SBS Fiber Ring Lasers Applications

There are a number of applications which can take advantage of the properties of SBS lasers. In this section, we will propose and demonstrate several such applications.

2.3.1 Laser Linewidth Reduction

One application of an SBS laser is for the reduction of frequency jitter in a single-frequency laser, such as a dye laser, without the use of fast feedback loops. As previously demonstrated in Fig. 2.15, even if a jittery laser is used as the pump for an SBS laser, the linewidth of the SBS laser is still very narrow. Thus, the jittery pump laser is downshifted by the SBS shift, e.g., 30 GHz for a visible pump laser, and converted into a narrow linewidth SBS laser. In addition, the directionality of the SBS gain also makes the SBS laser very resistant to the effects of optical feedback. Backscattering or back reflections into the SBS laser propagate in the direction opposite to that of the laser, thus do not perturb the lasing field, or the laser gain medium, due to the directionality of the SBS gain.

However, if the linewidth of the pump laser is greater than the linewidth of the fiber cavity, the resulting amplitude modulation of the SBS gain will broaden the linewidth of the SBS laser. As a concrete example, consider the problem of reducing the short-term linewidth of a single-frequency dye laser ($\lambda \sim 600$ nm) with an initial dye laser linewidth that has been reduced to 2 MHz using simple servo loops. The fiber cavity linewidth can be chosen to be 10 MHz, a little wider than the width of the dye laser pump. For a desired SBS laser output power of 10 mW, the pump threshold for the SBS laser is also selected to be 10 mW, for efficient pump power conversion. To find the required cavity length, or equivalently, the cavity finesse, Eq. (2.32) can rewritten using $F = \mathrm{FSR}/\Gamma = c/L\Gamma$ to give,

$$\mathrm{P}_{th} = \frac{A\pi^2}{F^2 g L} = \frac{A\pi^2}{g}\frac{L^2\Gamma^2}{c^2 L} = \frac{A\pi^2\Gamma^2}{gc^2}L \tag{2.33}$$

which in this case yields $L = 1$ m, for an FSR of 250 MHz and $F = 20$. With this large cavity FSR, thermal tuning of the SBS gain curve will be required to center the gain curve over a cavity resonance. The linewidth

of the resulting SBS laser is expected to be a few kilohertz, based on the observed SBS linewidth in Fig. 2.15.

If a lower threshold with the same linewidth is desired, the cavity length can be shortened, and the cavity finesse increased by the same factor. In this way, the cavity linewidth is unchanged, but the threshold, which is proportional to $1/(F^2L)$, is reduced. Similarly, to increase the threshold, the cavity length is increased, and the finesse reduced.

2.3.2 Wideband Frequency Shifter

Another possible application of solitary SBS lasers is as a wideband frequency shifter that requires neither high speed electronics nor high speed modulators. As previously demonstrated in Fig. 2.10, with a pump at 630 nm, the first SBS laser is shifted by 30 GHz. In addition, just as the pump laser generates gain for a counterpropagating SBS laser, with sufficient pump power, the SBS laser itself can become strong enough to generate a second SBS laser.

The generation of higher order SBS lasers can be demonstrated using the setup in Fig. 2.18, in which a strong pump laser, **P**, is coupled into the counterclockwise (CCW) direction of a ring resonator. With the pump well above SBS threshold, an SBS laser, **B**, is generated in the clockwise (CW) direction. With sufficient pump power, the first SBS laser, **B**, can become strong enough to act as the pump for a second SBS laser, $\mathbf{B}^2$, which will be generated in the CCW direction of the cavity.

After being coupled out of the cavity, the pump and both SBS lasers are then combined using a directional coupler and pass through a scanning Fabry-Perot before falling on detector **D**. Figure 2.19(a) shows the output of **D** with only the first SBS laser above threshold, where the largest peak is due to the pump laser, **P**, and the smaller peak is due to the SBS laser, **B**, is downshifted by 30 GHz. With increasing pump power, shown in Fig. 2.19(b),

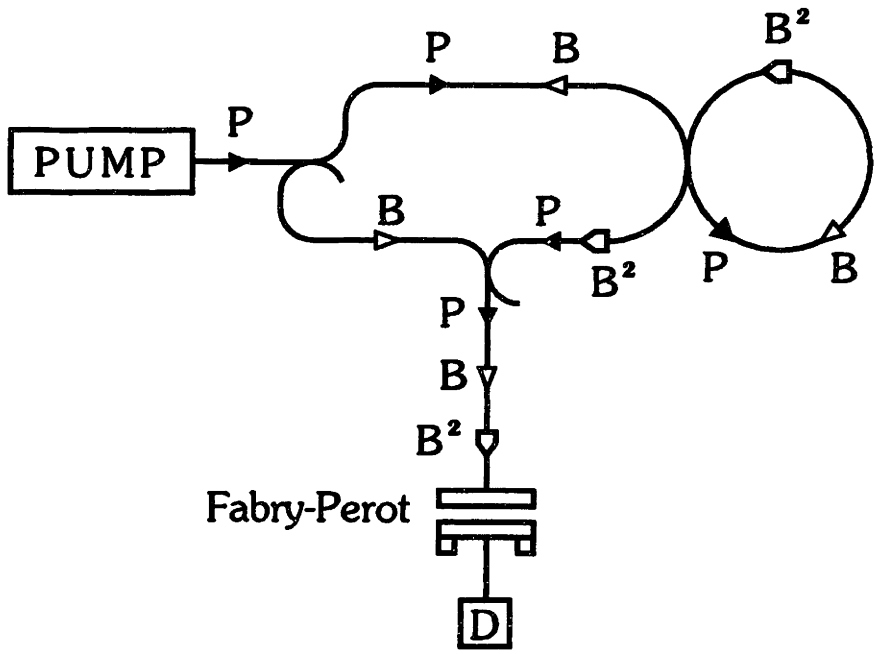

Figure 2.18 Setup for the observation of a higher order SBS laser.

the second SBS laser, $\mathbf{B}^2$, is observed, downshifted by 60 GHz, or twice the Brillouin shift, from the original pump.

Using a higher finesse cavity at 1.15 μm, we have also demonstrated tertiary SBS lasers, using the setup shown in Fig. 2.18. As before, for low pump powers, only a single SBS laser, labeled **B** is observed in Fig. 2.20(a), shifted by 15 GHz from the 1.15 μm pump, as expected for this wavelength. As the pump power is increased, in Fig. 2.20(b), a secondary SBS laser, $\mathbf{B}^2$, is also observed, and for the maximum available pump power, in Fig. 2.20(c), primary, **B**, secondary, $\mathbf{B}^2$, and tertiary, $\mathbf{B}^3$, SBS lasers are all observed.

Thus, the SBS laser can be used as a wideband frequency shifter which, using a pump around 600 nm, will provide shifted beams at multiples of 30 GHz, without the use of high speed electronics or modulators. Pumps at longer wavelengths will give smaller shifts.

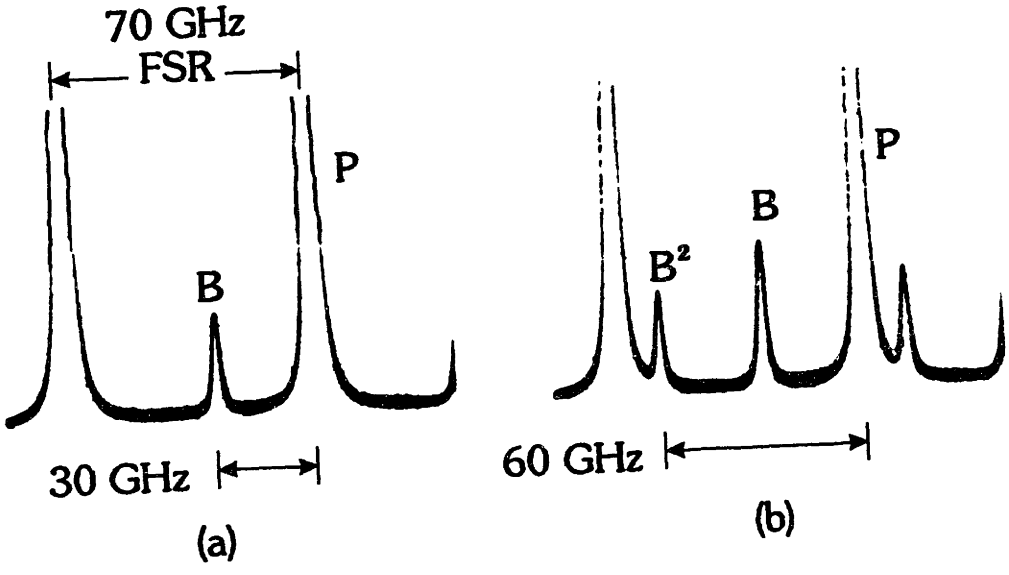

Figure 2.19 Scans of the output of the SBS laser (a) with the pump laser below secondary SBS threshold, and (b) above secondary SBS threshold. Cavity B.

2.3.3 Sensor Applications

Finally, there are a number of interesting sensor applications for the SBS laser. For example, in Fig. 2.21, two independent SBS lasers are used as a sensor. One of the lasers, labeled **Sense**, is perturbed, for example, by temperature or pressure and the second laser, labeled **Reference**, is used as a reference. Thee output of the sensor is the beat frequency between the lasers. Such a configuration can be used as a very sensitive thermometer since, as mentioned in Section 2.2.6, the output frequency changes by approximately 10 GHz/°C. In addition, various coatings can be applied to the **Sense** cavity fiber to allow the sensing of a wide range of phenomena, such as electric fields, magnetic fields, and acoustics.

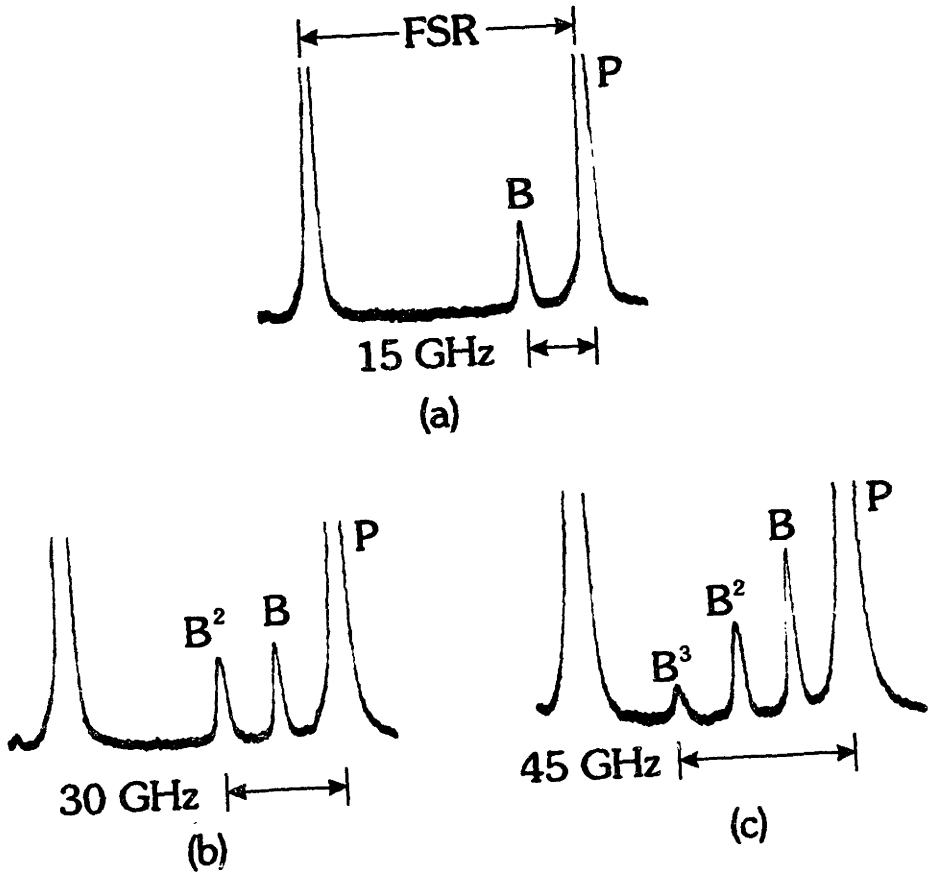

Figure 2.20 Demonstration of higher order SBS lasing as a function of increasing pump power. Cavity G.

2.4 Experimental Considerations

In this section, some of the important experimental considerations in the development of SBS fiber ring lasers will be discussed.

2.4.1 Optical Layout

Figure 2.22 shows a more detailed layout of a solitary SBS laser. As seen in the figure, the actual optical setup used in the previous experiments is a hybrid, using both fiber-optic and bulk-optic components. The pump laser, a 3 mW He-Ne laser, described in more detail in Section 2.4.3, is passed

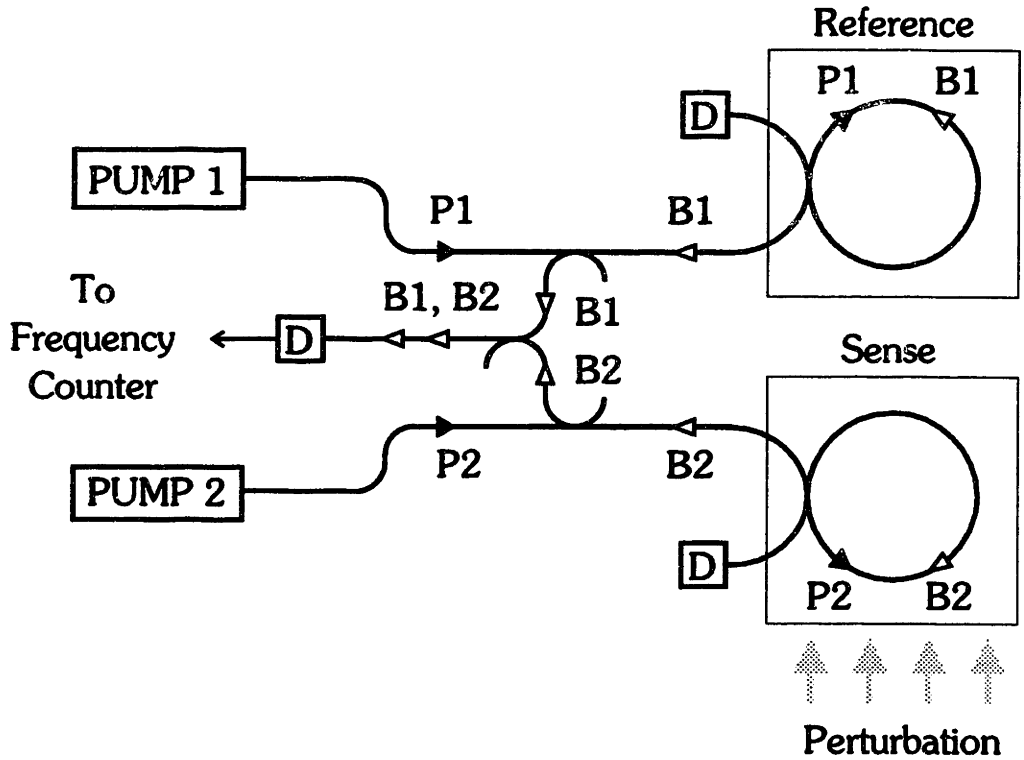

Figure 2.21 Schematic diagram for an independent SBS laser sensor with a reference cavity and a sensing cavity.

through an acousto-optic modulator (A/O), reflected by several steering mirrors, and then passed through a quarter-wave plate and a half-wave plate, and coupled into the fiber arm of the cavity. The A/O, typically driven at 40 MHz, is used to isolate the pump laser from intensity backscattering by the cavity, and also provides a convenient pump intensity control by adjusting the drive to the A/O.

The steering mirrors, in conjunction with the fiber coupling stage, are used to align the pump into the optical fiber. Due to the very small core of the optical fiber, this alignment is particularly sensitive, and the use of very high quality mirror mounts, securely fastened to the optical table, is strongly recommended. In addition, to minimize the sensitivity of the coupling to

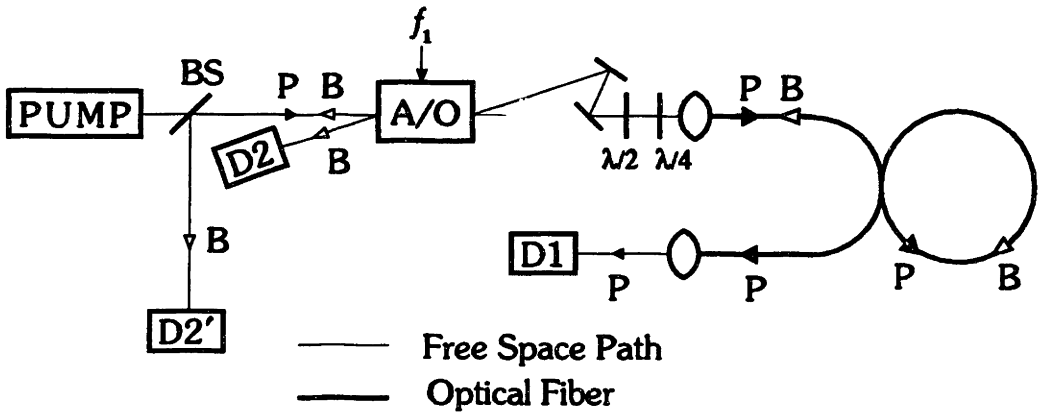

Figure 2.22 Detailed diagram of the optical setup.

thermal perturbations, it is important to minimize the length of the path between the pump laser and the fiber coupling stages.

Coupling into, and out of, the fiber arms was done using commercial fiber stages with either a high quality 20× microscope objectives or ball coupling lenses. In both cases, coupling efficiencies of 50% were routinely obtained. To minimize end reflections from the fiber, the fiber ends were mounted in glass sleeves and polished at a 7° angle. Despite this safeguard, intensity reflections from the fiber arms of approximately 0.1% were still observed. These reflections were apparently caused by either microbends of the fiber mounted in the glass sleeve, or from microfractures near the polished end of the fiber. One advantage of the ball coupling lenses, in addition to their low cost, is that index matching oil can be used between the end of the fiber and the lens, due to their very short working distances. This is the preferred configuration.

Since the eigenpolarizations of the fiber cavity are not linear, wave plates are used to match the pump's state of polarization to a cavity eigenpolarization. However, many high quality waveplates are manufactured with a small angle between the faces of the plates, typically 30 minutes of arc, in order

to eliminate any Fabry-Perot effect between the faces of the plate. Unfortunately, this angle also causes a small amount of beam steering as the plate is rotated, which misaligns the fiber coupling. The use of wave plates can be eliminated altogether by using a fiber polarization rotator on the input arm to the cavity, if there is enough fiber arm available. This has the obvious advantage of eliminating two components in the optical path, but is somewhat less convenient to align.

All of the cavities used in this chapter were made from nonpolarization maintaining fiber. Thus, with any perturbation to the cavity fiber, the birefringence of the fiber changes, thus changing the eigenpolarizations of the cavity. While this can be a problem in practical applications, in the laboratory environment, very little drift was observed in the cavity eigenpolarizations over the course of a day, or even the course of several days. Polarization adjustments were typically only needed when the cavity was significantly disturbed, e.g., if a PZT was added to the fiber or if the cavity was moved. On the other hand, the eigenpolarizations of cavities made from polarization maintaining (PM) fiber were studied in our laboratory and found to be quite sensitive to thermal perturbations, due to the large amount of birefringence between the two fiber axes.[34,35] Thus, polarization matching into PM cavities required much more care and adjustment than comparable non-PM cavities.

It is hard to overemphasize the sensitivity of the fiber cavity to thermal perturbations. Even the light from a 20 Watt light bulb focused on a single strand of optical fiber will cause significant changes in the optical length of the fiber, and this technique was frequently used to perturb the cavity. In a typical configuration, the fiber cavity is covered in a small box which is then enclosed in a larger box. Both enclosures are designed to minimize air flow around the cavity, since convective heating and cooling can produce large and

relatively abrupt thermal perturbations. In addition, the enclosures protect the cavity from physical damage and acoustic perturbations.

2.4.2 AC Servo

An AC servo was used to lock the pump laser to the center of a cavity resonance. This servo employed a frequency modulation technique to generate a discriminant with a zero crossing at the center of the cavity resonance which can can be used to lock the pump to the center of a cavity resonance.[18,36]

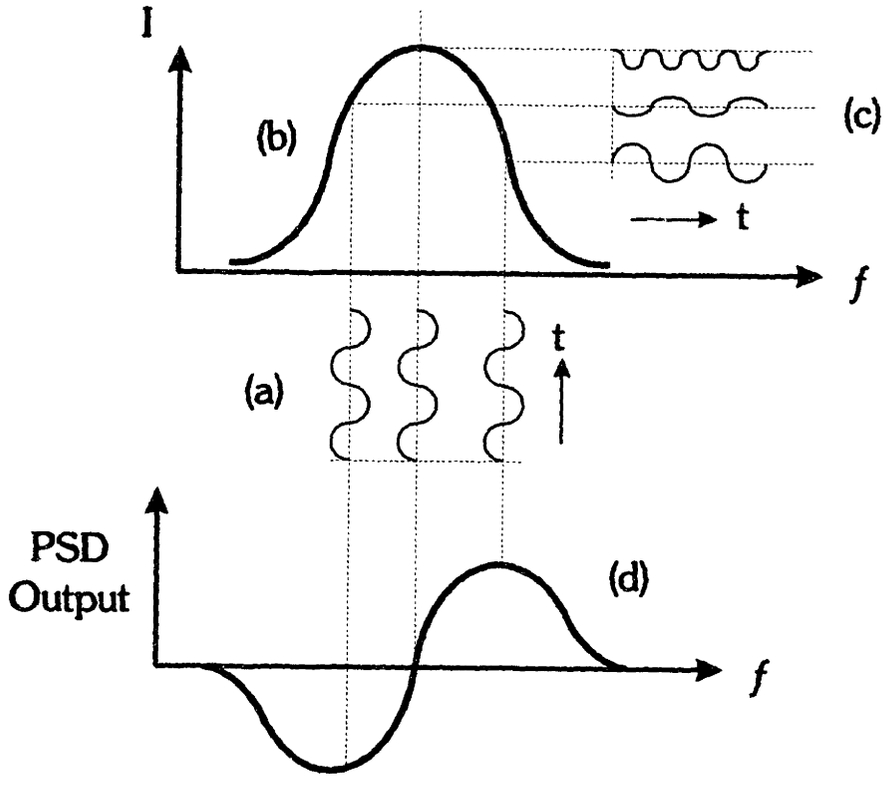

Figure 2.23 Intensity response of a frequency modulated laser at various detunings from the center of a resonance.

The generation of such a discriminant can be understood from a simple quasi-static model, shown in Fig. 2.23. As seen in the figure, the pump frequency is modulated at f_m, shown in part (a), which after passing through

the cavity resonance, (b), generates an intensity signal shown in (c). If the pump is exactly at the center of the resonance, the top waveform in (c), an amplitude modulation is observed, primarily at twice the modulation frequency, $2f_m$, with no component at f_m. However, if the pump is slightly below resonance, shown in the middle waveform in (c), a small intensity modulation at f_m is observed which is 180° out-of-phase with the applied modulation. Finally, the bottom waveform in (c) shows that if the pump is above the center of the resonance, a large amount of intensity modulation is observed which is in-phase with the applied modulation. If the intensity signal is demodulated at f_m using a phase sensitive detector (PSD), a discriminant can be formed, as shown in Fig. 2.23(d), which has a zero crossing at the center of the resonance and, as mentioned above, can be used as the error signal in a servo.

Figure 2.24(a) shows a scan of a cavity resonance without any applied modulation, and Fig. 2.24(b) shows the same resonance with frequency modulation applied. Note that the resulting intensity modulation is strongest on the sides of the resonance, is small in the center of the resonance, and goes to zero off resonance. Finally, Fig. 2.24(c) shows the modulated resonance (top) and the corresponding output from a PSD, the discriminant, (bottom) which goes through zero at the center of the cavity resonance as needed by the servo.

Figure 2.25 shows an example of an SBS laser using an AC servo in which the modulation is applied to the cavity. The intensity signal from detector **D** is demodulated by a PSD to generate an error signal which is then integrated to form the correction signal. The correction signal is then combined with the cavity modulation and then both signals are amplified and applied to a PZT that is used to tune the cavity. The PZT has several strands of cavity fiber mounted on it and, as a function of the applied voltage,

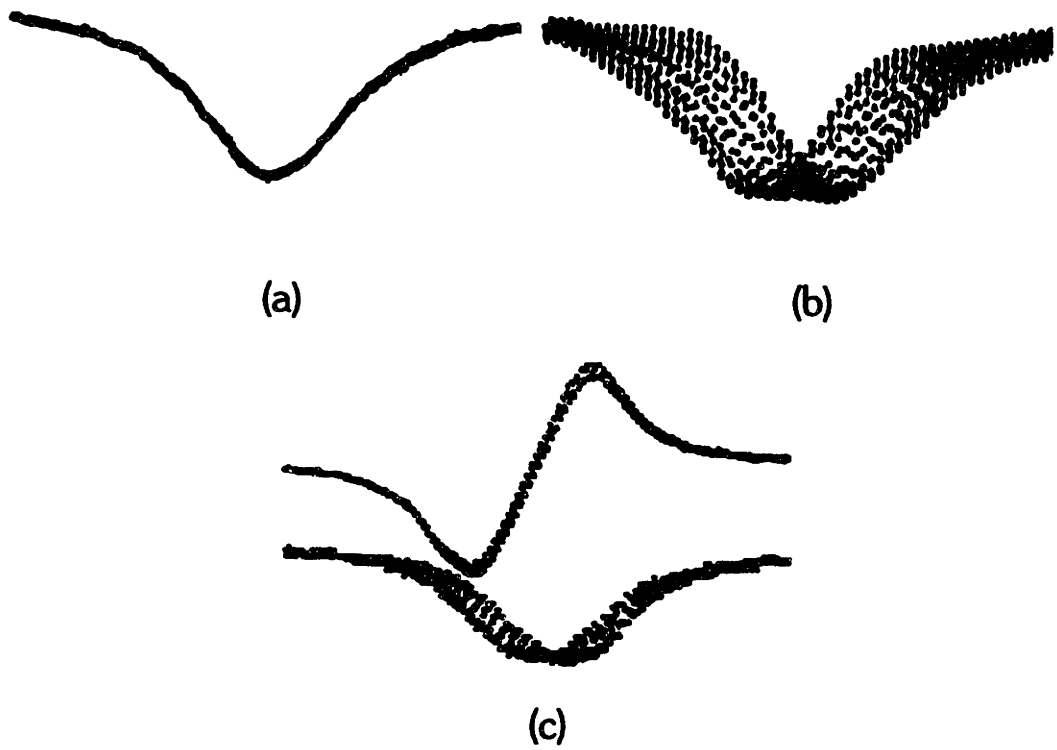

Figure 2.24 Cavity resonance scans (a) without modulation, (b) with modulation, and (c) with modulation and the corresponding discriminant. Cavity H.

the PZT changes dimension and therefore stresses the fiber, which in turn changes the optical length of the fiber and hence, the resonance frequency of the cavity.

The PZT can be either a radial mode cylinder with the fiber wrapped around it or a shear mode plate with the fiber mounted to the face of the plate. The optical fiber is usually mounted to the PZT using beeswax to allow the easy removal of the fiber without the use of solvents which can damage the fiber's protective jacket.

The servos were implemented with a combination of commercial and custom-built electronics. Commercial lock-in amplifiers, model 124a from

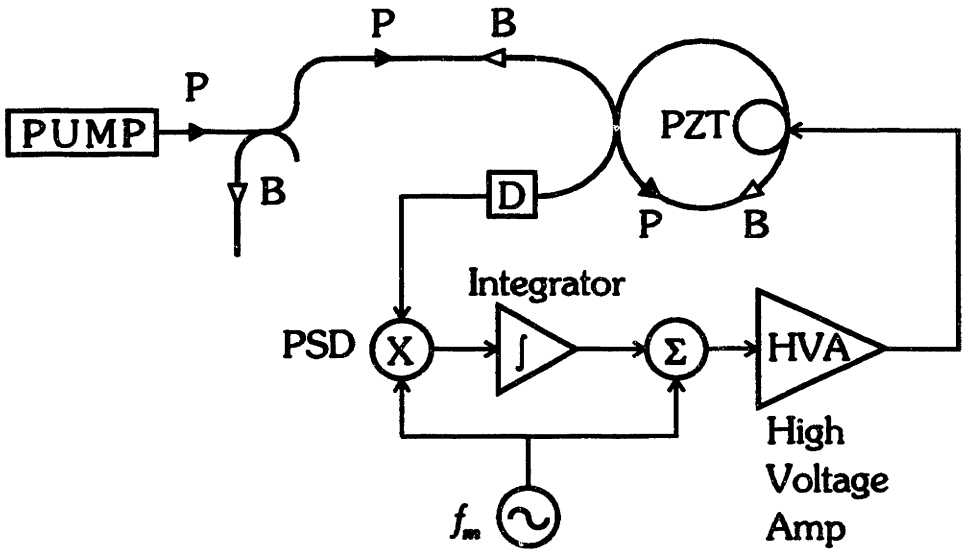

Figure 2.25 Example of a CW SBS laser using an AC servo.

Princeton Applied Research, were used as the PSDs and had a 3 dB bandwidth of 1.6 kHz, which typically limited the servo bandwidth. The high voltage amplifiers were designed and built in our laboratory and had a bandwidth of 3 kHz when driving a high capacitance PZT load.

Although the PZTs provided a good high speed response, they had a dynamic range of only a few cavity FSRs, which frequently limited the length of data runs. In order to achieve longer runs, two techniques were used that took advantage of the wide dynamic range possible with thermal perturbations of either the fiber cavity or the laser. In the first technique, shown in Fig. 2.26, the correction signal to the PZT is either integrated, as in the figure, or simply amplified, and used to drive a small (<1/4 Watt) heater in close proximity to the cavity. Thus, the PZT compensates for the fast fluctuations of the cavity while the heater takes care of the slower, large amplitude drifts. In the second technique, shown in Fig. 2.27, instead of heating the fiber cavity, the laser itself is heated. Thus, the fiber cavity is allowed to drift, while the laser follows it.

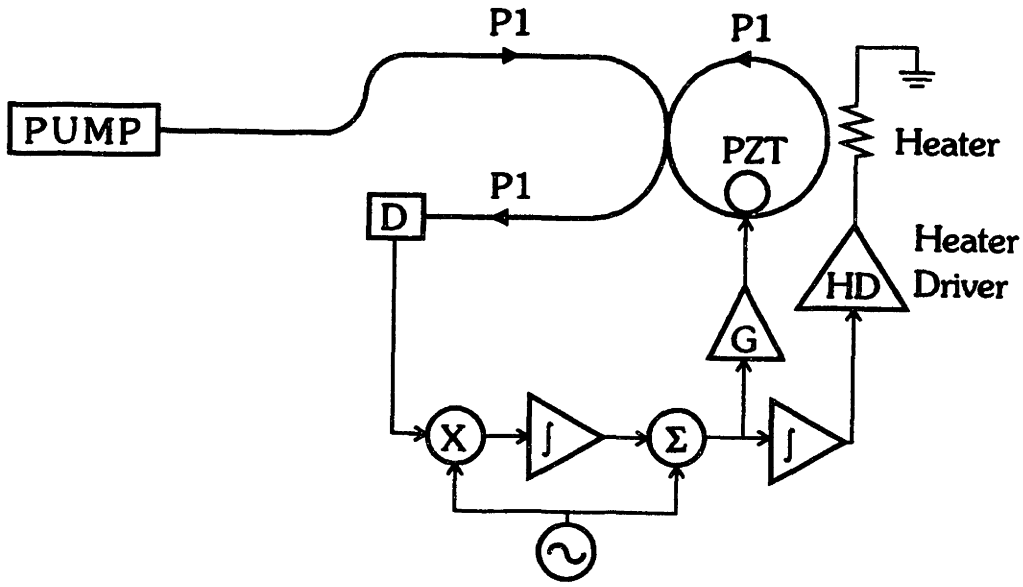

Figure 2.26 Extended dynamic range servo using a fiber cavity heater.

It should also be noted that in all the setups, except that in Fig. 2.27, the fiber cavity is locked to a stabilized laser. This configuration has the advantage of stabilizing the average temperature of the fiber cavity, but also results in a number of localized perturbations to the fiber cavity due to the PZT and the cavity heater. It is also possible to lock the laser to the cavity. The advantage of this technique is that the cavity is left unperturbed, however, the disadvantage is that the laser power will vary as the frequency of the laser tracks the cavity, and the length of the data runs will therefore be limited by the tuning range of the pump laser.

2.4.3 Pump Laser Stabilization

The He-Ne pump lasers used in this thesis were stabilized to their gain curve using a simple, home-built servo system. The lasers, as mentioned in Section 2.2.3, are nominally 2 mW, two-mode (FSR $\approx$ 680 MHz), randomly

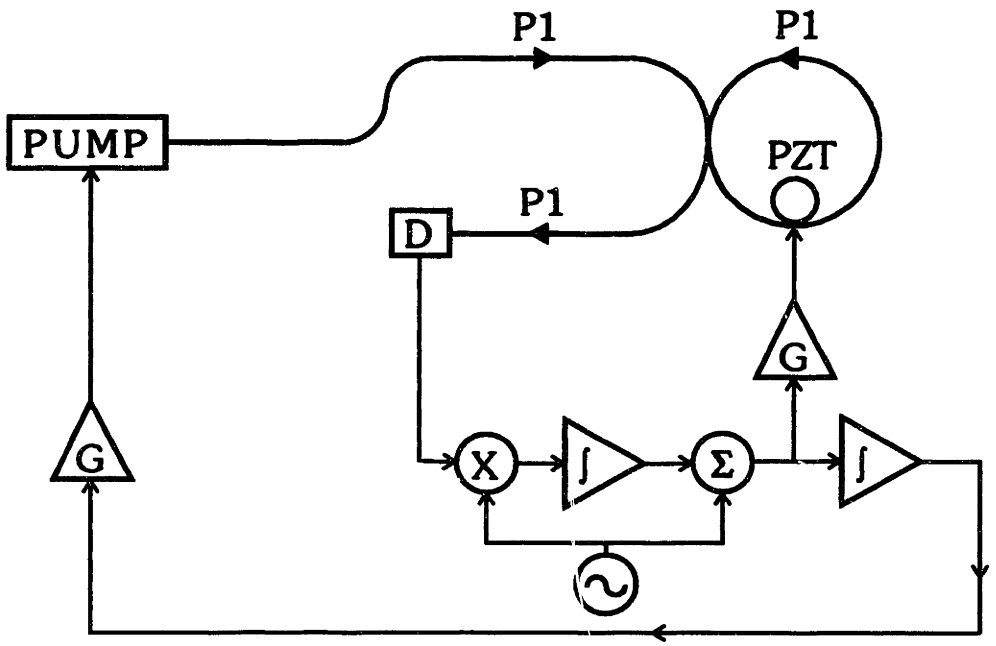

Figure 2.27 Extended dynamic range servo using a laser heater.

polarized lasers in which the modes are both linearly polarized, and mutually orthogonal. Thus, as seen in Fig. 2.28, a single mode of the laser can easily be selected using a simple polarizer at the output of the laser.

In addition, using the optical output from the back of the laser, the intensities of the two laser modes can be measured using two detectors, two polarizers, and a beamsplitter, as shown in the figure. By subtracting the intensities of the modes, an intensity independent discriminant can be generated to lock the average frequency of the laser modes to the center of the laser gain curve. Alternatively, since only one of the laser modes is used in this application, intensity independence can be sacrificed, and an adjustable gain stage, as shown in the figure, or an external bias, can be used to adjust the lock point of the laser in order to increase the amount of power in the laser mode of interest.

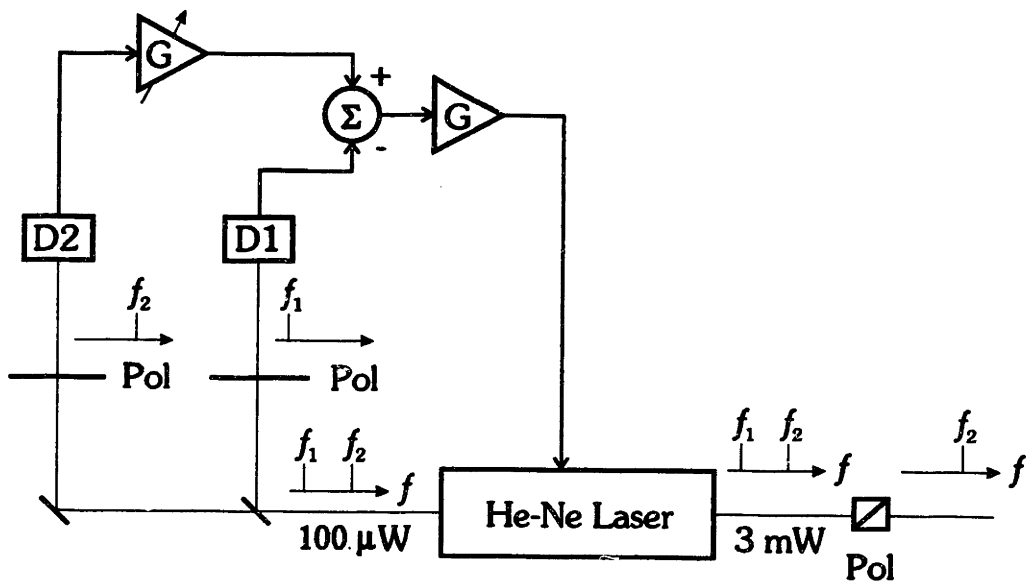

Figure 2.28 Schematic for a two-mode laser stabilization system.

Similar to the fiber cavity servo, this servo uses a PZT mounted to the laser for fast tuning, and a heater for large dynamic range. The beat between independently stabilized lasers indicates that the short-term stability of the servo is on the order 1 MHz, while the long-term drift is on the order of 10 MHz. This long-term drift is mainly due to dark current variations in the detectors, which were strongly driven by temperature. Further, the servo has also demonstrated a significant sensitivity to intensity backscattering into the laser, even when an A/O is used at the output of the laser. Even though backscattering from beyond the A/O is frequency shifted, a small amount of the backscattering still passes through the laser cavity and affects the stabilization servo.

2.5 SBS Laser Problems

There are several issues which must be addressed for proper operation of the SBS laser, and this section will explore some of the problems with this type

of laser, including the generation of higher order SBS lasers, spontaneous modelocking, and the effects of cavity backscattering.

2.5.1 Higher Order SBS

As mentioned in Section 2.3.2, it is possible to use the SBS laser itself as the pump for a second SBS laser which will copropagate with the pump, and be downshifted by twice the SBS frequency shift, or 60 GHz for a visible pump.

However, there a number of effects caused by the generation of higher order SBS lasers. One of these effects can be observed using the setup shown in Fig. 2.29. Figure 2.30(a) shows the output of **D1** (top) and **D2** (bottom) for modest pump powers, with the SBS laser showing its characteristic threshold behavior, followed by a smooth increase in power as the pump laser approaches the center of the cavity resonance. With an increase in pump power, in Fig. 2.30(b), a flattening is observed near the peak SBS laser power, and the flattening becomes more pronounced at even higher pump power levels, shown in Fig. 2.30(c). Finally with the maximum available pump power, Fig. 2.30(d), the peak of the first SBS laser trace is dramatically flattened and there are also significant distortions in the pump.

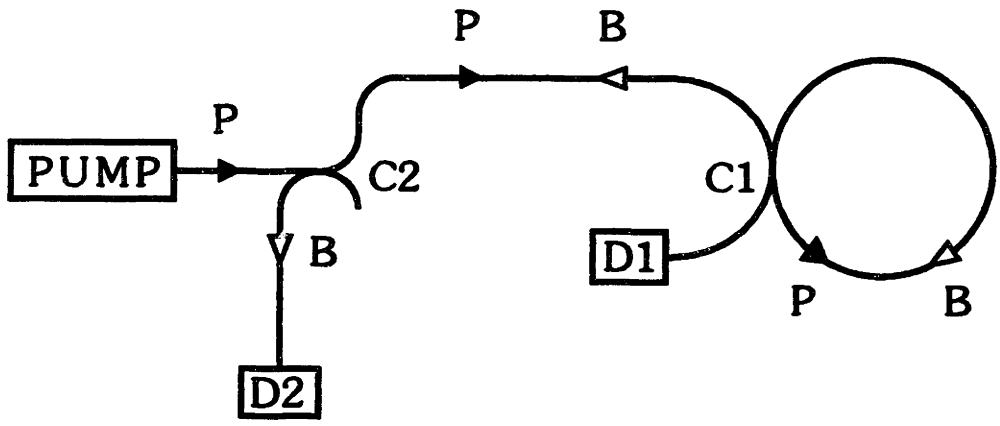

Figure 2.29 SBS laser setup for the demonstration of the effects of higher order SBS lasing.

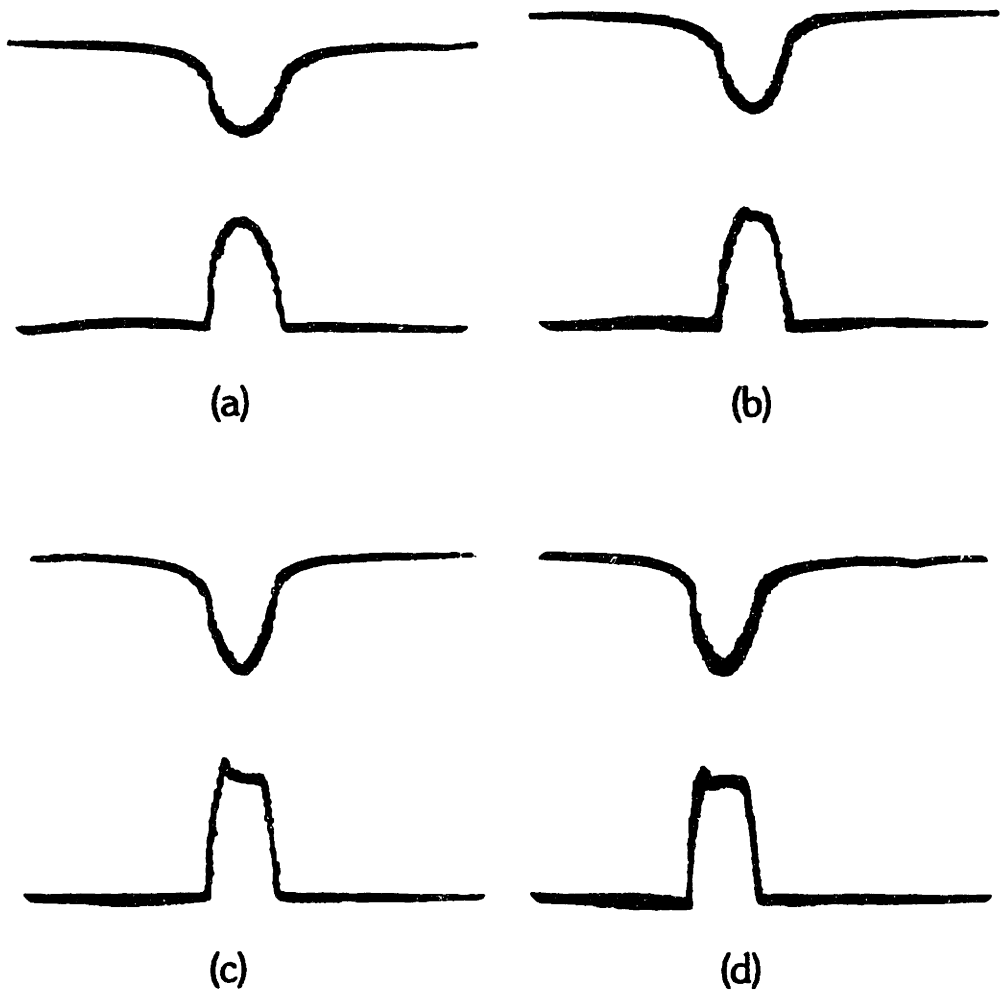

Figure 2.30 Scans of the pump over the fiber cavity resonance showing the pump (top) and the SBS (bottom) with the pump (a) below secondary SBS threshold, (b) slightly above secondary SBS threshold, (c) above secondary threshold, and (d) maximum pump power. Cavity B.

This behavior of the primary SBS laser can be also be demonstrated by plotting the primary SBS laser output power versus the pump power, as shown in Fig. 2.31. In the figure, the SBS laser power steadily increases as the pump power is increased above threshold, until the SBS power reached approximately 14 μW. At this point, secondary SBS lasing was observed,

and the primary SBS laser power remains approximately constant until the pump power reached 200 μW. At this point, the tertiary SBS laser was observed, and the primary SBS laser power once again began to increase with increasing pump power.

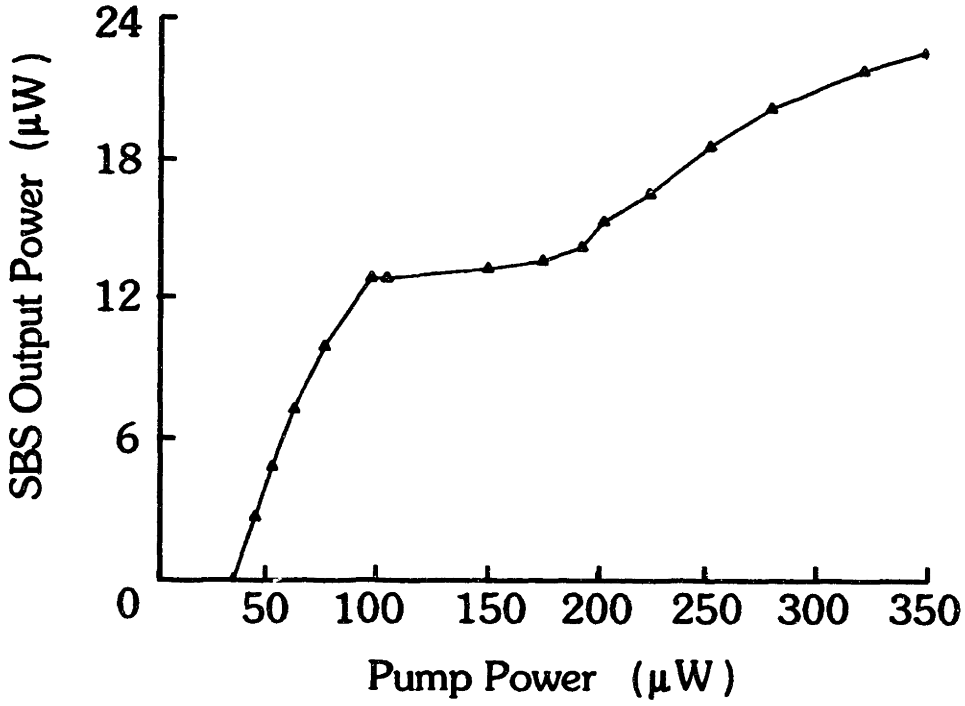

Figure 2.31 Primary SBS laser power as a function of increasing pump power. Cavity G.

This limiting of the primary SBS laser is caused by the generation of the secondary SBS laser. Recall that above the SBS threshold, the round trip gain is equal to the round trip loss in the cavity. However, the round trip gain for the secondary SBS laser is proportional to the power of the primary SBS laser. Thus, the threshold for the secondary SBS laser limits the amount of power that can be efficiently generated in the primary SBS laser.

2.5.2 Spontaneous Modelocking

The SBS laser discussed here has several modes under the SBS gain curve and, due to the interaction between the SBS laser and its gain medium, is able to, on occasion, spontaneously modelock.[37]

Figure 2.33 shows the beat between two independent SBS lasers, using the setup shown in Fig. 2.32. In this case, the pump power for one of the SBS lasers, **P1**, is increased so that it is very close to the threshold for secondary SBS, allowing the **B1** SBS laser to partially spontaneously modelock. Meanwhile, the second SBS laser, **B2**, continued to lase in only a single longitudinal mode. As seen in Fig. 2.33, seven beat notes, spaced by approximately 10 MHz, can be observed above the noise floor of the spectrum analyzer, which corresponds to seven longitudinal modes of the modelocked laser (FSR = 10 MHz).

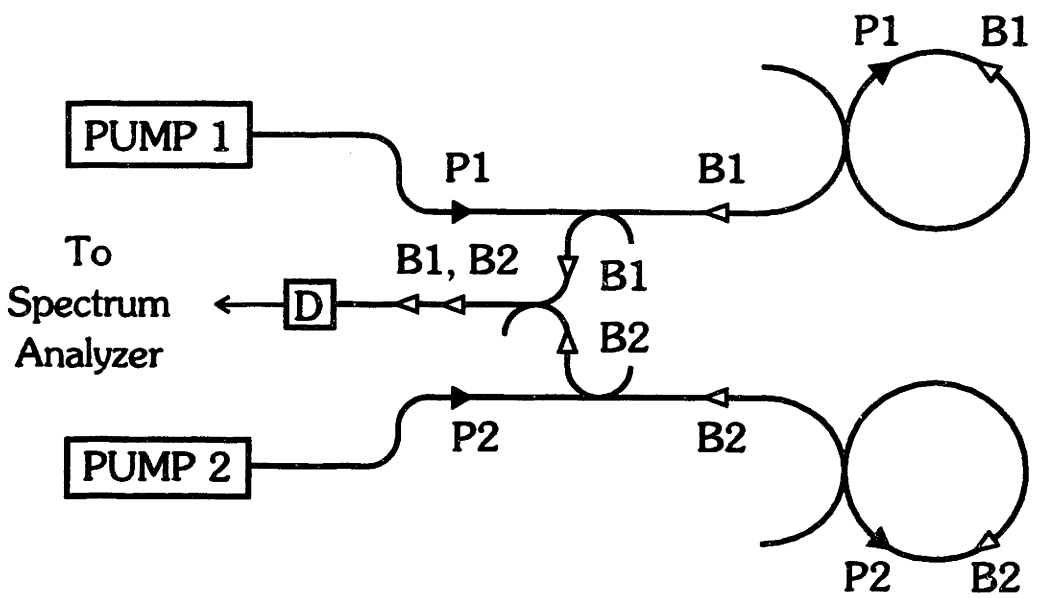

Figure 2.32 Setup for measuring independent SBS laser beatnote demonstrating partial spontaneous modelocking.

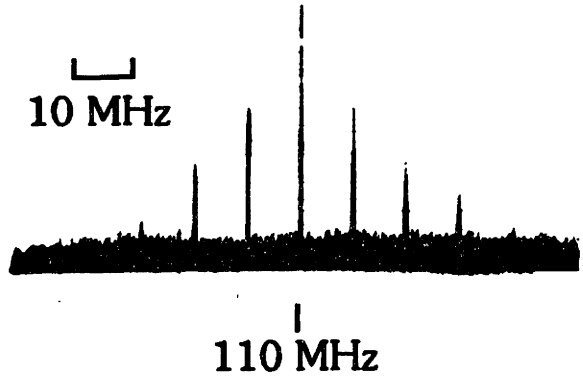

Figure 2.33 Spectrum of the beat between a single frequency SBS laser and a partially, spontaneously modelocked SBS laser. Cavities B and C.

While spontaneous modelocking can be a desirable characteristic in some laser systems, the relatively narrow linewidth of the SBS gain medium limits the length of the pulses that can be generated to only about 10 ns for a pump laser at 633 nm. Clearly for stable, single mode operation of the SBS laser, spontaneous modelocking must be prevented. One method of preventing spontaneous modelocking is to choose the cavity FSR to be greater than the half-width of the SBS gain.

2.5.3 Backscattering

The backscattering inside the fiber cavity can be from "hot spots", i.e., defects in the fiber or coupler that cause weak reflections, or from distributed Rayleigh scattering from the entire fiber. Since the total intensity backscattering is a function of the coherent addition of all the individual scatters, the amount of backscattering observed can vary dramatically as a function of the environment of the cavity.

In solitary SBS lasers, the main effect of these backscatter variations is to change the internal cavity loss, and hence the finesse and the SBS

threshold. To illustrate this, again we consider the simple SBS laser setup, shown in Fig. 2.34, where the fiber cavity is tuned by applying a triangle wave to a PZT mounted on the cavity.

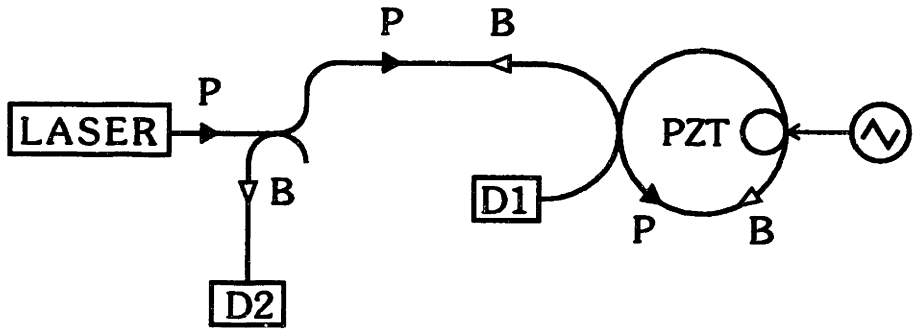

Figure 2.34 Simple SBS laser setup with scanned fiber cavity.

Figure 2.35 shows the pump laser, as measured by detector **D1**, in the top trace, and the resulting SBS laser , as measured by **D2**, in the lower trace, as the cavity is scanned through several FSRs. As seen in the figure, the amount of SBS generated varies widely from mode-to-mode of the cavity. In this case, the pump laser is at 140% of the SBS threshold for the mode on the right, but still generates very little, if any, SBS in the center mode.

By quickly reducing the pump power, the intensity backscattering for the three modes in Fig. 2.35 can also be examined. Figure 2.36 shows the reduced pump in the top trace, using an expanded scale, and the intensity backscattering in the bottom trace, also using an expanded scale. Note that the mode in Fig. 2.35 with the least SBS (center mode), i.e., the highest threshold, also has the highest backscattering in Fig. 2.36, i.e., the highest loss or lowest finesse. Similarly, the mode with the least backscattering (right) also has the smallest threshold.

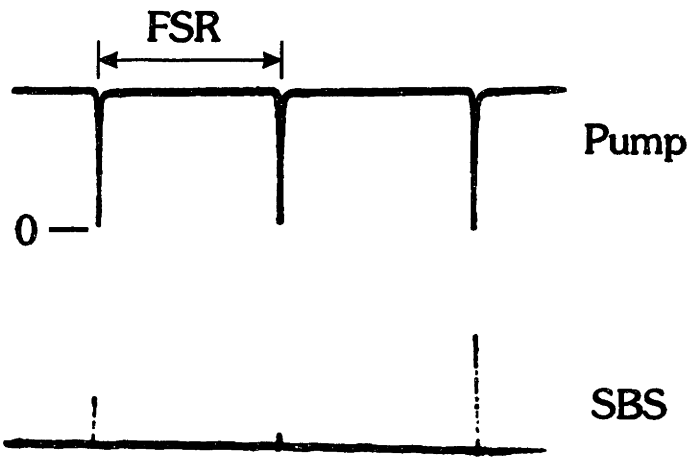

Figure 2.35 Fiber cavity scans showing the pump (top) and the SBS (bottom) for several longitudinal modes of the cavity. Cavity D.

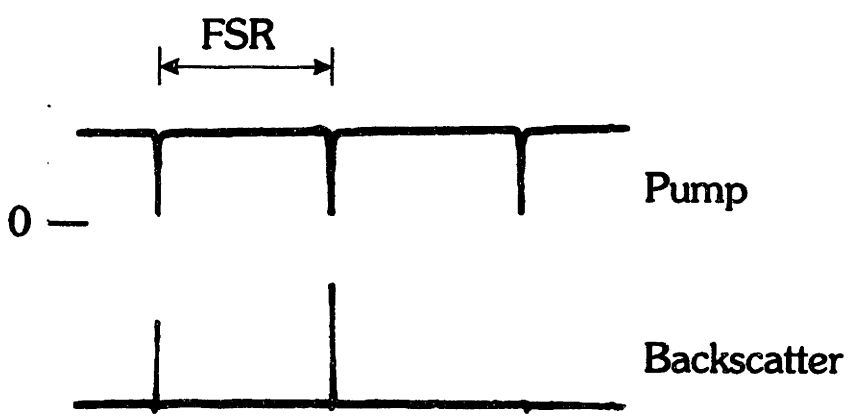

Figure 2.36 Fiber cavity scans showing the pump (top) and the intensity backscattering (bottom) for several longitudinal modes of the cavity. Cavity D.

The amount of internal backscattering in a fiber cavity is a complex function of the pump frequency and external perturbations to the fiber and coupler. For a given cavity, there is relatively little that can be done to reduce or even reliably perturb the amount of backscattering. However, it

is possible to increase the average amount of backscatter by perturbing the fiber, for example, tight bends in the fiber, or glues and adhesives on the fiber, can significantly increase the amount of backscattering. In general, since a component of the backscattering is due to Rayleigh scattering, which is proportional to λ^{-4}, moving to longer wavelengths, for example 1.3 or 1.5 μm, results in significantly lower backscattering than at 632 nm.

Chapter Three

Common Cavity SBS Fiber Lasers

Lasers generated in the same optical cavity, i.e., common cavity lasers, have a number of interesting properties. Most importantly, the lasers have very little relative frequency jitter, which makes them useful in many applications. The tunability and directionality of the SBS gain medium allows common cavity SBS lasers to be generated with great flexibility in the choice of frequency separation and configuration.

In this chapter, the operation of common cavity SBS lasers will be demonstrated, their properties examined, and applications suggested, ranging from optical clocks to microwave sources. The experimental considerations are then described along with some of the problems with these lasers.

3.1 Generation of Common Cavity Fiber Ring Lasers

In this section, the use of SBS as the gain medium for common cavity ring lasers will be described, and common cavity SBS lasers will be demonstrated.

3.1.1 Common Cavity SBS Fiber Ring Lasers

The directionality, tunability, and low threshold of SBS lasers make them nearly ideal for generating common cavity, fiber ring lasers. Recall that for a solitary SBS fiber laser, the directionality of the SBS gain medium allows laser operation in a single, predictable direction of a fiber ring cavity. As seen in Fig. 3.1, with the pump in the CCW direction of the cavity, the SBS gain is only in the CW direction, and with sufficient gain, unidirectional lasing in the CW direction is observed, as demonstrated in Section 2.2.3.

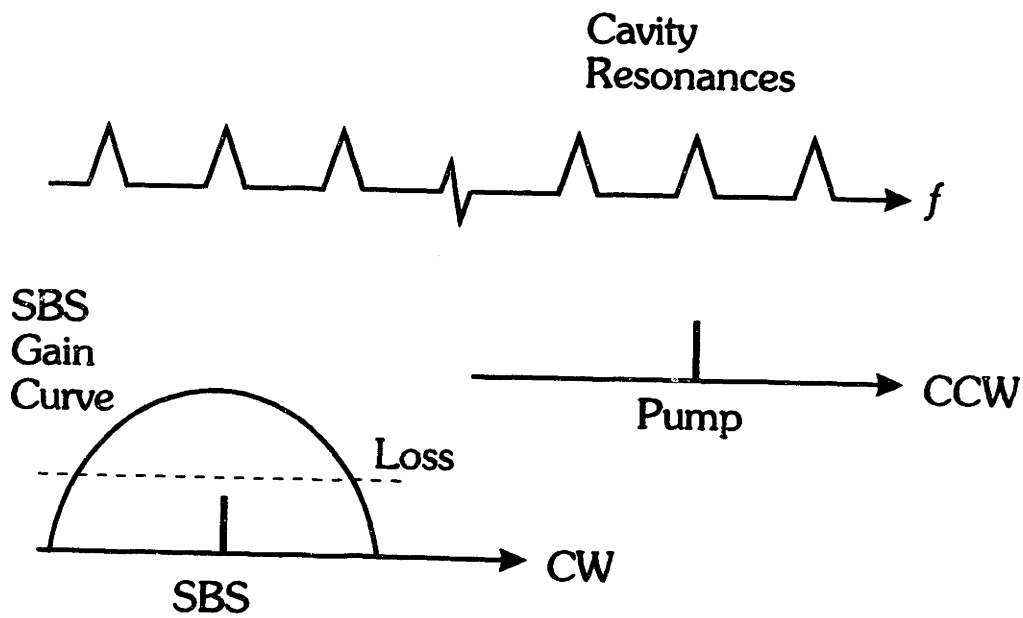

Figure 3.1 SBS gain curve and cavity resonances showing unidirectional SBS lasing.

By using an additional pump laser in the CW direction of the cavity, as shown in the setup in Fig. 3.2, it is possible to generate a second independent

SBS gain curve in the same cavity, illustrated in Fig. 3.3. The additional pump laser, **P2**, is in the CW direction and generates a second SBS gain curve, and a corresponding laser, **B2**, in the CCW direction of the cavity. Since the two pumps are separated by one FSR of the cavity, i.e., $\Delta q = 1$, their gain curves, and the resulting SBS lasers, are also separated by $\Delta q = 1$. The directionality of the SBS gain prevents gain competition between the counterpropagating SBS lasers, so simultaneous stable bidirectional lasing is observed.

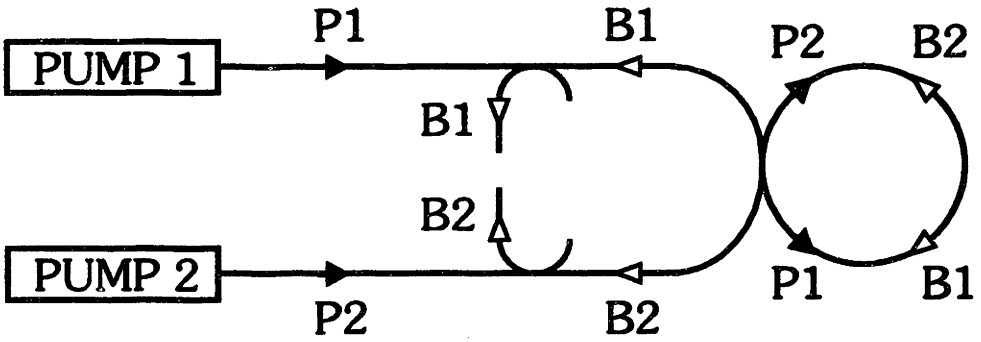

Figure 3.2 Two independent pump lasers are used to generate two SBS lasers in the same fiber ring cavity.

In addition, since the SBS gain curves are tied to the frequencies of their respective pump lasers, it is possible to generate SBS lasers with very large frequency separations by using widely tunable pump lasers, limited only by the tuning range of the pumps and the characteristics of the optical cavity.

Further, the pump lasers can also be used in the same direction of the cavity to generate copropagating SBS lasers. In this case, the pump laser separation should be large enough to prevent overlapping of the SBS gain curves.

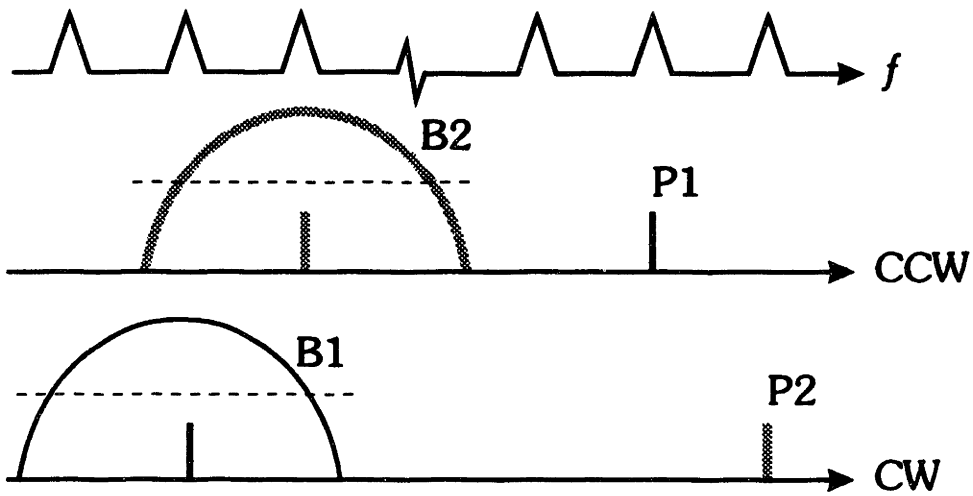

Figure 3.3 Two independent pumps, **P1** and **P2**, generate SBS gain for two simultaneous SBS lasers, **B1** and **B2**, which are separated by one cavity FSR.

3.1.2 Demonstration of Common Cavity SBS Fiber Ring Lasers

Figure 3.4 shows a common cavity SBS laser setup. Two independent, single frequency He-Ne pump lasers, in the directions labeled **P1** and **P2**, are coupled into the CCW and CW directions, respectively, of the same ring resonator, and their polarizations are adjusted to match the same eigenpolarization of the ring cavity. In this configuration, the fiber cavity is locked to **PUMP 1**, using the output of detector **D1** and an AC servo as previously described in Section 2.4.2. The second pump laser, **PUMP 2**, is locked to another longitudinal cavity resonance separated by approximately 92 MHz, or $\Delta q = 9$, using the output of detector **D2** and a second AC servo.

With both pumps, **P1** and **P2**, above SBS threshold, two SBS lasers, **B1** in the CW direction, and **B2** in the CCW direction, are generated. After leaving the cavity, a portion of each of the SBS lasers are combined using a directional coupler, and fall onto detector **D3**, whose output is observed on a

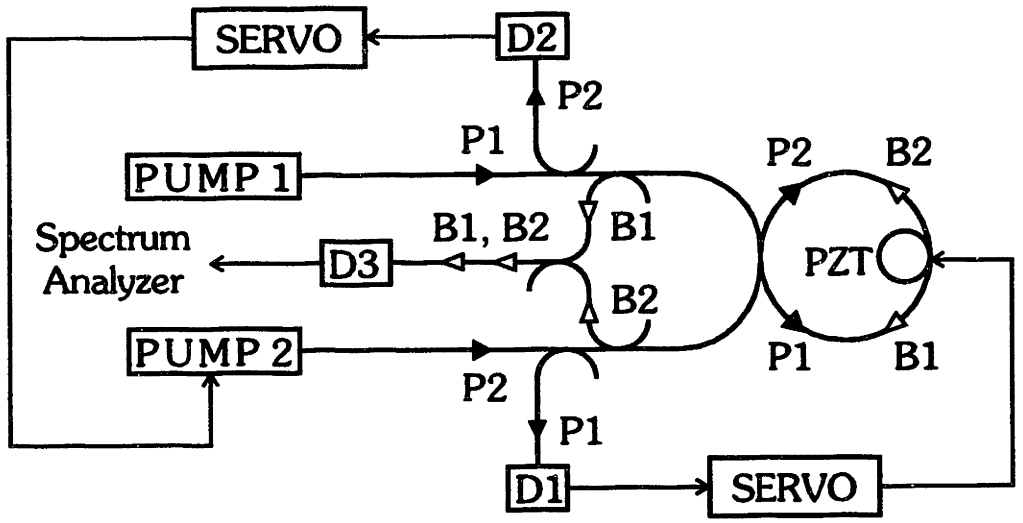

Figure 3.4 Independent pump lasers, in the directions labeled **P1** and **P2**, are coupled into opposite directions of the same ring cavity and generate two SBS lasers, **B1** and **B2**, respectively.

spectrum analyzer. Figure 3.5(a) shows the beat between the two SBS lasers, centered on 92 MHz, with a width of only 30 Hz. This linewidth, however, is approximately the same as the instrumental linewidth of the spectrum analyzer, i.e., 30 Hz, as shown in Fig. 3.6. Hence the actual linewidth of the beat between the common cavity SBS lasers could be much less than 30 Hz.

Since the SBS lasers are generated in the same cavity, fluctuations in the optical length of the cavity are, to a large degree, common to both lasers and thus, do not affect the width of the beat.

It is important to realize that this very narrow beat is not the result of using narrow pump lasers. The spectrum of the beat between the pump lasers, which were intentionally jittered, is shown in Fig. 3.5(b), demonstrating that the width of the pump laser beat, approximately 100 kHz, is over 3 orders of magnitude broader than the beat between the corresponding SBS lasers.

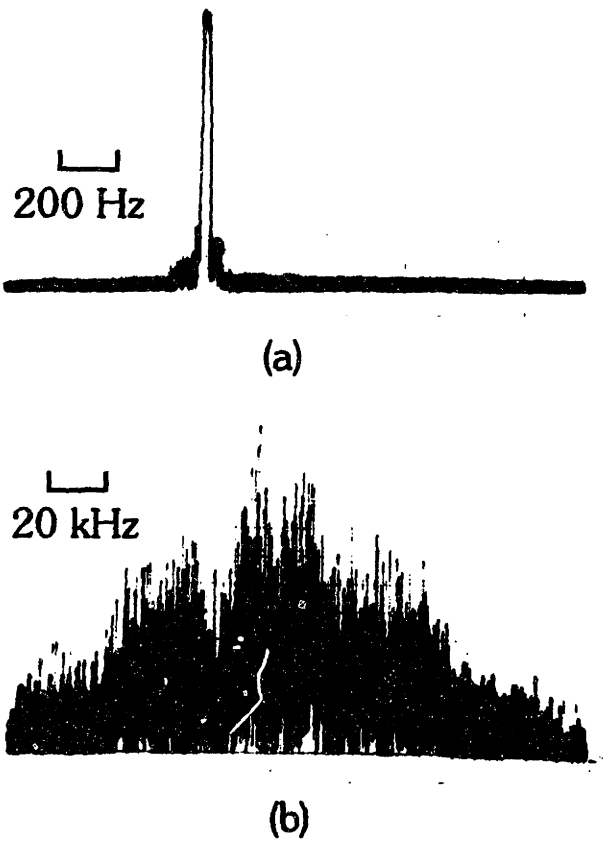

Figure 3.5 Spectrum analyzer scans of (a) the beat between independent SBS lasers and (b) their corresponding pump lasers. Both beats are centered on 92 MHz. Cavity B.

In order to measure the beat between two common cavity SBS lasers with greater precision, the beat was digitized and Fourier analyzed. The resulting spectrum, in Fig. 3.7, shows a 2 Hz wide beat note between the lasers, with the instrumental linewidth being less than 1 Hz, determined by the length of the sample.

This 2 Hz relative linewidth between the free-running SBS lasers was limited by slow drifts in the difference frequency between the SBS lasers caused by variations in the fiber cavity environment, which will be discussed

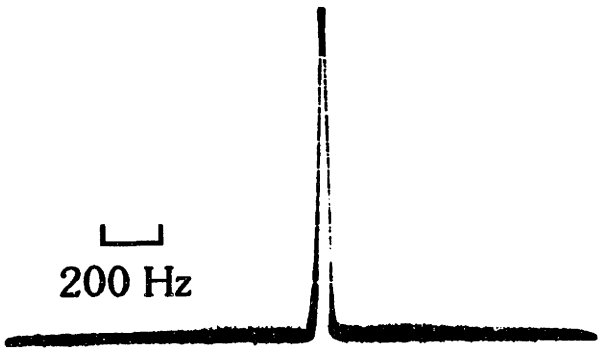

Figure 3.6 Spectrum analyzer scan of the output of a narrow linewidth oscillator demonstrating the 30 Hz instrumental linewidth of the analyzer.

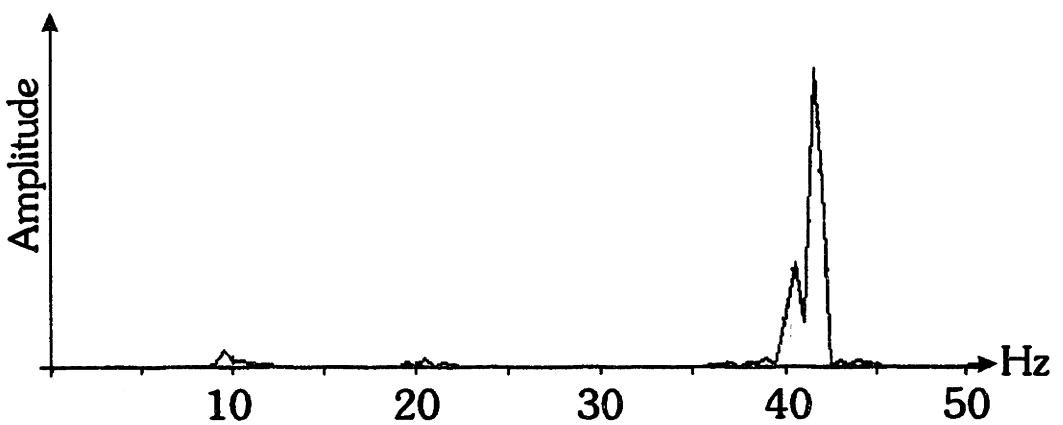

Figure 3.7 High resolution spectrum of a common cavity SBS laser beatnote at 1150 nm. Cavity G.

in Section 3.4. Thus, further narrowing of this linewidth would require either precise control of the fiber cavity environment, or the locking of the beat frequency to an external frequency reference.

3.1.3 Large Frequency Difference, Common Cavity SBS Lasers

Since the frequency of the SBS gain, and hence the SBS laser, is tied to the pump frequency, it is also possible to generate common cavity SBS lasers

with very large frequency separations, limited only by the tuning range of the pump lasers and the wavelength dependence of the cavity finesse. For example, in Fig. 3.8, the He-Ne pump lasers are locked to cavity resonances separated by 557 MHz, or $\Delta q \approx 55$. The linewidth of the resulting SBS beat, shown in Fig. 3.8, is again close to the 30 Hz instrumental linewidth of the spectrum analyzer, shown in Fig. 3.6. Thus, even with a large frequency difference between the SBS lasers, very little relative frequency jitter is observed.

In this case, the frequency separation between the common cavity SBS lasers, 557 MHz, was limited by the bandwidth of the available detection circuitry. However, even without this detector limitation, the limited tuning range of the He-Ne pump lasers would have only allowed frequency differences of up to approximately 1 GHz. Generation of SBS lasers with very large frequency differences requires the use of widely tunable pump lasers, such as dye lasers or semiconductor lasers.

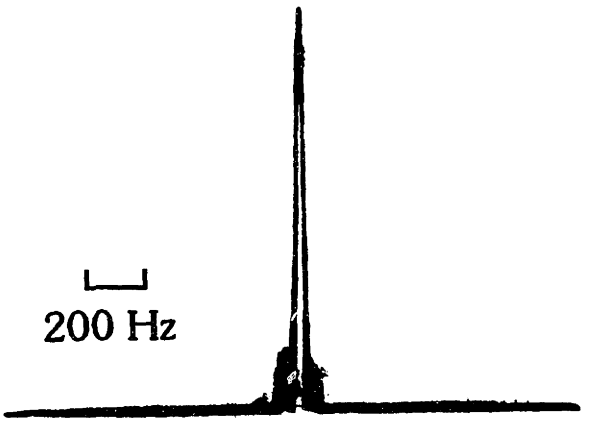

Figure 3.8 Spectrum analyzer scan of the beat between independent SBS lasers with a large frequency difference of 557 MHz. Cavity B.

Though we have only shown two SBS lasers in the same ring cavity, this common cavity setup can also accommodate additional SBS lasers simply by introducing additional pump lasers at other cavity resonance frequencies.

Further, the SBS lasers do not all have to be generated using the same cavity eigenpolarization. Since the polarization of the SBS laser is determined by the eigenpolarization of the cavity with the greatest gain, i.e., the pump eigenpolarization, by matching different the pump lasers into different cavity eigenpolarizations, the corresponding SBS lasers will be generated in different cavity eigenpolarizations.

3.1.4 Fundamental Limit on Laser Linewidth

The very narrow observed linewidth, less than 2 Hz, of the common cavity SBS laser beat in Fig. 3.7 is still much larger than the expected fundamental linewidth, $\Delta\nu_{st}$, as predicted by Schawlow-Townes.[38] This limit is due to spontaneous emission induced phase noise in the laser, and can be written as,

$$\Delta\nu_{st} \approx \frac{2\pi h\nu(\Delta\nu_c)^2}{P_L} \tag{3.1}$$

where h is Planck's constant, ν is the frequency of the laser, $\Delta\nu_c$ is the passive cavity linewidth, and P_L is the output power from the laser. Thus, with all other sources of frequency drift and noise removed, the laser linewidth would not decrease below this limit. Evaluating $\Delta\nu_{st}$ for a 100 μW laser output at 633 nm, using a cavity with a linewidth of 300 kHz, yields a laser linewidth of only 2×10^{-3} Hz. It should be noted, however, that thermally driven fluctuations in the optical length of the cavity could prevent the Schawlow-Townes limit from being achieved without the use of external servos.

3.2 Applications of Common Cavity SBS Lasers

There are a number of applications that require two laser beams with very little relative frequency jitter. Before discussing these applications, we will consider the various ways to generate such laser beams. One way is by frequency shifting one of the beams, for example using an electro-optic (E/O) or an acousto-optic (A/O) modulator. However, in order to generate large frequency differences, high speed modulators and high frequency drives are required. Another approach is the use of independent, tunable lasers, so that large frequency differences can be easily generated. However, correlating the frequency jitter in the two independent lasers is difficult, and may require wide bandwidth servo loops.

Since much of the frequency jitter of a typical laser is due to optical cavity fluctuations, lasers generated in the same optical cavity, i.e., common cavity lasers, can exhibit very little relative frequency jitter. However, using a homogeneously broadened gain medium, such as a typical dye or solid-state amplifier, lasing will be observed in only a single mode of the cavity. On the other hand, with an inhomogeneously broadened gain medium, such as a Doppler broadened gas, lasing in several adjacent longitudinal modes of a cavity can easily be achieved. If lasers are required in arbitrary longitudinal modes, however, an independent, tunable gain medium for each of the lasers is needed.

In contrast, SBS allows the generation of multiple, independent lasers in arbitrary longitudinal modes of the same ring cavity, with the frequency separation limited only by the tunability of the pump lasers and the wavelength dependence of the fiber cavity finesse. In the following sections, some applications of common cavity SBS lasers will be suggested.

3.2.1 SBS Fiber Ring Laser Gyroscope

A very important application of common cavity SBS lasers is as an optical inertial rotation sensor, i.e., "gyroscope", which will be discussed in detail in Chapter 4.

Briefly, in a ring laser gyroscope, two counterpropagating lasers are generated in the same longitudinal mode of a ring cavity, and the frequency difference between these lasers is proportional to the inertial rotation normal to the plane of the ring cavity. SBS is the only solid-state gain medium which can generate simultaneous, continuous, stable lasers in opposite directions of the same longitudinal mode of a ring cavity. This has led to our demonstration of the first fiber ring laser gyroscope, as discussed in Chapter 4.

3.2.2 Microwave and Millimeter-wave Sources

One application of common cavity SBS lasers is as a narrow linewidth, microwave or even millimeter-wave source. By combining the outputs of two common cavity SBS lasers with a large frequency separation, a narrow band, amplitude-modulated optical beam can be generated. This beam can then be detected and amplified for use as a microwave or even mm-wave source, as shown in Fig. 3.9, limited only by the bandwidth of the detection circuitry and the tuning range of the pump lasers. In addition, as previously shown in Fig. 3.8, the linewidth of the 557 MHz beat between the SBS lasers is very narrow, $\Delta\nu \ll 30$ Hz, even with a large frequency separation between the lasers.

Since the frequency of the SBS laser beatnote can only be tuned in increments of the cavity FSR, a frequency shifter with a tuning range equal to a cavity FSR, as seen in the figure, can be used to fine tune the beat frequency. Thus, to generate an arbitrary beat frequency, the difference frequency between the SBS lasers is first tuned to within a cavity FSR of the desired frequency by selecting the pump laser separation, and then the frequency shifter is used to tune the beat frequency to the desired frequency.

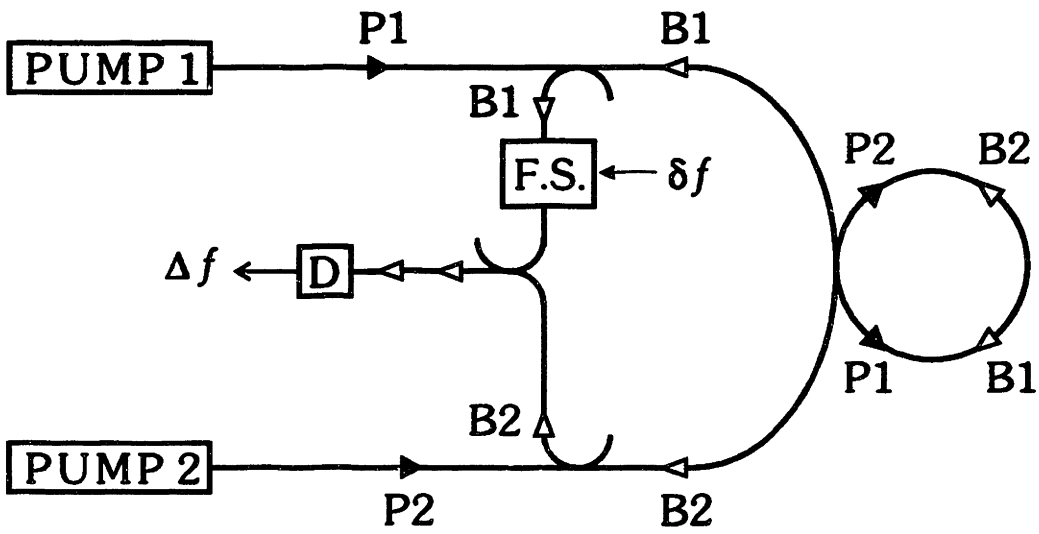

Figure 3.9 The use of SBS lasers as a narrow band, very high frequency source.

3.2.3 Two-Photon Spectroscopy

Another use of common cavity SBS lasers is for high resolution, two-photon spectroscopy based on the stimulated resonance Raman effect, as illustrated in Fig. 3.10. In stimulated Raman, the observed linewidth of a two-photon transition between closely spaced ground-state atomic levels 1 and 3, as shown in Fig. 3.10, is independent of the linewidth of both the 1–2, and 2–3 transitions. Thus, the linewidth of the two-photon transition can be extremely narrow, and the observed linewidth is usually transit time limited.[39]

However, if such a transition is excited using lasers **B1** and **B2**, any uncorrelated jitter between the lasers will broaden the observed linewidth. Thus, for very high resolution spectroscopy, very narrow linewidth lasers are needed. By using tunable pumps, SBS lasers with a large frequency separation and correlated frequency jitter can be generated at the required frequencies for the stimulated resonance Raman effect.

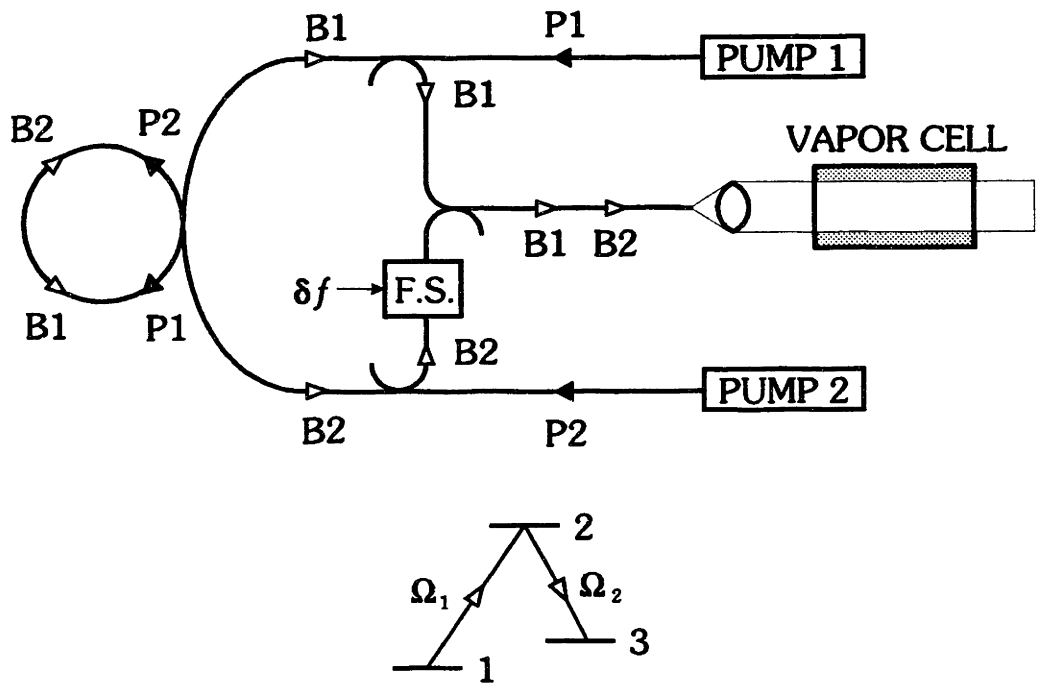

Figure 3.10 Example of the use of SBS lasers for two-photon spectroscopy using stimulated Raman effect.

3.2.4 Simple Atomic Clock

One practical application of two-photon spectroscopy using common cavity SBS lasers is a very simple atomic clock. Here, the frequency difference between the SBS lasers is locked to a stimulated Raman transition between the two closely spaced levels in the ground state, for example hyperfine levels in cesium, and this frequency difference becomes the frequency output of the clock.

Figure 3.11 shows a simple atomic clock setup, using a Raman transition in an atomic vapor cell with a buffer gas. The pump lasers are locked to different longitudinal modes with approximately the correct spacing for the desired stimulated Raman transition. The fiber cavity is then tuned, using **SERVO 1**, to bring SBS laser **B2**, on resonance with one of the atomic transitions, in this case the 2–3 transition. A second servo, **SERVO 2**, is

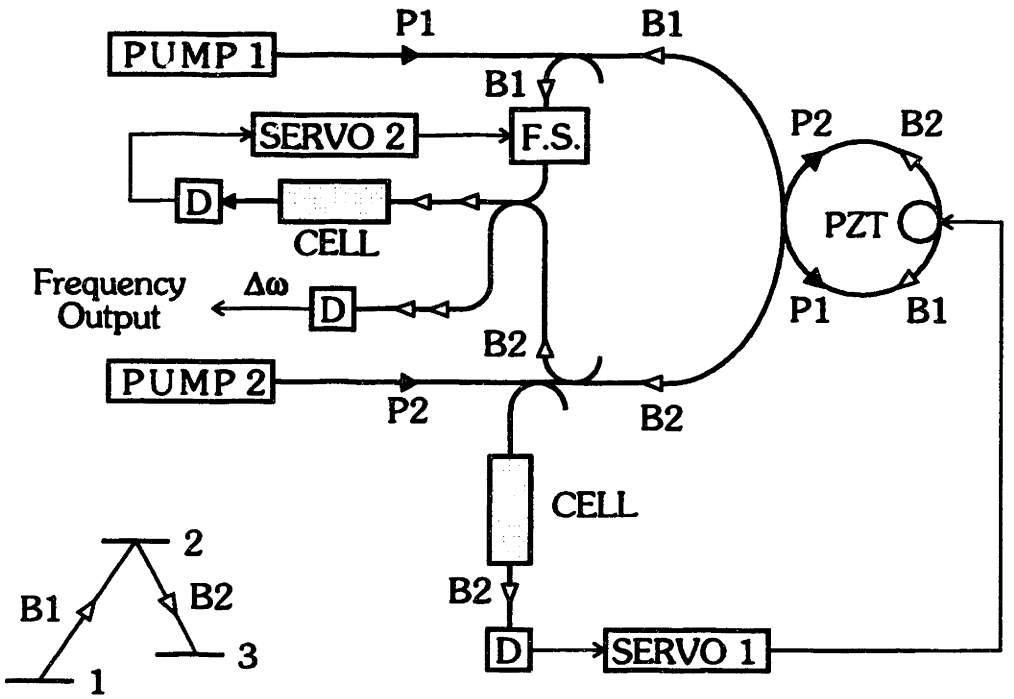

Figure 3.11 A simple optical clock using common cavity SBS lasers.

then used to fine tune the difference frequency between the SBS lasers, using a frequency shifter, **F.S.**, to exactly match the splitting between levels 1 and 3. Thus, the output of the clock is the difference frequency between the SBS lasers which can easily be detected, as shown in the figure.

The buffer gas is used to increase the effective transit time, thus reducing the observed linewidths. For example, using sodium vapor with helium as the buffer gas, a 1 kHz linewidth was observed in our laboratory. Otherwise, a Ramsey separated field excitation can be used in an atomic beam.[39]

3.2.5 Magnetic Field Sensor

Another application of two-photon spectroscopy and common cavity SBS fiber lasers is for precision magnetic field measurements. In this case, the Zeeman splitting of the lower levels of the stimulated Raman transition is used to measure the magnetic field, using an apparatus similar to that in

Fig. 3.11. Thus, the magnetic field strength is measured as a frequency change of the output frequency, $\Delta\omega$. This technique may have applications for high precision measurements of both very strong, and very weak magnetic fields.

3.2.6 Laser Doppler Velocimetry

Another simple application of common cavity SBS lasers is for very high flow rate laser Doppler velocimetry (LDV), as illustrated in Fig. 3.12. In LDV, the difference frequency between a reference beam and the Doppler-shifted scattering from seed particles in a flow is used to measure the velocity of the flow. By introducing a frequency difference between the reference and the scattered beams, the direction of the flow can also be determined. In such a scheme, however, the maximum velocity that can be unambiguously measured is limited by the frequency shift between the reference and the scattered beams, thus for very high flow rates, very large frequency differences are needed. Therefore, by using common cavity SBS lasers, very large frequency differences can be easily generated between the beams.

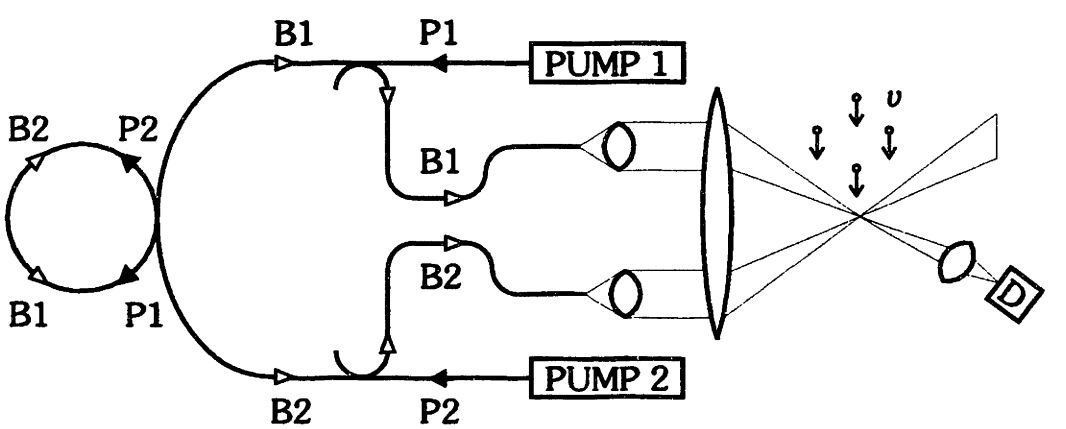

Figure 3.12 The use of common cavity SBS lasers for high rate laser Doppler velocimetry.

3.2.7 Absolute Interferometric Position Sensing

In many interferometric position sensing devices, an amplitude modulated optical beam is used to measure the distance to a target. Here, the amplitude modulated beam is generated by interfering the outputs of a pair of SBS lasers, as shown in Fig. 3.13. This beam is then reflected from a target, detected, and the phase of the modulation on the reflected light is measured using a phase sensitive detector (PSD). This phase, ϕ, is the phase, at the modulation frequency, of the round trip distance to the target. Thus, with only a single modulation frequency, the measured distance, d, is ambiguous, i.e., $d = (\phi/2\pi \pm n)\,\lambda$, and to resolve this ambiguity, multiple modulation frequencies can be used. In addition, the resolution of the distance measurement increases with the modulation frequency for a given signal-to-noise level.

It should be noted that the use of an amplitude modulated optical beam has several advantages over directly using RF radiation. The optical beam, due to its much shorter wavelength, can be collimated and focused much more easily than the RF beam and can effectively be used with target sizes much smaller than the RF wavelength.

As mentioned in Section 3.2.2, common cavity SBS lasers using tunable pumps allow the generation of several lasers at different frequencies in the same cavity that can be combined to generate an optical beam which is amplitude modulated at a particular frequency, or at several frequencies. In addition, using SBS, very high rate amplitude modulations can be generated for high resolution applications.

3.2.8 Direct Readout Sensors

We will now mention another application of SBS lasers in the area of sensors. There are a variety of perturbations that affect the optical path length of a fiber cavity, which in turn changes the resonant frequencies and FSR of

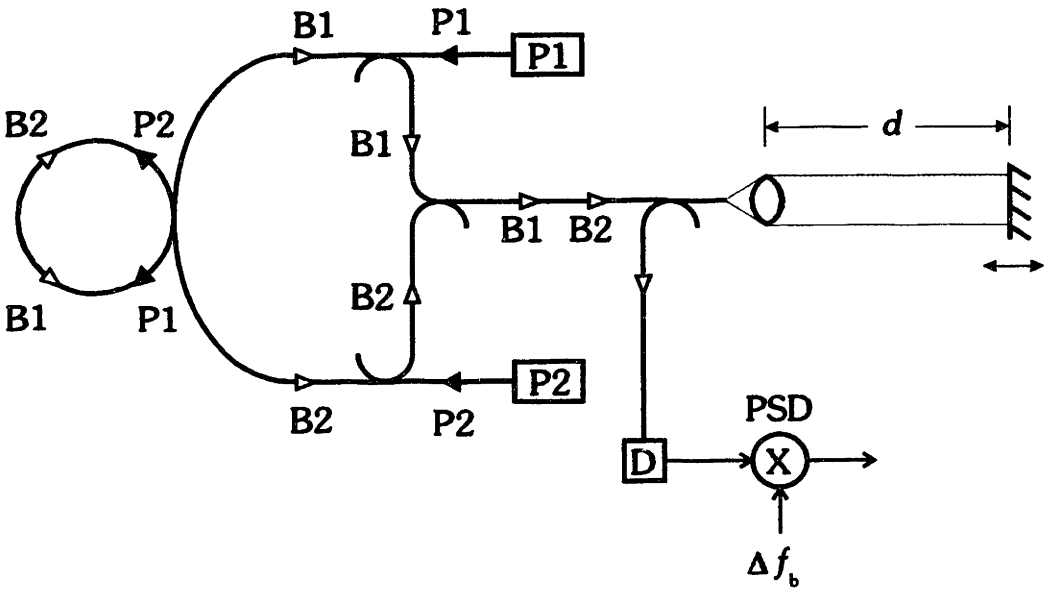

Figure 3.13 Application of common cavity SBS lasers to absolute interferometric position sensing.

the cavity. Thus, a passive fiber cavity can be used to sense any of these perturbations, for example, temperature. In addition, special coatings can be applied to the fiber to allow sensing of a wide range of phenomena, such as electric fields, magnetic fields and pH.

However, with a passive cavity, the change in the resonant frequency or FSR of the cavity must be measured externally. For example, servos, similar to those described in Section 2.4.2, could be used to lock lasers to adjacent cavity resonances, and the difference frequency between the lasers could then be used to measure changes in the cavity FSR. Thus, any errors in these servos will result in errors in the measurement of the perturbation.

On the other hand, the SBS lasers automatically lase at the center of their respective cavity resonances, so any change in the cavity FSR can be measured by simply measuring the change in the beat frequency between the lasers.[40] In addition, only a simple servo is required to lock the pumps to

their respective cavity resonances, and servo offsets will not easily affect the measured beat frequency.

3.3 Experimental Details

There were a number of considerations which had to be addressed in the design and implementation of the various experiments in this chapter. In this section, some of the more important details will be discussed.

3.3.1 Detailed Optical Layout

The optical setups used for this chapter were a hybrid of bulk-optic and fiber-optic components, as shown in Fig. 3.14. Each pump laser is isolated from external backscatter using an A/O, and is matched into the same polarization of the fiber cavity using bulk-optic waveplates. The resulting SBS lasers, **B1** and **B2**, are coupled out of the input arms using the unshifted beams from the A/O modulators which, with the A/Os optimized, are typically 10% of the shifted beams.

The use of the unshifted A/O beam has several advantages: it does not introduce any additional loss for the pump, the frequency of the SBS laser is not affected by the A/O frequency, and the coupling ratio is tunable by changing the alignment or drive to the A/O. However, there are also disadvantages: the SBS laser is not isolated from external optical feedback by the A/O, the unshifted A/O beam has poor spatial quality, and the exact coupling can vary with changes in room temperature. In this case, the unshifted beams were primarily used to maximize pump power into the cavity.

As shown in Fig. 3.14, to combine the SBS lasers, a directional fiber coupler was used, and bulk-optic waveplates were used to match the polarizations of the two SBS lasers for maximum beat amplitude. Though the poor spatial quality of the unshifted beam from the A/O significantly reduced the

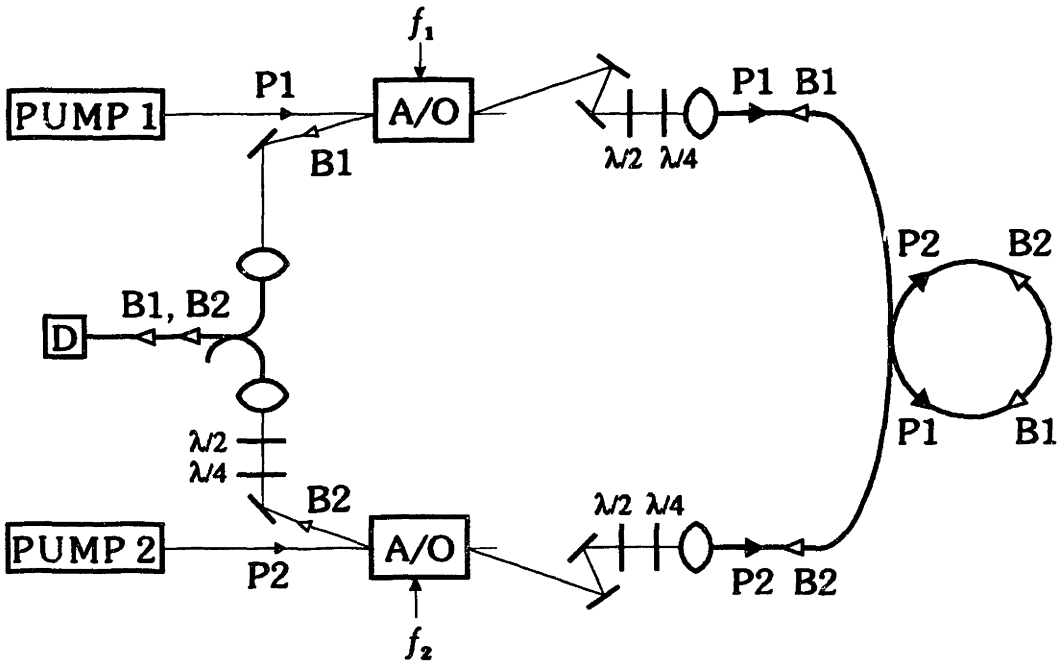

Figure 3.14 Detailed optical setup for independently pumped, common cavity SBS lasers.

amount of light that could be coupled into the fiber, typical coupling was only about 20%, the use of the fiber coupler allowed the decoupling of the alignment of the pump lasers into the cavity and the alignment of the SBS lasers. In addition, the fiber coupler guaranteed good spatial mode matching between the SBS lasers, despite the poor optical quality of the unshifted A/O beams.

While the A/Os isolated the pump lasers from backscattering, they did not protect the lasers from optical feedback from each other. For example, as the pump lasers are being locked to their respective resonances, the difference frequency between the pumps needed to be continuously varied. So, when the difference frequency was exactly the same as the sum of the A/O shifts, the pumps fed into one another and erratic pump laser operation resulted. Thus, care must be taken when locking the pump lasers to their respective cavity resonances.

3.3.2 Pump Filtering

Unlike the solitary SBS lasers, no optical filtering was used for the common cavity SBS lasers for two reasons. First, although both of the pump lasers were combined by the fiber directional coupler along with the SBS lasers, the beat between the pump lasers was much broader than the beat between the SBS lasers. Thus, when using a high resolution frequency scale on the electronic spectrum analyzer, the pump lasers' beat made a negligible contribution to the background noise. Second, since most of the cavities had good resonance depths, typically around 90%, only a small amount of the pump was reflected from the cavity.

3.3.3 AC Servo Modulation

With multiple pump lasers, the choice of modulations becomes more complicated. If the cavity is modulated, the same modulation frequency is applied to both pump lasers, and crosstalk between the pumps, caused by intensity backscattering from the cavities, can lead to servo instability. In the experiments of this chapter, a different modulation frequency was used for each pump, and the modulation frequencies were chosen to minimize interactions. As a rule of thumb, modulation frequencies, and their first harmonics, were separated by at least 5 kHz.

The separate modulation frequencies can be: applied directly to the pump lasers, used to modulate the frequency of the A/O drives, applied to PZT-mounted mirrors in the input arm of the cavity, or applied to PZTs on the fiber input arms to the cavity. However, if the modulation is applied between the SBS pick-off and the fiber cavity, the SBS beat will also be frequency modulated, which in most cases is undesirable.

3.4 Common Cavity SBS Laser Problems

There are a number of problems with common cavity SBS lasers, in addition to those already discussed for solitary SBS lasers. The most important additional problem is the change in the difference frequency between the lasers due to thermal effects, dispersion pulls, nonlinear optical effects and mode hopping. These errors are also very important in the operation of an optical gyroscope. Only thermal effects and mode hopping will be examined here, and the remaining errors will be discussed in detail in Section 4.5.

3.4.1 Thermal Effects

One cause of drift in the difference frequency is the thermal expansion of the cavity. With the lasers separated by several cavity FSRs, any change in temperature changes the optical length of the cavity, the cavity FSR and hence, the beat frequency. In a typical physical layout, the fractional change in the optical length of the cavity with temperature has been measured to be 2×10^{-5}. Thus, with a frequency separation of 500 MHz, the thermal tuning of the beat frequency is approximately 10 kHz/$^{\circ}$C.

For applications where a very stable beat frequency is required, several methods are available to stabilize this beat frequency including the use of an atomic resonances, as discussed in Section 3.2.4, locking the difference frequency to an external frequency reference, stabilizing the pump laser frequency, or stabilizing the temperature of the fiber cavity.

3.4.2 Longitudinal Mode Hopping

Another, more dramatic change in beat frequency can be caused by longitudinal mode hopping. If the center of the SBS gain curve is in the middle of two cavity resonances, the gains for the two resonances will almost be exactly the same. Thus, very small changes in cavity loss, for example due to

changes in backscattering, can cause the laser to change longitudinal modes, i.e., mode hop.

During this mode hopping, solitary SBS lasers will exhibit an increased amplitude noise. However in common cavity SBS lasers, when one of the SBS lasers mode hops, a large change in the difference frequency is observed. In order to avoid such mode hopping, the center of the SBS gain curve can be thermally tuned to the center of a cavity resonance.

Chapter Four

SBS Fiber Ring Laser Gyroscope

Inertial rotation sensors, i.e., gyroscopes, play an important role in modern inertial navigation systems for use in airplanes, spacecraft, submarines, and even automobiles. For many years, mechanical gyroscopes were used in such navigation systems, however, in the last few years, they have been replaced, in some applications, by optical gyroscopes based on bulk-optic ring lasers. The bulk-optic ring laser gyroscopes are attractive because of their better reliability, lower maintenance, and strapped-down operation. More recently, fiber interferometer gyroscopes have been developed which have the additional benefits of reduced mass, low cost, very high shock resistance, and long lifetimes.

In this chapter, we will demonstrate the first solid-state ring laser gyroscope, based on SBS in optical fibers. This is the fiber-optic analog of the bulk-optic ring laser gyroscope. The Sagnac effect, which is the basis for all optical gyroscopes will be discussed first, along with several methods for measuring this effect. An SBS fiber ring laser gyroscope will then be demonstrated, and techniques for eliminating important error sources, for example lock-in and the optical Kerr effect, will be examined. Two optical techniques for eliminating the effects of lock-in are then demonstrated.

4.1 Optical Gyroscope Theory

All optical gyroscopes are based on the Sagnac effect which states that there is an optical path length difference for light traveling along opposite directions around a rotating frame.[41] In this section, a simple physical model for the Sagnac effect in a vacuum will be presented, along with a derivation for the Sagnac effect in a dielectric medium. Methods for measuring the Sagnac effect will then be presented, including the use of interferometers, passive ring cavities, and ring lasers.

4.1.1 A Physical Model for the Sagnac Effect

The Sagnac effect in a vacuum can be explained by considering the simple physical model of a circular optical path around the edge of a disk. With the disk initially at rest, shown in Fig. 4.1, two photons, one in CW direction and the other in the CCW direction, are introduced into the optical path at the position labeled **S**. They will propagate around the ring and return to their starting position in times, t_{cw} and t_{ccw}, for the CW and CCW photons respectively, given by,

$$t_{cw} = \frac{L_{cw}}{c_{cw}} \tag{4.1}$$

and,

$$t_{ccw} = \frac{L_{ccw}}{c_{ccw}} \tag{4.2}$$

where $L = L_{cw} = L_{ccw} = 2\pi R$ is the circumference of the disk, and $c_{cw} = c_{ccw} = c_o$ is the speed of light in a vacuum.

If the disk is rotating about an axis perpendicular to the plane of the disk, as shown in Fig. 4.2, the starting point **S** will move as the photons propagate around the ring, lengthening the effective perimeter of the ring for the photon in the CW direction and shortening the effective perimeter for the photon in the CCW direction.

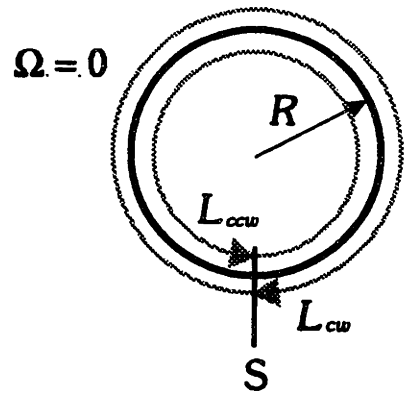

Figure 4.1 Circular optical path with counterpropagating photons at rest.

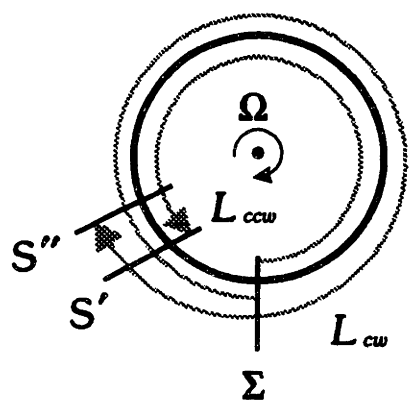

Figure 4.2 Circular optical path experiencing rotation in the plane of the ring.

Thus, the time it takes the photon in the CCW direction to return to the starting position, which has moved to the position marked S′, is given by,

$$t_{ccw} = \frac{L + \Omega R t_{ccw}}{c_o} = \frac{L}{c_o} \cdot \left(1 - \frac{\Omega R}{c_o}\right) \tag{4.3}$$

where Ω is the angular velocity of the disk, and ΩR is the tangential velocity of the edge of the disk. Similarly, the time it takes the photon in the CW direction to return to the starting point, which is this case will have moved

to position S″, is given by,

$$t_{cw} = \frac{L - \Omega R t_{cw}}{c_o} = \frac{L}{c_o} \cdot \left(1 + \frac{\Omega R}{c_o}\right) \tag{4.4}$$

Thus, the difference in the round trip propagation time in the CW and CCW directions is given by,

$$\Delta q = t_{cw} - t_{ccw} = \frac{L}{c_o}\left(\frac{2\Omega R}{c_o}\right) = \frac{4\pi R^2 \Omega}{c_o^2} = \frac{4A}{c_o^2}\Omega \tag{4.5}$$

where $A = \pi R^2$ is the area enclosed by the ring. This will generate an optical path length difference, ΔL, given by,

$$\Delta L = c_o \Delta t = \frac{4A}{c_o}\Omega \tag{4.6}$$

This simple expression for the inertial rotation induced path length difference in a vacuum is identical to that obtained from the exact calculation.[42,43]

4.1.2 Sagnac Effect in a Medium

To find an expression for the Sagnac effect in a medium, relativistic corrections to the addition of velocities must be incorporated into the previous calculation for the Sagnac effect in a vacuum.

The correct expression for c_{cw} in a medium is given by,

$$c_{cw} = \frac{(c_o/n) + R\Omega}{1 + \frac{(c_o/n)R\Omega}{c_o^2}} = \frac{c_o/n + R\Omega}{1 + R\Omega/nc_o} = \frac{c_o}{n} + R\Omega(1 - 1/n^2) + \cdots \tag{4.7}$$

and similarly,

$$c_{ccw} = \frac{(c_o/n) - R\Omega}{1 - \frac{(c_o/n)R\Omega}{c_o}} = \frac{c_o/n - R\Omega}{1 - R\Omega/nc_o} = \frac{c_o}{n} - R\Omega(1 - 1/n^2) + \cdots \tag{4.8}$$

Thus, in a medium, the round trip propagation time difference in Eq. (4.5) becomes,

$$\Delta t_m = 2\pi R \left(\frac{2R\Omega - (c_{cw} - c_{ccw})}{c_{cw} c_{ccw}} \right) \tag{4.9}$$

and using Eq. (4.7) and (4.8) gives,

$$\begin{aligned} \Delta t_m &= 2\pi R \, \frac{2R\Omega - 2R\Omega(1 - 1/n^2)}{c_o^2/n^2} \\ &= 2\pi R \, \frac{2R\Omega}{c_o^2} \\ &= \frac{4A}{c_o^2}\Omega \end{aligned} \tag{4.10}$$

Hence, in a medium the expression for ΔL becomes,

$$\Delta L = c_o \Delta t = \frac{4A}{c_o}\Omega \tag{4.11}$$

which is identical to the expression for ΔL in a vacuum, given by Eq. (4.6).

4.1.3 Magnitude of the Sagnac Effect

To appreciate the small size of ΔL, consider the length change of a circular path with an area of 10^{-2} m^2 on the north pole, experiencing only the rotation of the earth, i.e., $\Omega_e \approx 7 \times 10^{-5}$rad/s. For this rotation, the path length difference, ΔL, is only about 10^{-14} m, or about 10^{-4} of the width of a hydrogen atom. Further, for navigation grade performance the rotation sensitivity needs to be about $10^{-4}\,\Omega_e$, so the fractional change in optical path length, $\Delta L/L$, needs to be measured to a few parts in 10^{18}.

4.1.4 Fiber Interferometer Gyroscopes

Any area enclosing interferometer or resonator can be used to measure the Sagnac effect due to inertial rotation. In this section, we will discuss the use of an interferometer for the measurement of the Sagnac effect, and in the next section, a ring cavity will be discussed.

The interferometer method is based on the so called Sagnac interferometer and a fiber-optic implementation of this interferometer is shown in Fig. 4.3(a).[44] Light from the optical source, **S**, is coupled into both directions of a circular optical path, in this case formed using an optical fiber and a fiber-optic directional coupler **C1**. After traversing the path, the light from each direction is combined using coupler **C1**, and monitored using coupler **C2**. In the absence of inertial rotation, the light from each direction of the interferometer constructively interferes producing an intensity maximum, as measured by **D**. In the presence of an inertial rotation, the length difference, ΔL from Eq. (4.11), causes a phase difference between the beams given by,

$$\Delta\phi = \frac{2\pi}{\lambda_o}\Delta L = \frac{8\pi A}{\lambda_o c_o}\Omega \tag{4.12}$$

where λ_o is the free space wavelength of the source. As shown in Fig. 4.3(b), this phase shift causes a displacement along the interference fringe formed by light from the counterpropagating directions of the ring.

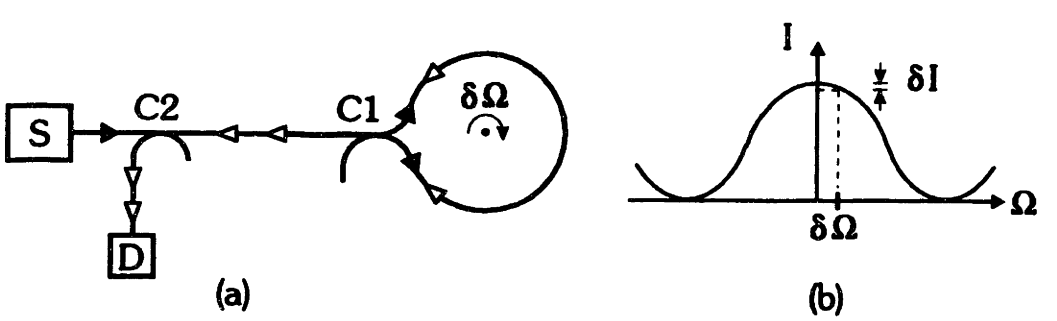

Figure 4.3 A fiber-optic implementation of a Sagnac interferometer, (a), and its intensity output, (b), as measured by **D**, as a function of rotation rate.

The measurement of earth's rotation using a Sagnac interferometer was first demonstrated by Michelson and Gale in 1925 using a bulk-optic interferometer sealed inside evacuated tubes with an enclosed area of 2×10^5 square meters to generate a quarter of a fringe of phase shift for Ω_e.[45]

Of course for a practical interferometer, such a large size is not feasible. For a more reasonable size, 10^{-2} m^2, the phase shift due to Ω_e is just $\Delta\phi \approx 10^{-7}$ radians, thus for navigation grade performance, i.e., errors of less than $10^{-4}\,\Omega_e$, the fringe shift must be measured to approximately 10^{-11} radians.

Instead of measuring such a small phase shift, the Sagnac effect can be enhanced by allowing the light to propagate around the ring many times using a multiple fiber turns. The resulting phase shift is then simply proportional to the number of times, N, that the light propagates around the ring, i.e.,

$$\Delta\phi_n = N\frac{8\pi A}{\lambda_o c_o}\Omega \tag{4.13}$$

The low loss of optical fibers allow path lengths of more than 10^4 m, thus for a realistic ring size, the enhancement of the phase shift can be several thousand. For example, for a 10^3 m long interferometer wrapped around a cylinder of area 10^{-2} m^2, the phase shift is increased by a factor of approximately 3000, so the phase shift due to earth rate becomes $\Delta\phi \approx 3 \times 10^{-4}$ radians.

While this is an improvement, nevertheless measurement of such small phase shifts requires the use of precision techniques. Further, error sources must be carefully controlled to achieve navigation grade performance. Fiber interferometer gyroscopes are under serious development in several laboratories and are beginning to make inroads in some specialty applications.[46]

4.1.5 Fiber Ring Cavity Gyroscopes

The Sagnac effect can also be measured using a fiber ring cavity, as illustrated in Fig. 4.4.[17,18] In this case, the path length difference, ΔL, causes a shift in the frequencies of the longitudinal modes of the cavity in the CW and CCW directions. Since a phase shift of 2π corresponds to a change in resonance frequency of a cavity FSR, the relative frequency shift due to the Sagnac effect, $\Delta\phi$ given by Eq. (4.12), can be written as,

$$\Delta f = \frac{c}{P}\frac{1}{2\pi}\Delta\phi = \frac{4A}{\lambda_o P}\Omega \tag{4.14}$$

where c is the speed of light in the medium and P is the perimeter of the cavity. Thus for a circular fiber cavity with an area of 10^{-2} m^2, a perimeter of 3.5×10^{-1} m, and a refractive index of 1.5, with an applied rotation rate of Ω_e, the frequency shift, Δf, is 8 Hz and, for comparison, the cavity FSR is 600 MHz. Thus for navigation grade performance, i.e., $10^{-4}\,\Omega_e$, Δf needs to be measured to 800 μHz.

In contrast to the fiber interferometer gyroscope, adding more turns to the resonator gyroscope does not increase the frequency shift, Δf, for a given rotation rate. As turns are added to the resonator, the phase shift, given by Eq. (4.13), increases with the number of turns. However, adding turns lengthens the cavity, and since the FSR is proportional to the inverse of cavity length, the frequency shift for an N-turn cavity is given by,

$$\Delta f_N = \frac{c}{N \cdot P}\frac{1}{2\pi}N \cdot \Delta\phi = \frac{4A}{\lambda_o P}\Omega \tag{4.15}$$

which is identical to the expression for a single-turn cavity in Eq. (4.14). However, if the N-turns can be added without increasing cavity losses, the cavity linewidth, FSR/F, will decrease with N thus, allowing a more accurate measurement of the frequency shifts due to the Sagnac effect.

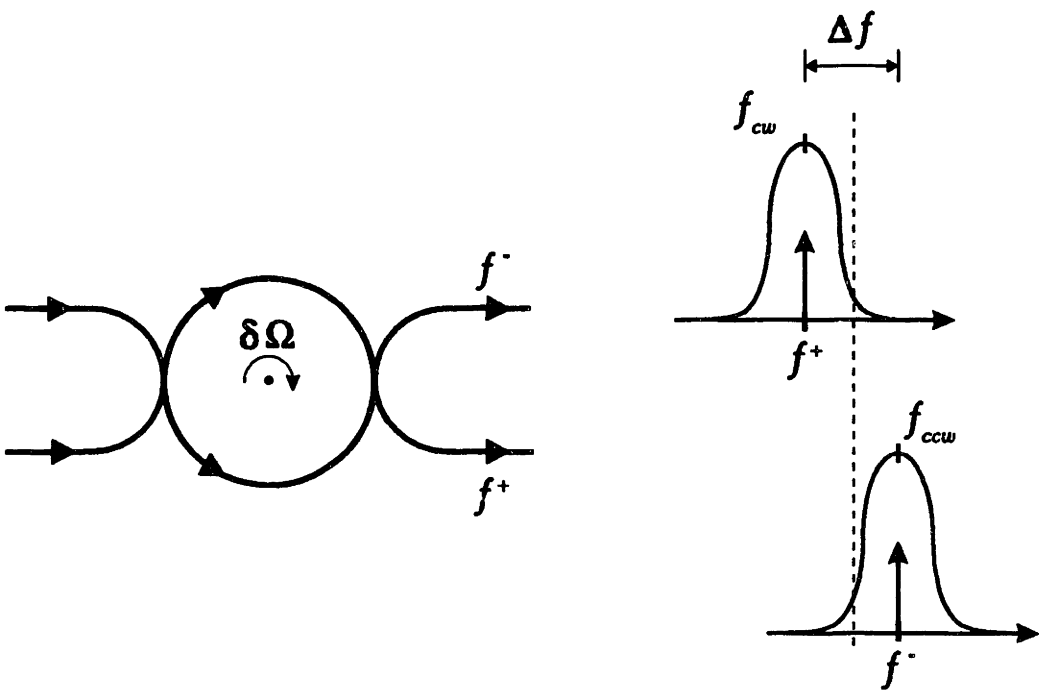

Figure 4.4 Measurement of inertial rotation using a ring resonator.

In addition, in applications where the size of the cavity is not constrained, for example, in geophysics applications, such a long fiber cavity need not be kept in a multi-turn ring, but can be used as a single large loop. For example, a fiber cavity with an area of 10^2 m^2, a perimeter of 3.5 m, a refractive index of 1.5, and an applied rotation rate of Ω_e, the frequency shift is 800 Hz.

Similar to the interferometer gyroscope, the frequency shift between the resonances along opposite directions of the ring cavity must be measured using precision modulation techniques. Due to the very small size of this frequency difference and the high precision with which it must be measured, such a measurement becomes challenging.[18]

4.1.6 The Ring Laser Gyroscope

Rather than externally measuring the frequency shift due to the Sagnac effect in a passive resonator, a ring laser gyroscope (RLG) performs this measurement automatically. In an RLG, two lasers are generated along opposite directions of the same cavity longitudinal mode. Since these lasers both oscillate at the centers of their respective cavity resonances, the frequency difference between the lasers is simply Δf. Thus, Δf can be measured by simply counting the beat frequency between the lasers.[47]

However, in order to create an RLG, simultaneous lasing along opposite directions of the same ring cavity must be achieved. If the two lasers use the same gain, such as in a conventional solid-state gain medium, mode competition between the counterpropagating lasers will lead to lasing in only one direction of the cavity at a time.

A Doppler broadened gaseous gain medium, on the other hand, is able to support simultaneous, bi-directional lasing. In Fig. 4.5(a), a Doppler broadened gaseous gain medium is shown schematically in a bulk-optic ring cavity. In this gain medium, as illustrated in the figure, the homogeneous linewidth of the lasing transition, Γ_H, is much smaller than the Doppler broadening induced by the thermal motion of the gain atoms, for example neon atoms. Thus, with the center of the cavity resonance below the frequency of the lasing transition, as shown in Fig. 4.5(b), the lasers will use atoms moving at some velocity v, along the direction opposite to that of the lasing field. In this way, in the atoms' reference frame, the laser field is Doppler-shifted to a higher frequency and is on resonance with the atom.

By plotting the distribution of atoms as a function of velocity, as shown in Fig. 4.5(c), we can show that, in this case, the CW laser will use atoms traveling at velocity $-v$, and the CCW laser will use atoms at velocity $+v$. Thus, even though both lasers are using the same cavity resonance and are

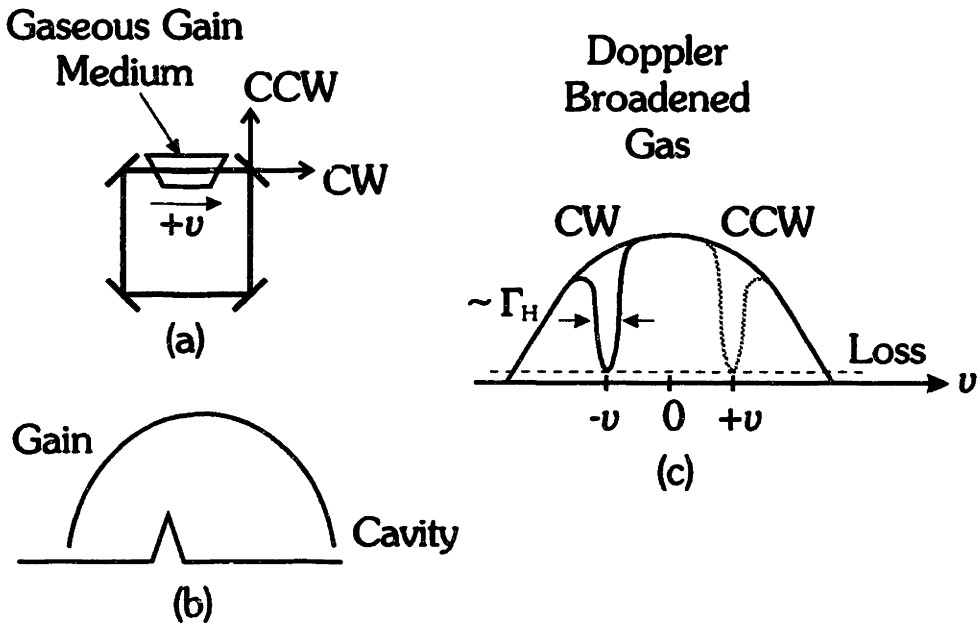

Figure 4.5 The gain curve and cavity resonances for a Doppler broadened gain medium in a ring resonator. The directionality of the Doppler shift allows counterpropagating lasers to use different velocity groups of atoms for gain, thus preventing gain competition.

at the same frequency, they are using different groups of atoms for gain and do not compete, so, simultaneous bi-directional lasing is observed.

The first RLG was demonstrated using a Doppler broadened, He-Ne gain medium and this type of RLG has been commercially successful and is now widely used in commercial and military aviation.[48,49,50] However, due to errors caused by dispersion, the cavity resonance in the RLG needs to be locked to the center of the gain curve. At this position, as illustrated in Fig. 4.6, both lasers have to use the same atomic velocity group, i.e., atoms with zero velocity component along the direction of laser propagation, and therefore, gain competition takes place between the counterpropagating lasers.

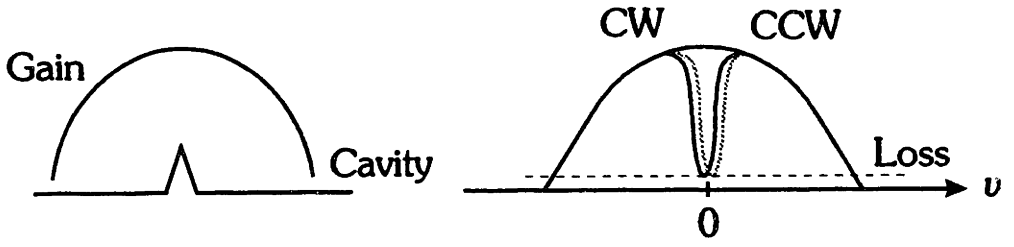

Figure 4.6 Gain competition between counterpropagating lasers when the cavity mode is at the center of the gain curve.

Obviously, for proper RLG operation such gain competition must be avoided. In the He-Ne RLG, this problem was solved by the fortuitous availability of two isotopes of neon with slightly displaced gain curves. Thus, by using a 1:1 mixture of these neon isotopes, the cavity resonance can be locked to the center of this composite gain curve, but still be far away from the center of either of the atomic resonances.[49]

4.2 SBS Fiber Ring Laser Gyroscope

As discussed in Section 3.1.2, the directionality of the SBS gain medium prevents gain competition between counterpropagating lasers and, as shown in Fig. 4.7, allows the generation of simultaneous, stable lasers in counterpropagating directions of the same longitudinal mode of a ring cavity.

A simplified schematic diagram for a fiber RLG based on SBS is shown in Fig. 4.8. A diode pumped, single-frequency, non-planar ring, Nd:YAG pump laser at 1.3 μm is split into two beams, in the directions labeled **P1** and **P2**, respectively, which are coupled into counterpropagating directions of the same ring cavity (Cavity **G**, $A = 4.5 \times 10^{-3}$ m^2, and $P = 0.25$ m). The ring cavity is mounted on a rotation stage so that a sinusoidal rotation, with a peak rotation rate equal to several thousand Ω_e, can be applied to the cavity.

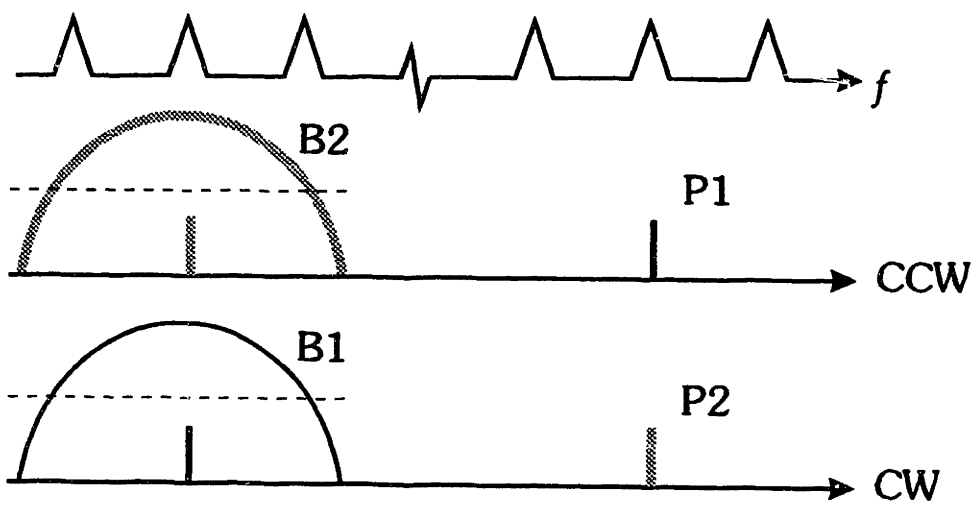

Figure 4.7 Two pump lasers **P1** and **P2**, generate independent gain curves for two SBS lasers, **B1** and **B2**.

With the pump beams locked to the center of a cavity resonance using an AC servo, not shown in the figure, two SBS lasers, labeled **B1** and **B2**, are generated by **P1** and **P2**, respectively. After leaving the cavity, the SBS lasers are combined using directional coupler **C**, pass through a short Fabry-Perot, used to filter out the residual pump laser, and fall onto detector **D**.

To demonstrate the sensitivity of the gyroscope to rotation, a rotation of approximately 7×10^{-2} r/s, or $\sim 1000\ \Omega_e$, is applied to the cavity, and a sinusoidal beat frequency of 3 kHz is observed at the output of detector **D**, as shown in Fig. 4.9(a). As the rotation rate is decreased to 4×10^{-2} r/s, the beat frequency decreases to 1.7 kHz, in Fig. 4.9(b), as predicted by Eq. (4.14). These beats clearly demonstrate that the SBS lasers are simultaneously oscillating and that there is no gain competition between the counterpropagating lasers.

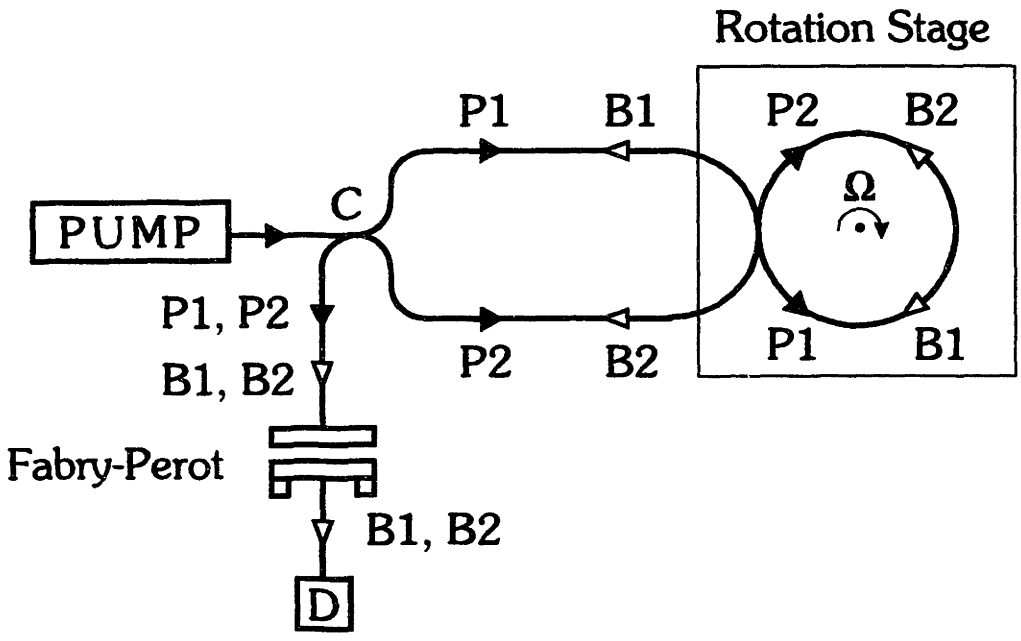

Figure 4.8 Simplified schematic diagram for an SBS ring laser gyroscope.

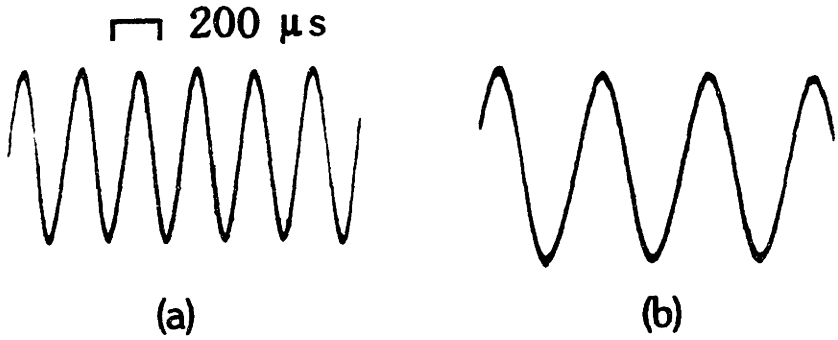

Figure 4.9 Beat between the SBS lasers for (a) large rotation rate, and (b) moderate rotation. Cavity G.

Another way of observing the rotation response of the RLG is by measuring the SBS laser beat frequency as a function of time using a frequency counter, as shown in Fig. 4.10. The digital output of the counter was converted into an analog signal and then recorded on a stripchart recorder. In addition, in order to measure the sign of the rotation, a frequency offset, f_b,

was introduced between the SBS lasers, using frequency shifters, δf_1 and δf_2, in the arms of the resonator, as shown in Fig. 4.10. Thus, with no applied rotation, a beat frequency equal to the applied bias frequency, f_b, was observed, and with rotation, this beat frequency either increased or decreased, depending on the direction of the applied rotation.

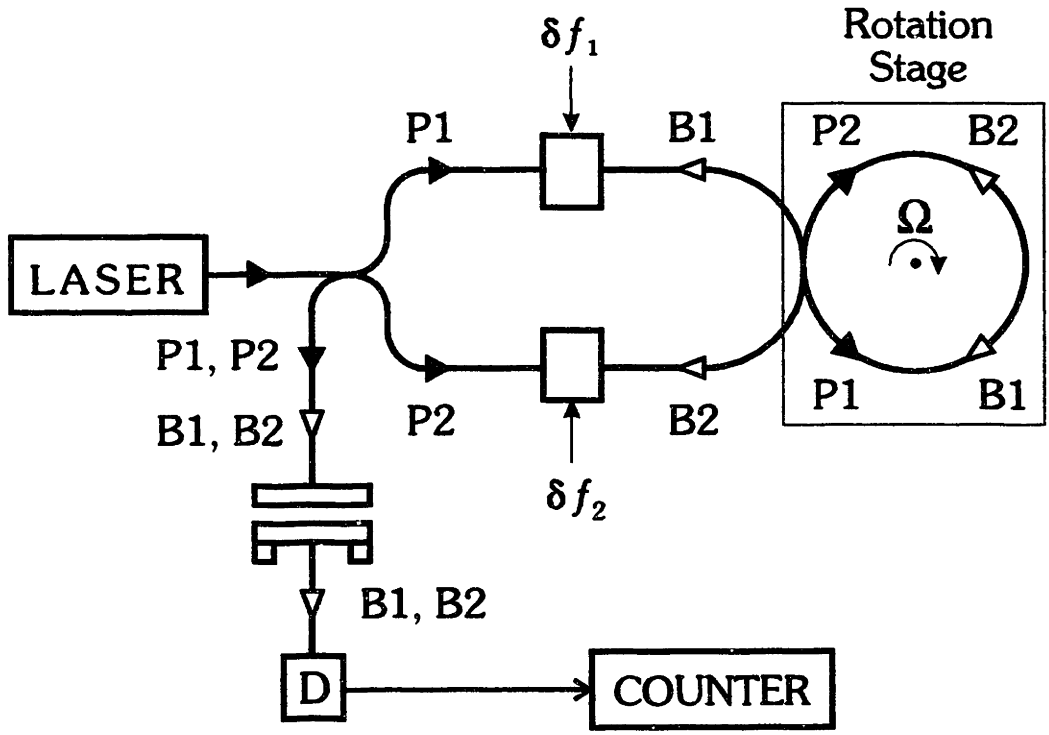

Figure 4.10 Simplified schematic diagram for an SBS ring laser gyroscope using a frequency offset to recover the sign of the rotation.

Figure 4.11(a) shows the output of the counter as a function of time in response to the applied sinusoidal rotation angle, shown in Fig. 4.11(b), which has a period of 17 seconds. As seen in the figure, the measured beat frequency, Δf, is proportional to the applied rotation rate, and hence, is 90° out-of-phase with the applied rotation angle shown in the figure. The wobble

observed in the rotation angle is an artifact of the angular measurement, and does not represent variations in angular velocity.

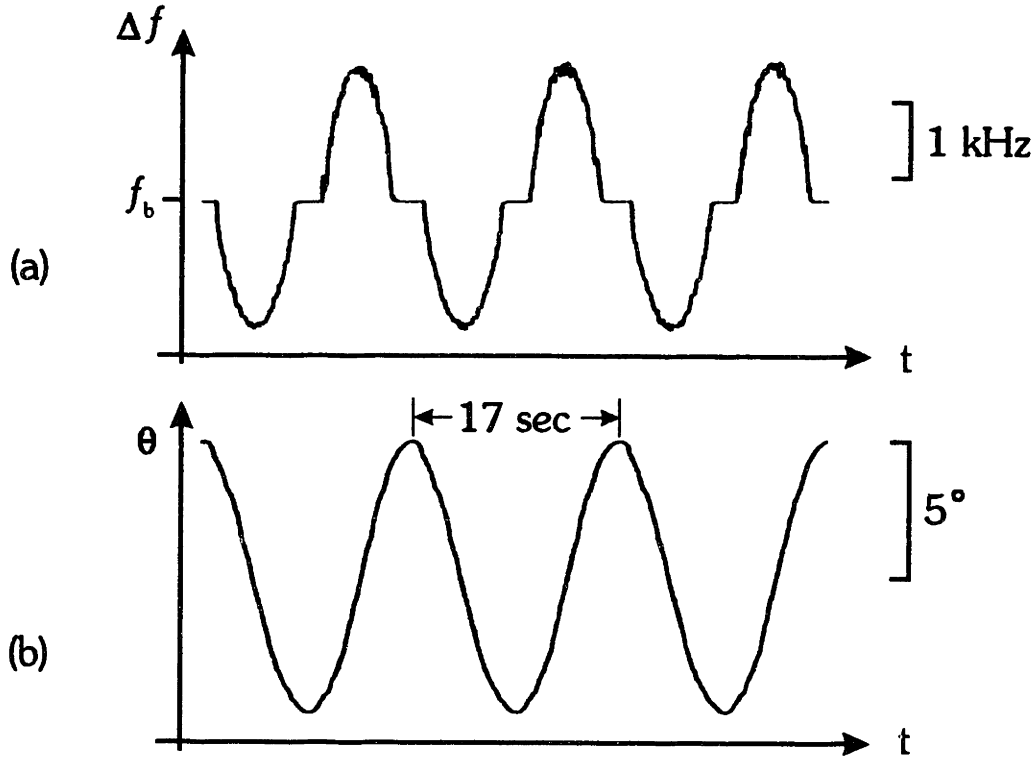

Figure 4.11 Simultaneous recording of (a) the difference frequency between the SBS lasers and (b) the angle of the applied rotation. Cavity H.

Also visible in Fig. 4.11(a) is a range of small rotation rates for which the frequency difference between the SBS lasers is zero, called the lock-in zone, which appears at f_b, the applied bias frequency. Lock-in is caused by the coupling of the counterpropagating lasers through backscattering inside the cavity and is an important error source in RLGs. Lock-in will be discussed in detail in the next section.

The response of Δf for different applied rotation rates is shown in Fig. 4.12, where the period of the rotation is abruptly changed between

three values. The peak-to-peak Δf, shown in Fig. 4.12(a), is 3.9 kHz for the first rotation rate, 5.9 kHz for the second, and 2.15 kHz for the third, in good agreement with the measured rotation periods of 20, 13.5 and 35 seconds, as predicted by Eq. (4.14). Also, the effect of the approximately 300 Hz wide lock-in zone on Δf can be seen for the three rotation rates, with Δf for the slower rotations being much more seriously distorted.

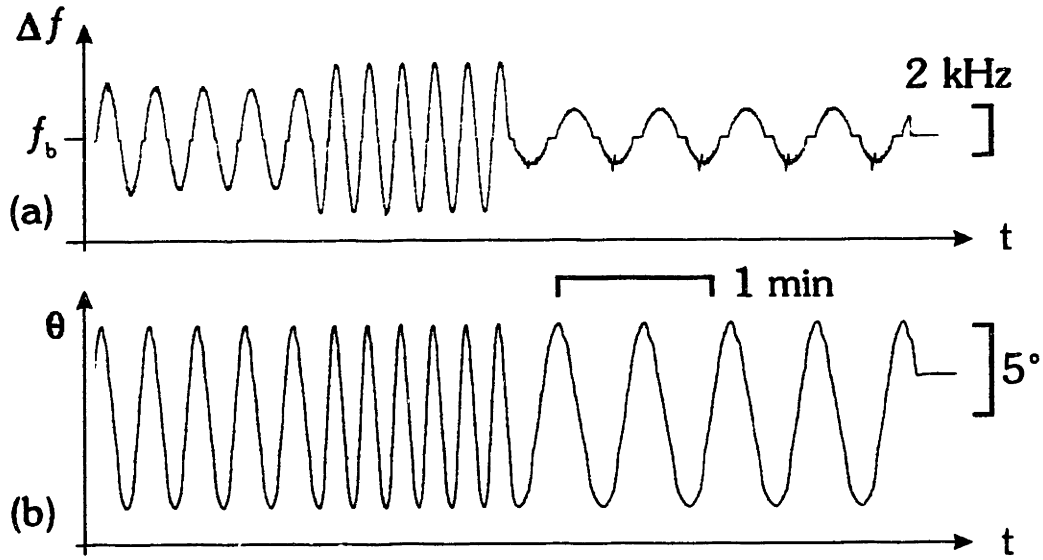

Figure 4.12 Simultaneous recording of (a) the beat frequency between the SBS lasers and (b) the angle of the applied rotation for three rotation rates. Cavity H.

4.3 Backscatter Induced Lock-in Effect

The lock-in effect is caused by the coupling of the counterpropagating lasers through optical backscattering inside the cavity, and has been observed and extensively studied in the He-Ne bulk-optic RLG.[51,52,53] It should be noted that lock-in, or frequency locking, has been studied for many years in a wide range of systems with lightly coupled, driven oscillators, such as pendulum

clocks, electrical oscillators, or driven mass-spring systems.[54] Also, in contrast to mode competition where only a single direction of the cavity lases at any one time, lasing occurs in both directions of the cavity under lock-in, but the frequencies of the counterpropagating lasers are the same.

To illustrate the effects of backscattering inside the cavity, we will consider the analytically simple case of weak, single direction scattering, for example, scattering from the CW electric field, E_{cw}, into the CCW field, E_{ccw}.[49] As seen in Fig. 4.13, the phase pull caused by the scattering of E_{cw} into E_{ccw}, $\Delta\psi$, is given by,

$$\Delta\psi = \alpha \sin(\psi + \theta)\frac{E_{cw}}{E_{ccw}} \tag{4.16}$$

where α is the magnitude of the scattering, ψ in the phase between the fields, and θ is the angle associated with the scattering process. Thus, the maximum phase pull occurs when $\theta + \psi = 90°$ and is given by,

$$\Delta\psi_{max} = \pm\alpha\frac{E_{cw}}{E_{ccw}} \tag{4.17}$$

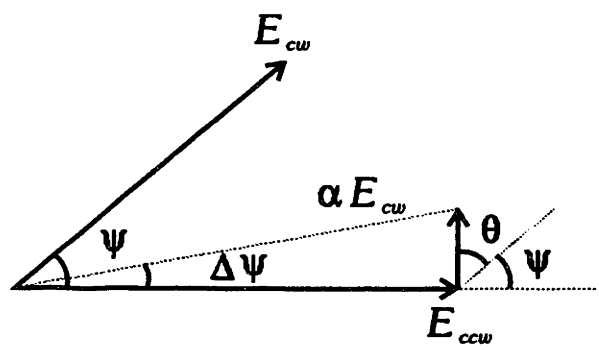

Figure 4.13 Phase pull due to scattering.

This phase pull can be related to a frequency pull by recalling that a phase pull of 2π results in a cavity resonance frequency shift of one FSR. Thus, the maximum frequency pull, assuming equal field strengths, $E_{cw} = E_{ccw}$, is given by,

$$\Delta f_{max} = \frac{\Delta\psi_{max}}{2\pi}\frac{c_o}{nP} = \frac{\alpha}{2\pi}\frac{c_o}{nP} = \frac{\Omega_L}{2\pi} \tag{4.18}$$

where Ω_L is the width of the lock-in zone and represents the maximum frequency difference between the counterpropagating lasers for which frequency locking will occur.

To find the exact behavior of the system, we will derive a differential equation for the phase difference between the counterpropagating lasers. In the absence of lock-in, a constant rotation rate will generate a constant frequency difference, or equivalently a linearly increasing phase difference, ψ, between the two lasers, given by,

$$\psi = \Omega t \tag{4.19}$$

where Ω is the difference frequency caused by the rotation, or equivalently,

$$\dot{\psi} = \Omega \tag{4.20}$$

The perturbation due to the backscattering can be included using Eq. (4.16) and assuming equal amplitudes for the counterpropagating lasers, yielding,

$$\dot{\psi} = \Omega + \Omega_L \sin(\psi + \theta) \tag{4.21}$$

This differential equation has two types of steady state solutions, i.e., solutions for constant applied rotation rates, ignoring the dynamics of lock-in. One solution is for $\Omega < \Omega_L$ where the frequencies are locked, and the other for $\Omega > \Omega_L$ where a beat frequency is observed between the lasers.

First consider the case where $\Omega < \Omega_L$. Since $\dot{\psi} = 0$, the phase difference can easily be shown to vary from $-\pi/2$ to $\pi/2$ as Ω varies from $-\Omega_L$ to Ω_L.

In the case where $\Omega > \Omega_L$, the solution is more complicated, and is given by,

$$\tan\left(\frac{\psi + \theta - \pi/2}{2}\right) = \left(\frac{K+1}{K-1}\right)^{\frac{1}{2}} \tan\left(\frac{1}{2}\Omega_L(K^2-1)^{\frac{1}{2}}t\right) \tag{4.22}$$

where $K = \Omega/\Omega_L > 1$. For large input rates, $K \gg 1$ the equation simplifies to,

$$\tan\left(\frac{\psi + \theta - \pi/2}{2}\right) = \tan\left(\frac{1}{2}\Omega t\right) \tag{4.23}$$

which can be further simplified to give

$$\psi = \Omega t + \pi/2 - \theta \tag{4.24}$$

which generates the same beat frequency as in the case without backscatter, only with a phase shift.

For gyroscope operation, the frequency difference between the lasers is usually the desired output. Equation (4.22) can be used to find an apparent frequency, defined as $\Omega_m = 1/\tau$ where τ is the amount of time required for ψ to increase by 2π and is given by,

$$\Omega_m = (\Omega^2 - \Omega_L^2)^{\frac{1}{2}} \tag{4.25}$$

Figure 4.14 shows a plot of theoretical frequency, $\Delta f = \Omega_m/2\pi$, versus the applied rotation rate, Ω, for several values of Ω_L ranging from zero to eight. As seen in the figure, for a range of low rotation rates, $\Omega < \Omega_L$, the measured frequency is zero, and for $\Omega > \Omega_L$, the measured frequency asymptotically approaches the lock-in free value as the magnitude of Ω increases.

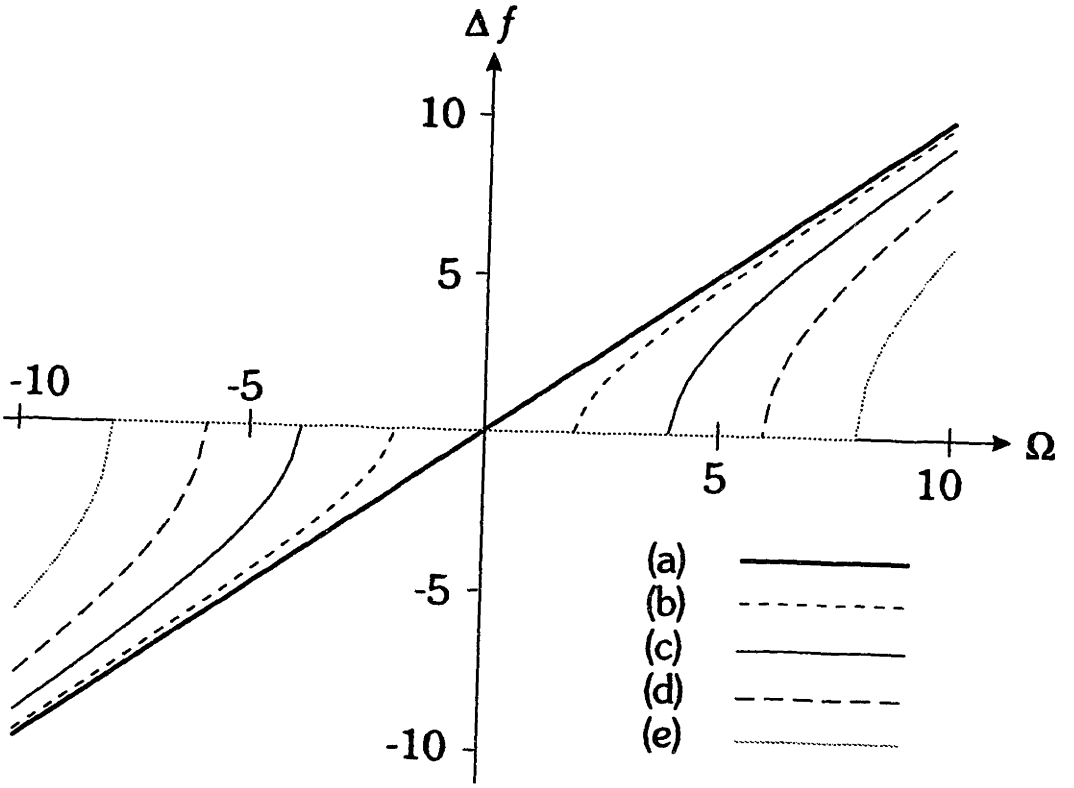

Figure 4.14 The theoretical output frequency as a function of applied rotation for (a) no lock-in, and a lock-in zone of (b) 2, (c) 4, (d) 6, and (e) 8.

However, instead of a constant rotation rate, in our experiments a sinusoidal rotation is applied to the RLG. Figure 4.15 shows the theoretical frequency output, Δf, for a sinusoidally varying rotation rate with a peak value of 10, for several values of Ω_L, from zero to eight. Similar to the observed data, the rotation signal is most severely distorted for Ω_L close to the peak Ω induced by rotation.

4.3.1 Size of the Lock-in Zone

The lock-in zone can be accurately measured by fitting digitized rotation data. In this case, the SBS beatnote is digitized, and a series of 2048 point FFTs are used to find the corresponding spectra, and Δf is then obtained

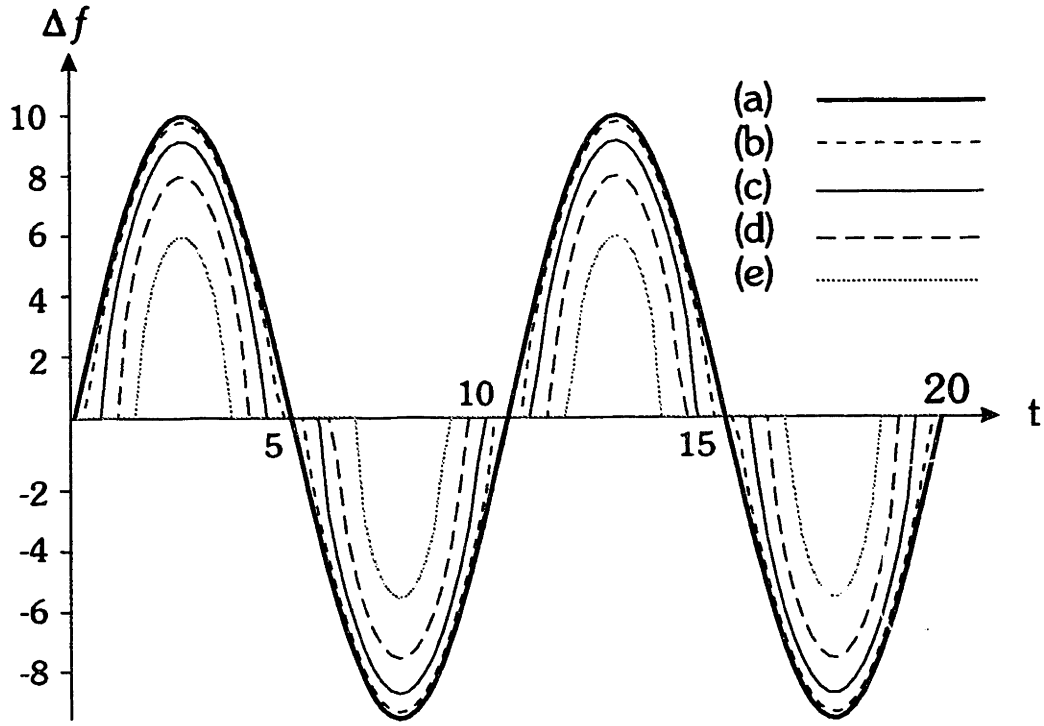

Figure 4.15 Theoretical output frequency with a sinusoidal applied rotation for various lock-in zone sizes, (a) zero, (b) 2, (c) 4, (d) 6, and (e) 8.

from these spectra. The frequency measurement from each FFT is shown as a single point in Fig. 4.16, and an approximate fit of the data is shown as a solid line. The lock-in zone of the fitted curve is 150 Hz.

In Fig. 4.17, the observed Δf is shown for several rotation cycles with the cavity only subject to random thermal perturbations. As seen in the figure, the width of the lock-in zone varies from a maximum of approximately 500 Hz, to a minimum of lock-in that is barely detectable. These variations in the size of the lock-in zone are due to variations in the cavity backscattering.

For this cavity, lock-in zones as wide as 2 kHz and as small as 100 Hz or less have been observed, corresponding to a maximum field backscattering ratio of $\alpha = 10^{-4}$.

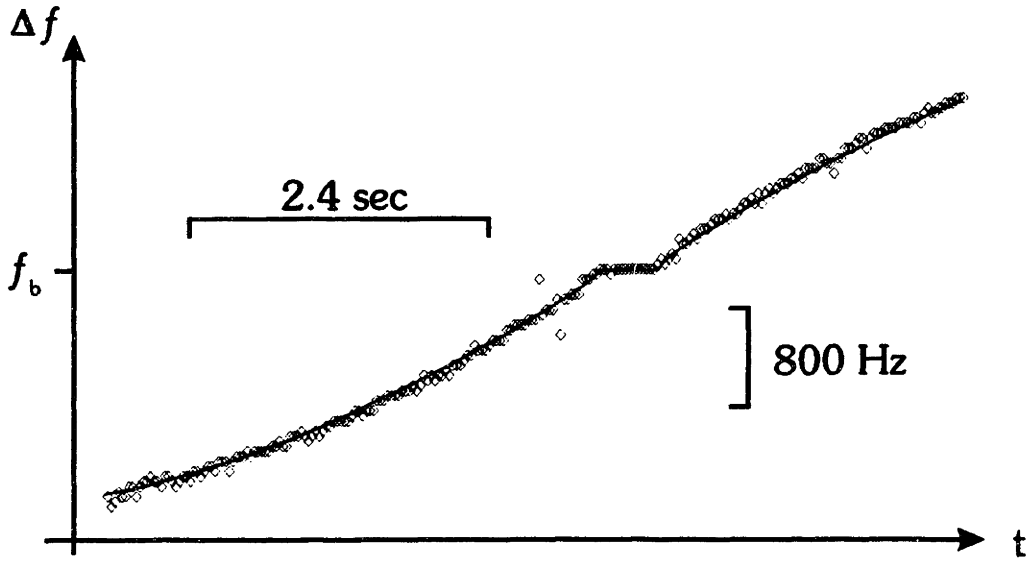

Figure 4.16 Rotation signal as a function of time with a fit of the data. Cavity H.

4.3.2 Backscattering Variations

The backscattering in a fiber cavity is the coherent sum of backscattering from several sources, including scattering from defects and inhomogeneities in the fiber or coupler, and Rayleigh scattering from the entire fiber. Due to the many sources of scattering, the observed variations of the net backscattering in a fiber cavity are a complex function of the pump frequency and external perturbations to the fiber cavity and coupler.

The setup in Fig. 4.18 was used to demonstrate the sensitivity of the backscatter to perturbations. In the figure, the pump laser is locked to the center of a cavity resonance and, with the laser well below the SBS threshold for this cavity, the intensity backscattering at the pump frequency is measured using detector **D2**. In addition, a slow triangle wave is also applied to the fiber cavity PZT to demonstrate the effect of local changes in the optical length of the fiber cavity on the backscattering. Since the laser is

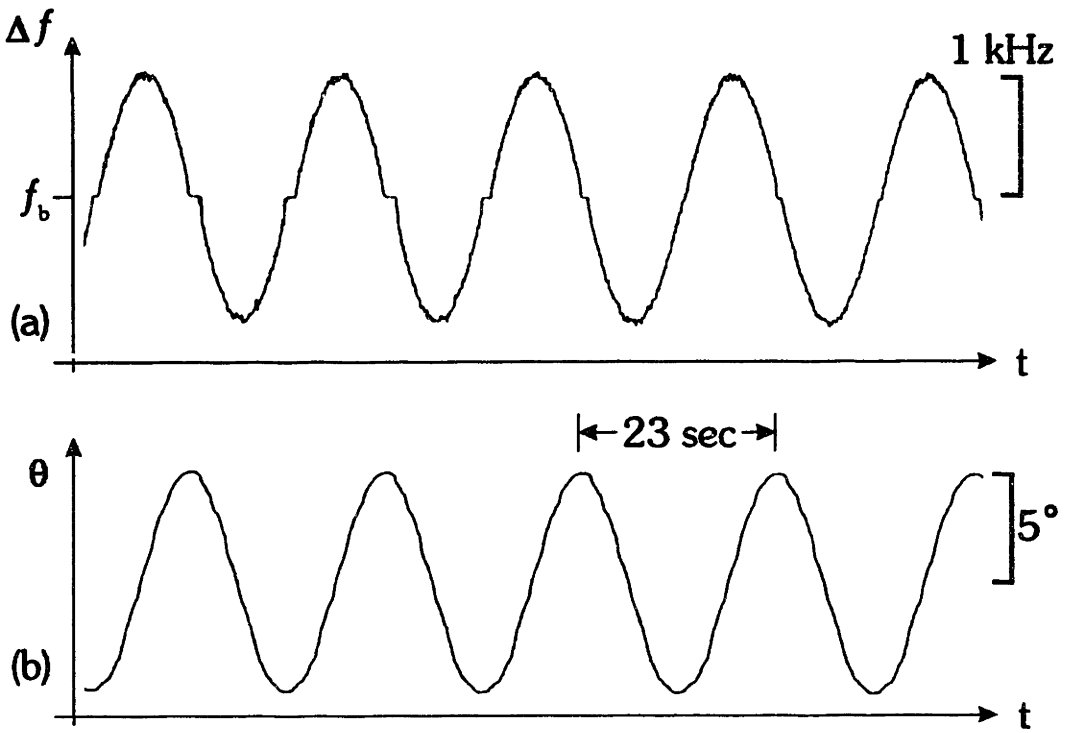

Figure 4.17 Measured frequency difference with a constant applied rotation demonstrating variations in size of lock-in zone. Cavity H.

locked to the fiber cavity, this slow triangle wave also causes the frequency of the laser to be tuned.

Figure 4.19 shows the variations in intensity backscattering, as measured by detector **D2**, as the cavity drifts with changes in the room temperature. The faster variations of the backscattering, with approximately a 10 second period, are caused by the triangle wave applied to the cavity PZT. Initially, this perturbation caused a 10% change in the observed backscattering, and, over the course of several minutes, this increased to approximately 30%. At the same time, the average intensity of the backscattering, which is initially approximately 20% of the input intensity, slowly drops to approximately 6% by the end of the 10 minute run.

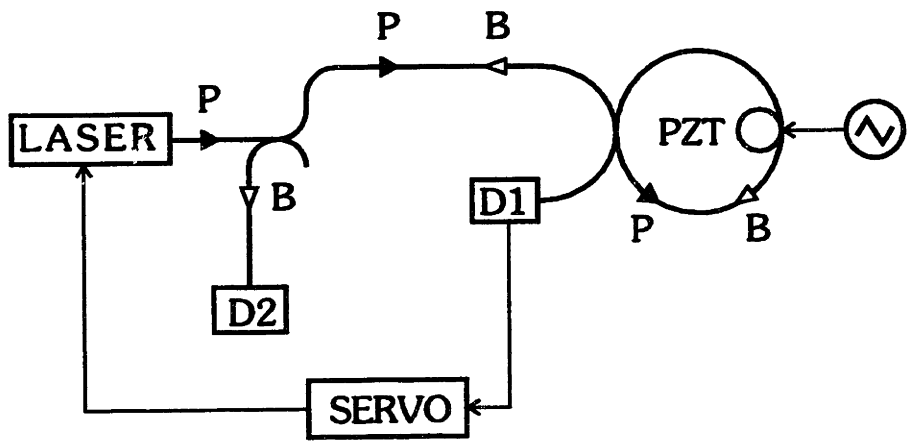

Figure 4.18 Fiber cavity setup to study the effects of cavity perturbations on backscattering.

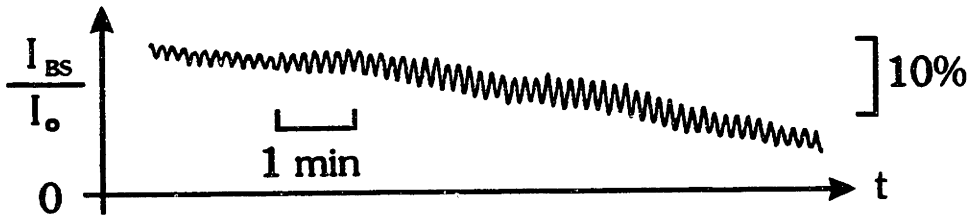

Figure 4.19 Intensity backscattering changes with cavity drift and cavity PZT perturbations. Cavity A.

Much more dramatic variations in the backscattering can be observed if the cavity is intentionally perturbed, in this case by very gently heating a small section of cavity fiber by shining a weak light it. Figure 4.20(a) shows the variations in the backscattering as the small light is turned on and off. As seen in the figure, this perturbation immediately causes large changes in the size of the backscattering which varies from almost zero to about 25%. In addition, this perturbation also causes variations in the effect of the cavity PZT.

In Fig. 4.20(b), the variation in the effect of the cavity PZT can more

easily be seen. Initially, the cavity is perturbed by shining a very weak light on it, and as the average level of the backscattering changes, the variation of the backscattering caused by the cavity PZT varies from almost zero to 30%.

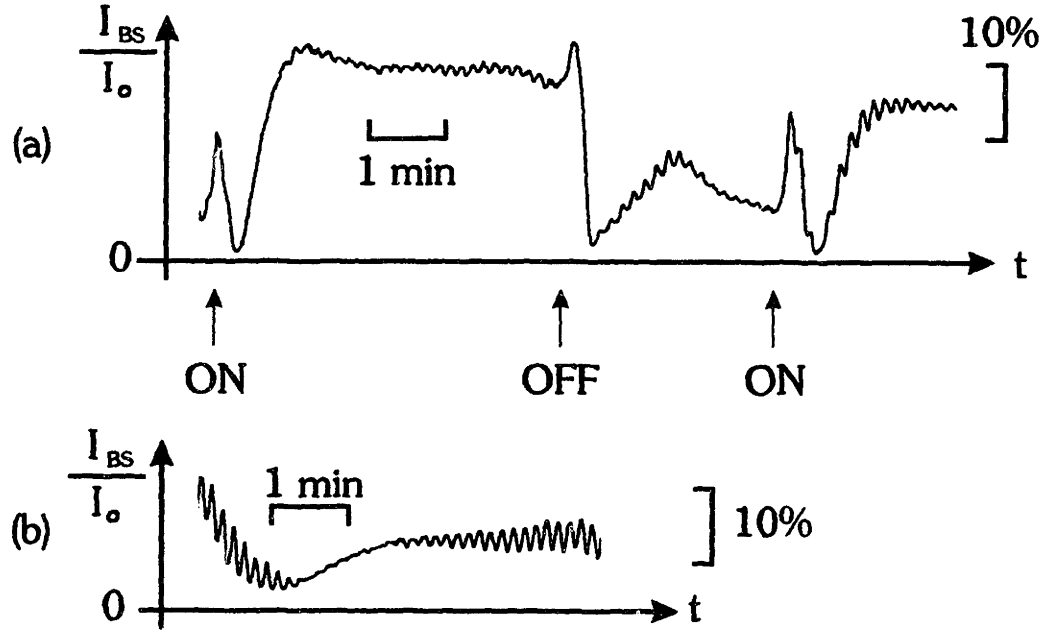

Figure 4.20 Variation in backscattering for (a) for several cycles of perturbations, and (b) for a single, weak cavity perturbation. Cavity A.

Changes in the cavity longitudinal modes also affect the backscattering, as shown in Fig. 4.21. Figure 4.21(a) shows the intensity backscattering, and Fig. 4.21(b) shows the laser PZT voltage, which is a measure of laser frequency. As the laser is sequentially locked to a series of adjacent cavity longitudinal modes, large changes in backscattering can be observed. Also notice that the variations are not due to other perturbations to the cavity, since the backscattering for a given longitudinal mode, e.g., the four marked modes in the figure, is almost constant throughout the run.

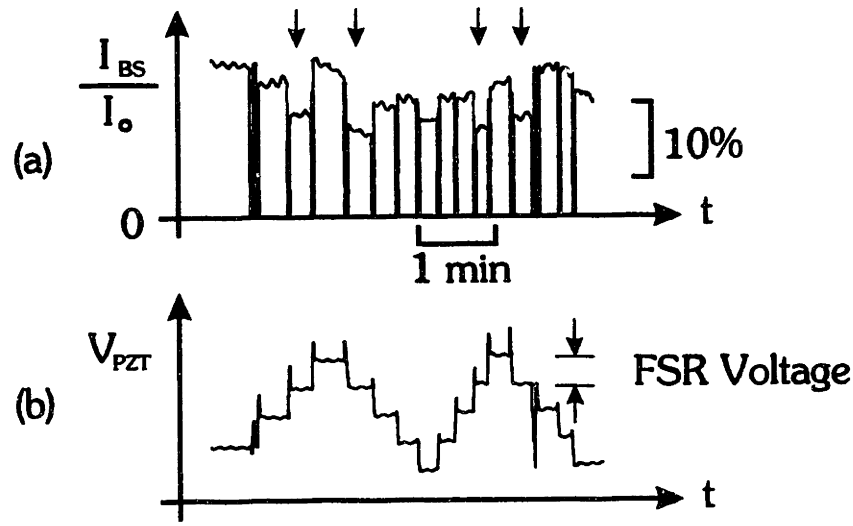

Figure 4.21 Backscatter variations with cavity longitudinal mode. Cavity A.

4.4 Techniques for Lock-in Elimination

Lock-in has been observed in both bulk-optic and fiber-optic RLGs and for precision navigation applications, it must be greatly suppressed or eliminated. Since the lock-in is caused by backscattering, the most obvious method for reducing or eliminating it is to reduce or eliminate the backscattering. In a bulk-optic RLG, the dominant source of backscattering is the mirrors and extraordinary care is taken during the manufacture of the mirrors to minimize the amount of backscattering, nevertheless, some small scattering still remains, around $\alpha \sim 10^{-8}$.

In an SBS fiber RLG, on the other hand, there is Rayleigh backscattering along the entire length of the cavity, in addition to scattering from defects and inhomogeneities in the fiber and in the coupler. Thus, the observed levels of backscatter in the fiber RLG are typically much larger than those observed in the bulk-optic RLG, and they are also much more variable, as discussed in Section 4.3.2. One method to reduce the scattering is to move to

longer wavelengths to take advantage of the λ^{-4} dependence of the Rayleigh scattering.

It is clear, however, that backscattering cannot be completely eliminated. Therefore, techniques for the elimination of the effects of backscatter-induced lock-in are required. There are two basic classes of techniques that are applicable to the SBS RLG. The first approach introduces an alternating bias that minimizes the amount of time that the gyro spends in the lock-in zone, thus while lock-in is still present, its effects are greatly diminished. The second approach prevents or suppresses the coupling between the counterpropagating lasers caused by the backscatter. Thus, even though the backscattering is present it does not lead to coupling between the lasers and hence, no lock-in.

4.4.1 Alternating Bias for Lock-in Removal

One conceptually simple technique for eliminating the effects of lock-in is to introduce a large constant nonreciprocal phase shift (NRPS), i.e., a phase shift that is different for the two directions of the cavity, like the Sagnac effect, between the counterpropagating lasers. If the size of the NRPS is such that the resulting frequency difference is much greater than the width of the lock-in zone, this NRPS will prevent frequency locking even when the gyroscope is at rest. In practice, however, this technique is not used due to the stability requirements on the bias and the lack of a suitable method for generating such a large, constant NRPS.

One way to reduce the requirements on the stability of the bias is to periodically reverse the sign of the bias, i.e., apply an alternating bias. In this way, by averaging over several bias reversal cycles, no net bias would be observed.

For the He-Ne RLG, lock-in was completely eliminated by mechanical dither.[55] In this case, the bulk-optic cavity is mounted on a piezoelectric

torsion spring which is sinusoidally driven at the mechanical resonance of the system. In addition, pseudo-random rotation noise is added to the sinusoidal dither to randomize the errors due to any residual lock-in.[56] Mechanical dither is very successful for several reasons: no additional components are introduced into the optical cavity, it is difficult for the dither to introduce a bias, it is relatively easy to implement, and the suppression is not dependent on the precise amplitude or frequency of the dither. Mechanical dither could also be used with the SBS RLG, where the small mass of the fiber cavity would allow such a dither to be more easily accomplished.

A number of other methods for introducing an alternating bias have been suggested and demonstrated for the bulk-optic RLG, including those based on the Faraday effect.[57]

4.4.2 Coupling Suppression

Three techniques for the suppression of coupling between the lasers will be discussed here. The first technique generates the SBS lasers in different longitudinal modes of the cavity, i.e., $\Delta q \neq 0$, and the second technique uses a time dependent NRPS to "wash out" the coupling between the lasers. The third method uses modelocked lasers so that only backscattering from a very limited area of cavity will contribute to lock-in.

The directionality and tunability of the SBS gain medium allows the counterpropagating lasers of the RLG to be generated in different longitudinal modes of the same cavity, as demonstrated in Section 3.1. The large frequency difference between such lasers prevents frequency locking, however, the zero rotation beat frequency between the lasers is now centered on an offset of $\Delta q \cdot \mathrm{FSR}$. Thus, the measurement and stability of the bias is an important issue for the performance of such a gyroscope. However, there are also additional problems with this technique which will be explored in detail in Section 4.5.

Another method to decouple the lasers is through the use of a time dependent, NRPS, i.e., time-dependent nonreciprocal suppression, TD-NRS. TD-NRS uses the time delay between phase modulations in the fiber cavity to generate a direction dependent optical phase shift, similar to that caused by rotation. By carefully adjusting the amplitude and frequency of this dither, the coupling between the counterpropagating lasers can be completely washed out. This technique will be discussed in Section 4.6.

Yet another method to decouple the lasers is through the use of modelocked lasers.[58,59,60] A modelocked laser simultaneously oscillates in several modes of the cavity, with a fixed phase relationship between the modes. Thus, instead of a continuous output, the modelocked laser output is a periodic series of pulses. Two such modelocked lasers can be generated in opposite directions of the same cavity for use as an RLG and, in this case, only scattering from the region where the laser pulses overlap will contribute to lock-in. Thus, with very short pulses that cross in free space, lock-in can be virtually eliminated. However, the application of this technique in the SBS RLG is not clear and needs to be investigated.

4.5 Performance of the Δq Gyroscope

The tunability and directionality of the SBS gain curve allows the generation of counterpropagating lasers in different longitudinal modes of the same cavity, as demonstrated in Section 3.1.2. In such a configuration, backscattering will not lead to frequency locking, due to the large frequency difference between the lasers.

The operation of a Δq gyroscope will be demonstrated using the setup shown in Fig. 4.22. In this case, a single pump laser is used, and frequency shifters in the arms of the cavity generate the frequency difference between the pumps, **P1** and **P2**, which is $\delta f_1 - \delta f_2 = \text{FSR} = 96$ MHz, i.e., $\Delta q = 1$. In this configuration, the SBS lasers, **B1** and **B2**, initially have a frequency

difference of approximately 96 MHz as they leave the resonator. However, they experience an additional shift due to the frequency shifters, and thus their beat frequency is centered on approximately 2 · FSR or 192 MHz.

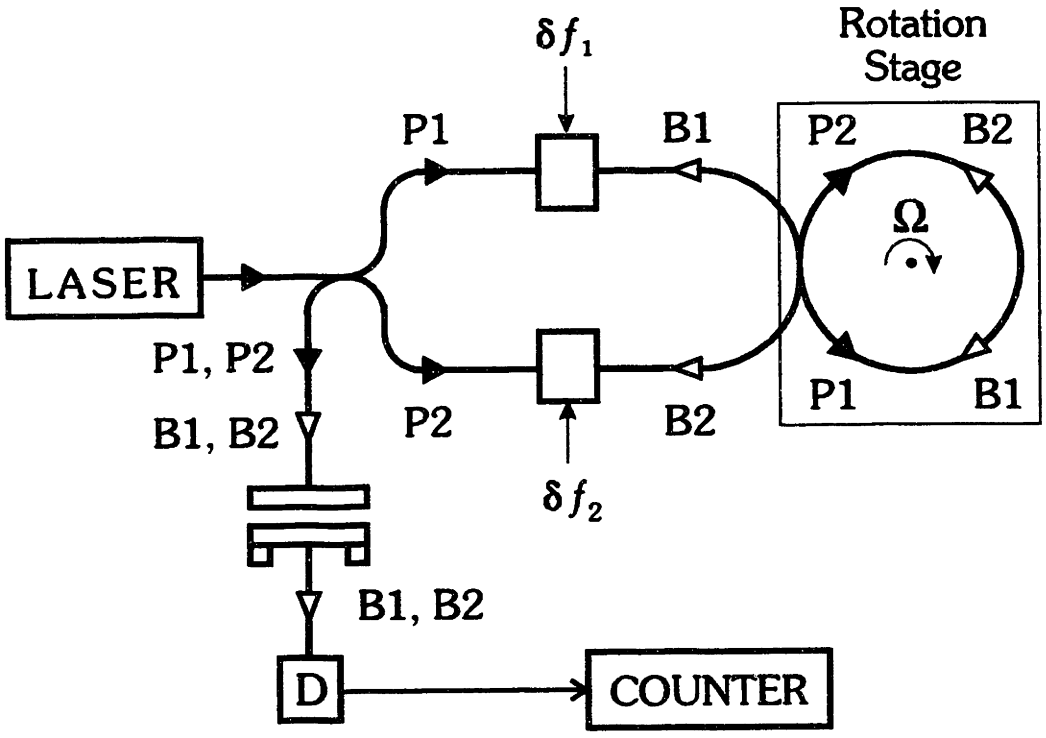

Figure 4.22 Simplified schematic diagram for an SBS ring laser gyroscope.

The response of Δf to the applied rotation is shown in Fig. 4.23(a) with the corresponding rotation angle in Fig. 4.23(b). In the center of the figure, the time scale is expanded to demonstrate that Δf is 90° out-of-phase with the rotation angle in Fig. 4.23(b), and that no lock-in is observed, as expected.

Figure 4.24 only shows the difference frequency, Δf, between the SBS lasers, first with applied rotation, and then as the cavity is brought to rest. As expected, with the cavity at rest, Δf is approximately at the midpoint of the

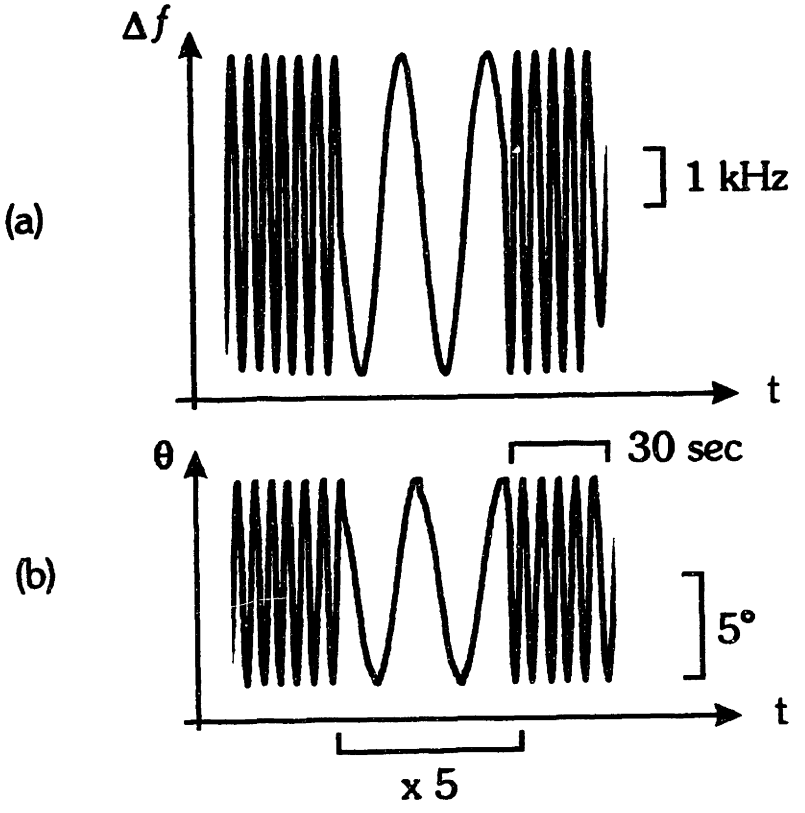

Figure 4.23 Simultaneous recording of (a) the difference frequency between the SBS lasers, as a function of (b) the applied rotation. Cavity E.

sinusoidal variations caused by the rotation. However, even on this relatively short time scale, variations in the RLG bias of 200 Hz can be observed. In this configuration, bias variations of 1 kHz were typically observed at 1.15 μm, and variations of 10 kHz were observed at 633 nm. In both cases, the variations were driven by cavity perturbations.

Thus, while the Δq gyroscope eliminates lock-in, it exhibits other sources of drift and bias variations. In the following sections, several sources of drift for the Δq gyroscope will be examined, including thermal perturbations, dispersion pulls, and backscattering variations.

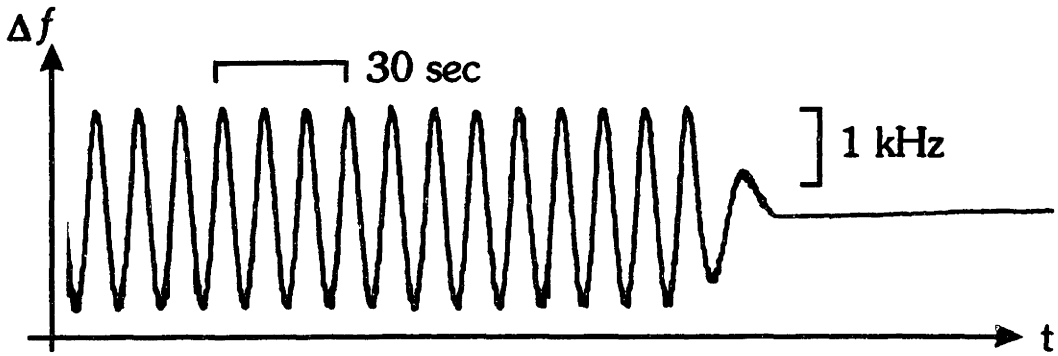

Figure 4.24 The difference frequency between the SBS lasers with and without rotation. Cavity D.

4.5.1 Thermal Drifts

One cause of bias drift in the Δq fiber RLG is the thermal expansion of the cavity, as discussed for common cavity SBS lasers in Section 3.4.1. As expected, with the SBS lasers separated by several FSRs of the cavity, any change in temperature changes the cavity FSR and hence the frequency bias. In a typical physical layout, the fractional change in optical length of the fiber cavity with temperature has been measured to be 2×10^{-5}, thus with frequency separation of 100 MHz, the thermal tuning of the beat frequency is $\sim 2\text{kHz}/^{\circ}\text{C}$, or about $400 \cdot \Omega_e/^{\circ}\text{C}$. Clearly, stabilizing the cavity will reduce this error, but for navigation grade performance, the cavity temperature would have to be held constant to within several microdegrees Celsius. In our case, the changes in temperature of the fiber cavity were only on the order of millidegrees Celsius, thus they were much too small to account for the observed drifts.

One possible method to eliminate or reduce this error is to use more than one pair of SBS lasers, or to periodically switch the directions of the lasers. These technique will be discussed further in Section 6.1.2.

4.5.2 Dispersion Pulls

An important additional source of drift is due to dispersion pulling of the SBS laser frequencies resulting from intensity backscattering of the pump lasers.

Consider a single pump laser, **P1**, in the CCW direction and the resulting SBS gain curve and SBS laser, **B1**, in the CW direction, as shown in Fig. 4.25. If there is any pump backscattering, a small amount of pump will also be present in the CW direction of the cavity, labeled **P1′**. Though this pump will be below the SBS lasing threshold, it will still generate a small SBS gain curve, labeled **B1′**. In a single direction SBS laser, this extra gain curve has no effect since it is in the opposite direction as the SBS laser.

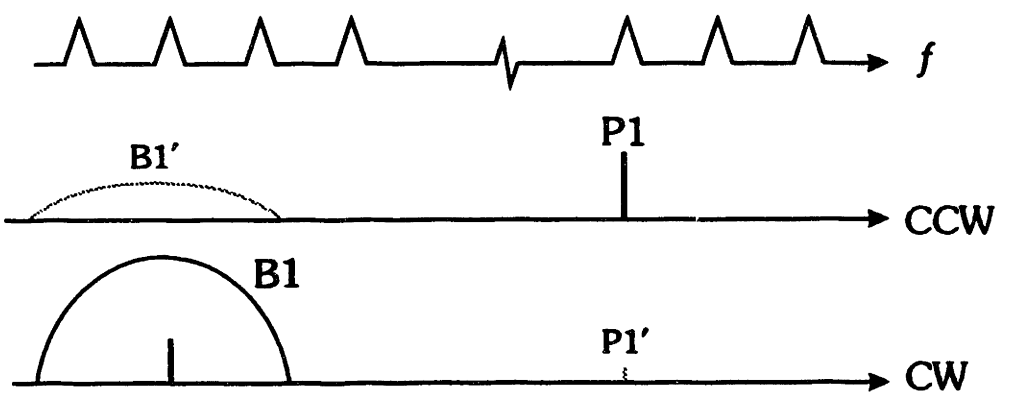

Figure 4.25 Generation of an extra SBS gain curve due to pump backscattering.

However, as shown in Fig. 4.26, if two counterpropagating SBS lasers, **B1** and **B2**, are generated in the same cavity, this extra SBS gain curve, **B1′**, due to its dispersion, will pull the frequency of the **B2** SBS laser. Thus, as the intensity of **P1** changes, or as the backscattering at the pump frequency changes, the size of the dispersion pull will also change and cause a bias drift in the gyroscope.

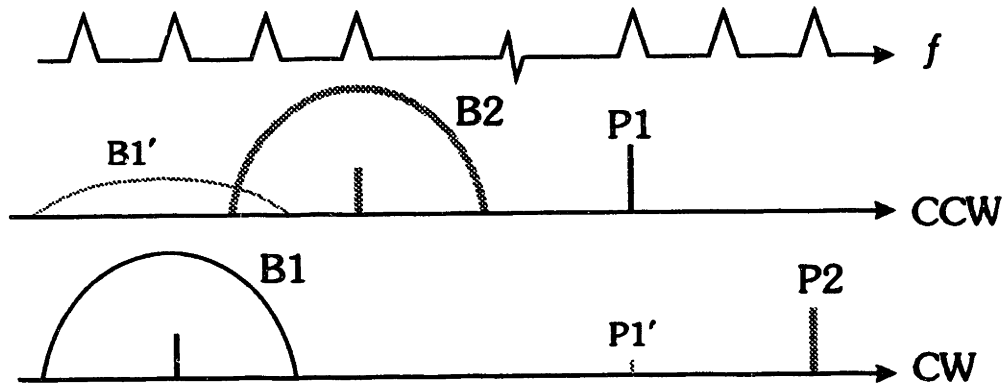

Figure 4.26 Extra SBS gain curve due to pump scattering.

4.5.3 Measurement of Dispersion Pulling

The size of the dispersion pull can be directly measured using the setup shown in Fig. 4.27. A single pump laser, **Pump**, is used for the pump beams labeled **P1** and **P2**, which generate a pair of SBS lasers, **B1** and **B2**, separated by several cavity FSRs through the use of frequency shifters. With the cavity locked to this pump laser, an additional pump laser, **PUMP 3**, in the direction labeled **P3**, is introduced into the cavity. This pump is asymmetrically coupled into the cavity so that there is much more coupled into the CCW direction of the cavity than the CW direction, as described in Section 4.9.1. Due to this imbalance in **P3**, a much larger SBS gain curve is generated in CW direction of the cavity than in the CCW direction, so the net dispersion pull is directly proportional to the intensity difference. Thus, in the figure, **P3** is only shown in the CCW direction of the cavity, representing the net effect of this additional pump.

To measure the dispersion pull as a function of power, **PUMP 3** is locked to a cavity resonance at a known separation from the original pumps, in this case about 30 MHz less than pump **P1**, as shown schematically in

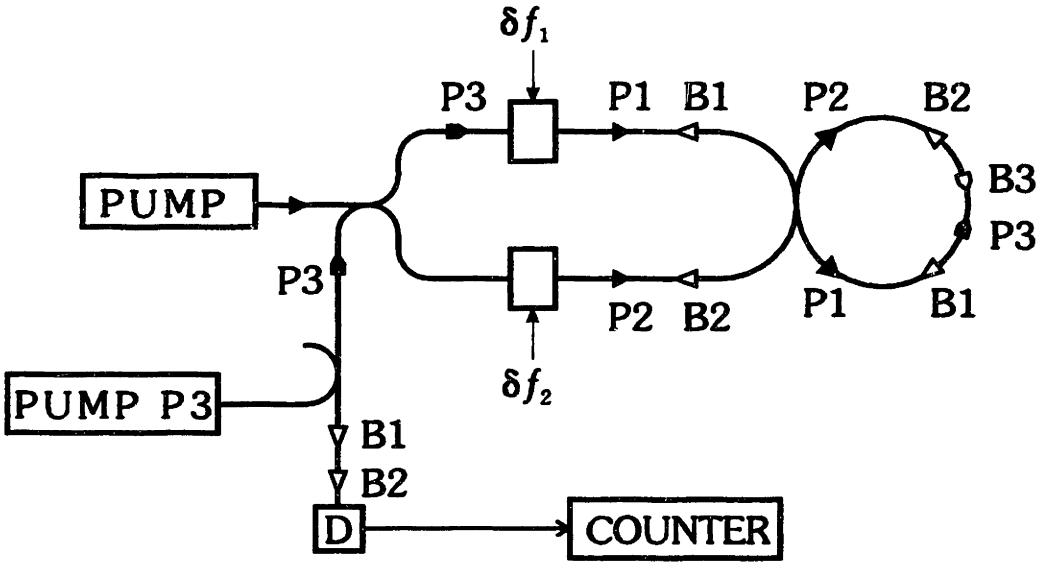

Figure 4.27 Experimental setup to measure the dispersion pull of an extra SBS gain curve.

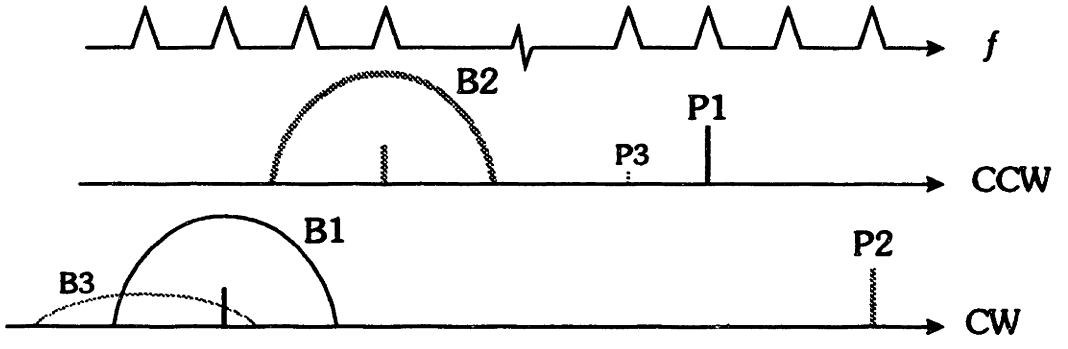

Figure 4.28 Effect of second pump laser on SBS lasers **B1** and **B2**.

Fig. 4.28. Figure 4.29(a) shows the difference frequency between the lasers, and Fig. 4.29(b), power in the perturbation laser. With **Pump 3** unlocked, the unperturbed Δf between SBS lasers **B1** and **B2** is measured, and, as the power is increased in increments, obvious changes in the SBS difference frequency is observed. The variation near the peak of the dispersion curve

was measured to be 680 Hz/μW of net input power. This is in good agreement with the predicted value of 700 Hz/μW for this cavity using the results of the derivation in Section 2.1.2.

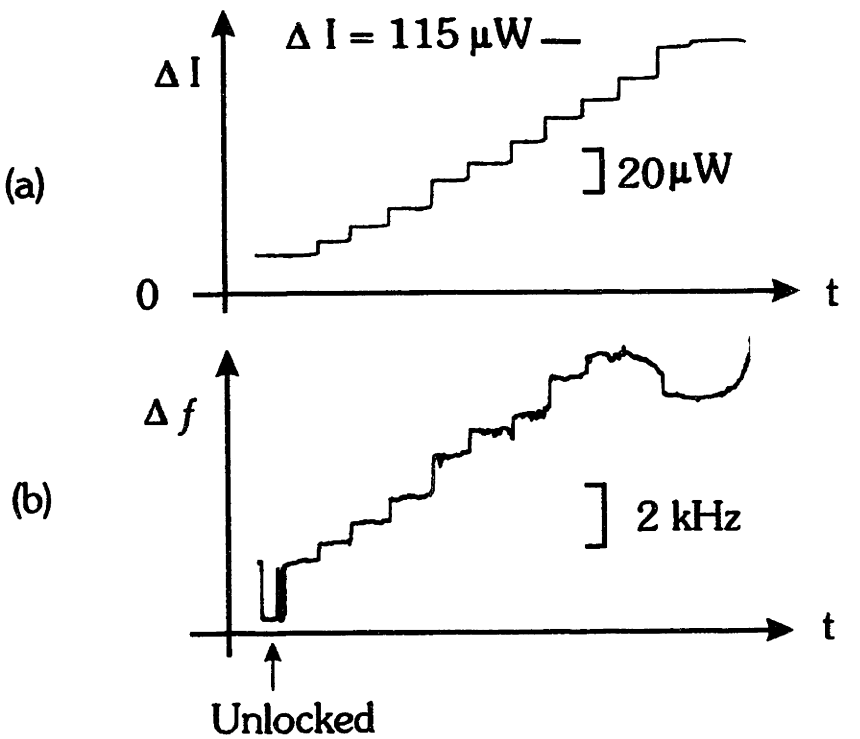

Figure 4.29 Dispersion pull versus perturbing pump power. Note the saturation for higher pump powers is a result of the generation of a third SBS laser. Cavity B.

The flattening and subsequent change in sign of the frequency pull as a function of power observed near the maximum power in Fig. 4.29 is caused by the **P3** laser power in the CCW direction of the cavity exceeding the SBS threshold. At this point, the pump power due to **PUMP 3** in the CCW direction becomes fixed, but the pump power in the CW direction continues to rise, since it is still well below threshold, and the net dispersion pull is reduced.

4.5.4 Frequency Dependence of Dispersion Pull

In addition, the frequency dependence of the dispersion pull can be measured by changing the frequency separation between the perturbation laser, **PUMP 3**, and the pump lasers. For a constant power in **PUMP 3**, the dispersion pull as a function of frequency was measured by locking **PUMP 3** to consecutive longitudinal modes of the fiber cavity.

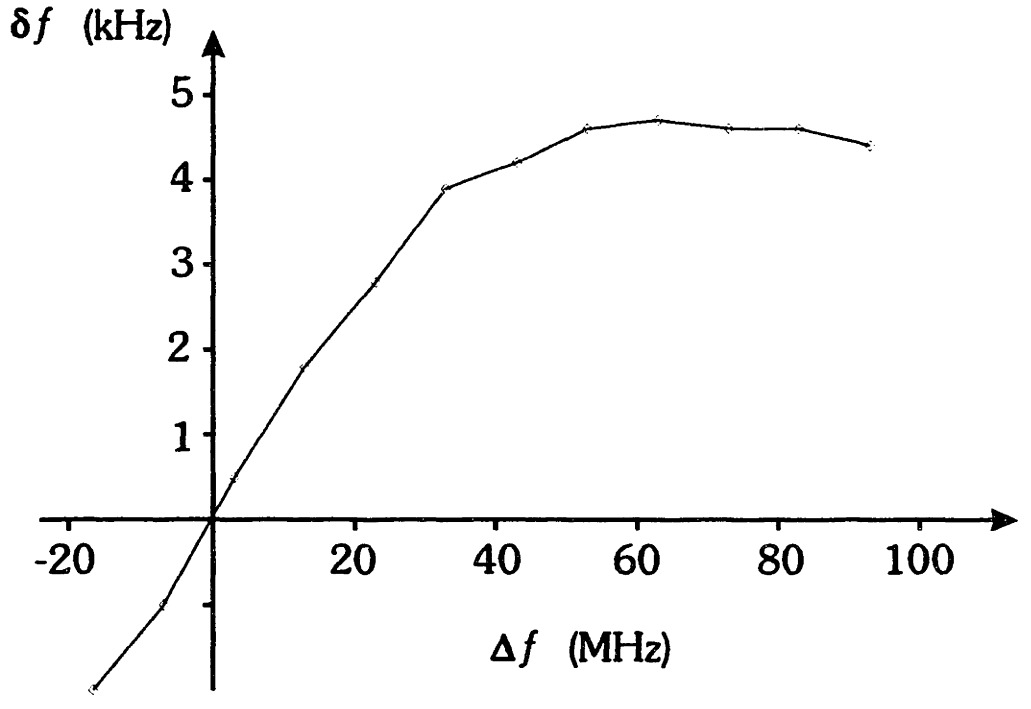

Figure 4.30 Dispersion pull as a function of perturbation laser tuning. Cavity B.

Figure 4.30 shows the plot of the dispersion pull, δf, as a function of frequency separation between **P1** and **P3**, Δf, demonstrating the change in sign of the dispersion pull around zero difference frequency. The peak dispersion pull occurs with a frequency difference of approximately 70 MHz, indicating the width of the SBS gain curve is approximately 140 MHz. This

is somewhat wider than the measured width for bulk silica and needs further study. It should also be noted that the dispersion curve is unusually flat near its peak. There are several possible explanations for this flattening, including fiber inhomogeneities, and stress variations in different parts of the fiber cavity.

To reduce the size of the dispersion pulls, SBS laser frequency spacings comparable to the half-width of the SBS gain should be avoided, since the dispersion pull is at a maximum at that separation. Thus, either a large frequency difference, or a very small frequency difference, i.e., $\Delta q = 0$, should be used between the SBS lasers.

4.5.5 Self Dispersion Pulls

Backscattering at the SBS frequency also can lead to frequency pulls on the SBS lasers themselves. In this case, the frequency pull is the result of backscatter-induced changes in cavity loss at the SBS frequency which cause a change in the self dispersion pull due to the SBS laser's gain curve.

Normally, the internal losses of the cavity at the SBS frequency are considered to be constant. However, variations in backscattering can lead to significant variations in the cavity loss as a function of the cavity environment, as demonstrated in Fig. 2.35. This loss variation will cause a corresponding change in the SBS gain, since the gain always equals the loss while the SBS laser is lasing. Thus, if the cavity mode is not exactly at the center of the SBS gain curve, this variation in the SBS gain will cause a variation in the dispersion pull of the SBS gain curve. For example, for a cavity mode 70 MHz from the center of the SBS gain curve with a 100 μW threshold, a 1% variation in the cavity loss will result in a 680 Hz offset change.

This source of drift can be eliminated by thermally tuning the SBS gain curve so that the cavity resonance is in the center of the gain curve, since the dispersion is zero there.

4.5.6 Other Possible Error Sources for the Δq Gyroscope

Though thermally and dispersively driven drifts appear to limit the present performance of the Δq SBS fiber RLG, there are a number of other error sources which may become important as the performance improves. These errors include eigenpolarization mismatch between the SBS lasers which would reduce reciprocity between the SBS lasers, eigenpolarization mismatch between the pump and the SBS laser which could lead to polarization pulling, frequency pulls due to frequency dependent backscattering, and excess phase noise due to finite common mode suppression of cavity jitter. In Section 6.1, other techniques will be suggested for the implementation of a Δq gyroscope.

4.6 Demonstration of TD-NRS

Another method to reduce or eliminate the backscattering-induced coupling between the counterpropagating lasers in an RLG is through the introduction of a time dependent NRPS.

To understand the time dependent NRPS, first we will consider a single phase modulator attached to a straight piece of fiber, as shown in Fig. 4.31(a). Initially, the net phase through the fiber is ϕ_o, and at time $t = 0$, a linear phase sweep is applied to the fiber by the modulator so the phase becomes,

$$\phi(t) = \phi_o + kt \tag{4.26}$$

where k is the magnitude of the phase sweep.

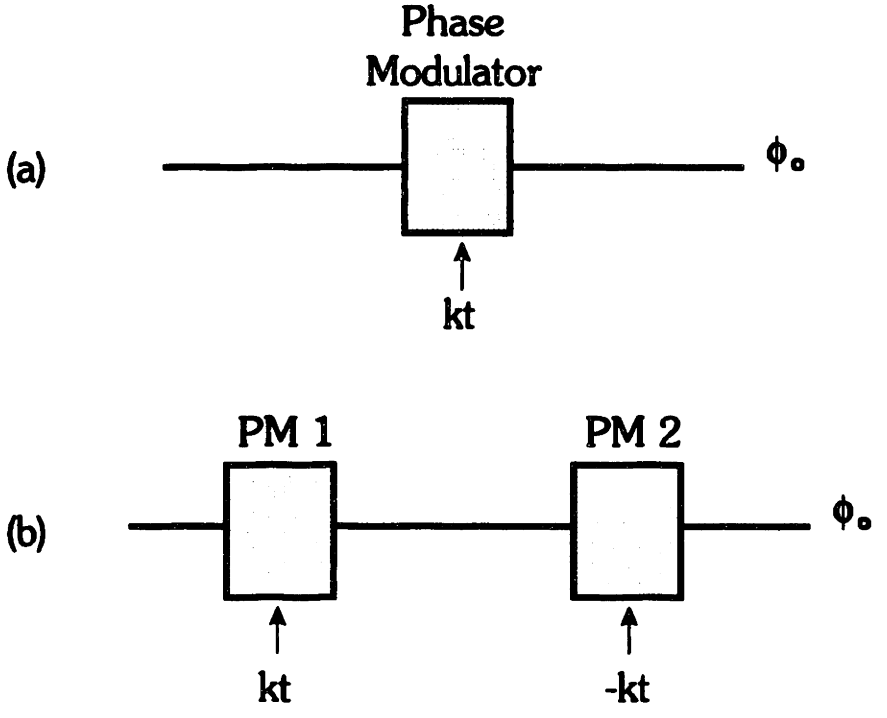

Figure 4.31 Demonstration of time dependent, nonreciprocal phase shift.

If a second modulator is added some distance L away and driven with the same magnitude phase shift, but opposite in sign, as shown in Fig. 4.31(b), the total observed phase shift, $\phi^+(t)$ becomes,

$$\phi^+(t) = \phi_o + kt - k\left(t + \frac{L}{c}\right) = \phi_o - k\left(\frac{L}{c}\right) \tag{4.27}$$

where c is the speed of light in the medium, and L/c is the time delay between the modulators. Hence, the residual phase shift is due to the time delay experienced by the light as it travels between the modulators. However, if the phase shift is observed along the opposite direction, the measured phase shift $\phi^-(t)$ is given by,

$$\phi^-(t) = \phi_o - kt + k\left(t + \frac{L}{c}\right) = \phi_o + k\left(\frac{L}{c}\right) \tag{4.28}$$

Thus, the sign of the residual phase shift changes with direction of propagation.

Therefore, by placing two such modulators on the fiber of a fiber ring cavity, as shown in Fig. 4.32, a NRPS can be generated which is similar to that generated by an applied rotation. Thus, these phase modulators can be used to dither the cavity by optical, rather than mechanical means.

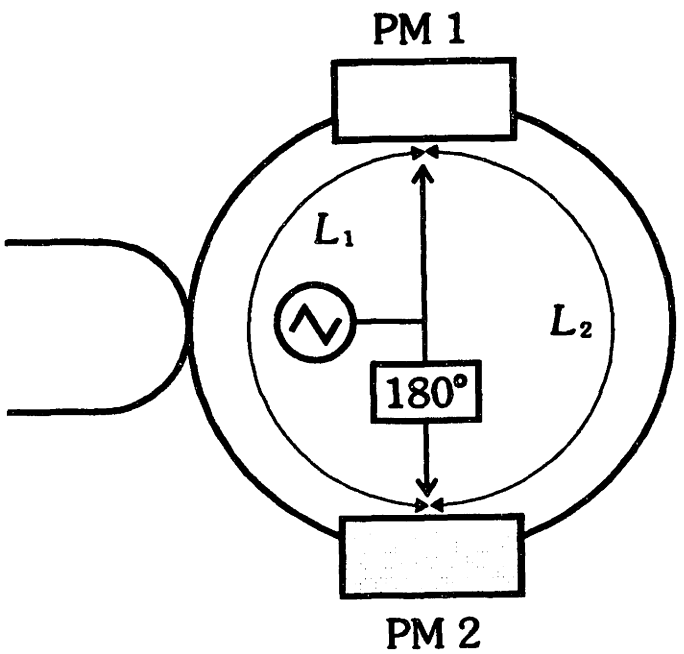

Figure 4.32 Ring cavity with attached phase modulator for TD-NRS.

Unlike mechanical dither, where very large peak phase differences can be easily generated between the paths, on the order of 6000 radian, this time dependent dither can only generate a NRPS of about 6 radians with the PZT phase modulators that are available to us. Thus, in its present form, it is not very suitable for generating the large alternating bias needed for lock-in elimination in our present setup.

4.6.1 Sinusoidal Suppression

One method for eliminating the coupling between the lasers is to sinusoidally modulate the difference frequency between the lasers, i.e, the creation of a time dependent, nonreciprocal suppression, TD-NRS. Recall that if the difference frequency between two lasers is sinusoidally modulated, the spectrum of the beatnote between the lasers has components at harmonics of the modulation frequency, with the amplitude of the m^{th} harmonic given by $J_m(\phi)$, where J_m is the m^{th} order Bessel function of the first kind, and ϕ is the phase excursion of the modulation. Figure 4.33 shows the magnitude of the spectrum between such sinusoidally modulated lasers for a variety of phase excursions. As seen in Fig. 4.33(c), by carefully adjusting the depth of modulation, the component at f_d, the unmodulated difference frequency between the beams, given by $J_0(\phi)$, can be made to go to zero, at $\phi \approx 2.41$. Thus, all the coupling between the lasers occurs at harmonics of the modulation frequency, and there is no coupling between the lasers at the original difference frequency.

This suppression technique can be used in any RLG. In our case, a sinusoidal NRPS may be applied to the RLG, to generate a sinusoidal frequency modulation of the beat frequency between the lasers. By adjusting the depth of this modulation, ϕ, to be approximately 2.41, the low frequency coupling between the lasers will be eliminated. Further, by choosing the modulation frequency to be much greater than the width of the lock-in zone, the lock-in zone can be completely eliminated for low rotation rates. However, there is still coupling between the lasers at the harmonics of the modulation frequency, thus, smaller lock-in zones will be observed for Δfs that are around these harmonics.

This technique was first suggested and demonstrated for a bulk-optic RLG,[61] and a similar technique is used to prevent spatial hole burning in

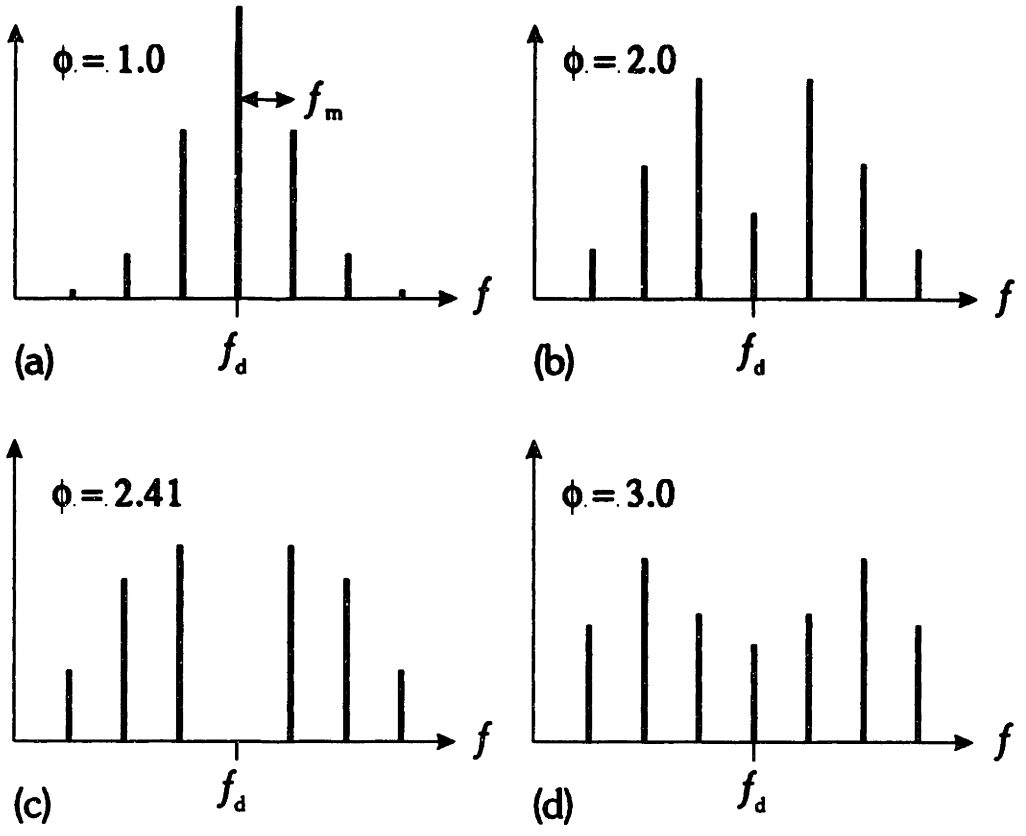

Figure 4.33 Magnitude of the spectrum of the a sinusoidally modulated laser beatnote.

solid-state lasers.[62] The technique is well suited to a fiber RLG since the phase modulators can be implemented using PZTs attached to the optical fiber, thus no additional components need to be added to the fiber cavity.[28]

One concern with TD-NRS is the placement of the phase modulators. For the elimination of lock-in, the coupling between the lasers must be prevented over the entire length of the cavity, however, until now, we have only considered suppression of the coupling at the output of the cavity. The NRPS induced by the phase modulators is proportional to the time delay, hence the separation, between the modulators. In this way, as viewed from the coupler labeled 1 in Fig. 4.34, the NRPS is proportional to L_2. Similarly, as viewed

from the coupler labeled **2**, the NRPS is proportional to L_1. Thus, for complete suppression, $L_1 = L_2 = L/2$. If the spacing between the modulators is not correct, then simultaneous suppression of lock-in due to the backscatter from both halves of the cavity will not be possible.

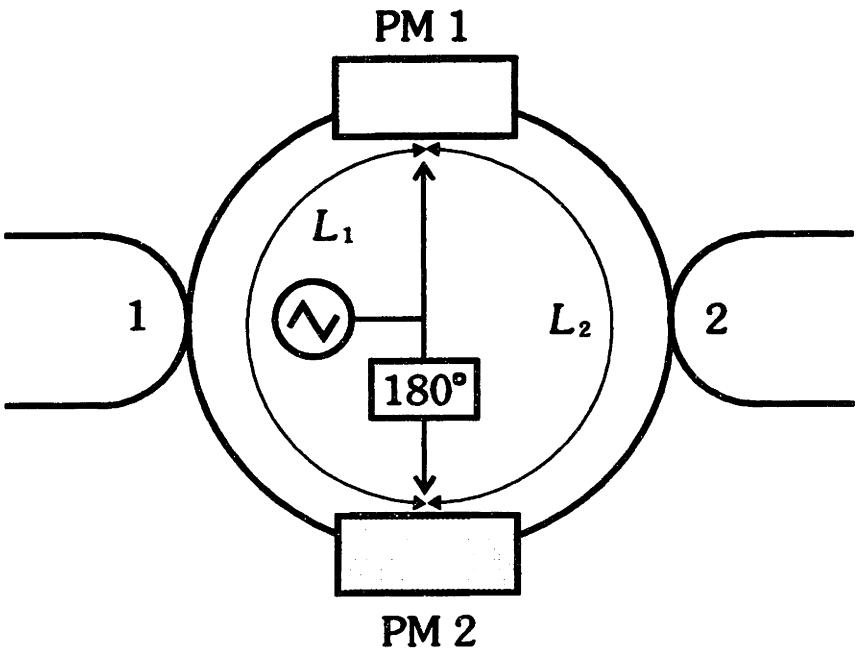

Figure 4.34 Fiber ring cavity with phase modulators attached for TD-NRS.

4.6.2 Generation of a TD-NRS

In order to generate a NRPS of the required size, as discussed above, two very well matched, large phase modulations must be applied to the fiber cavity at the correct spacing. In our case, the phase modulations were applied to the cavity using PZTs which drove a mechanical resonance in a small length of the optical fiber. Figure 4.35 demonstrates our ability to generate large, well matched phase modulations at a 35 kHz rate. A close-up of the cavity resonance ($F \approx 170$) in Fig. 4.35(a), shows the cavity without modulation,

demonstrating only the effects of laser noise and room acoustics on the cavity resonance. With a drive applied to only one of the PZT modulators, in Fig. 4.35(b), the cavity resonance frequency is swept by almost an entire FSR, indicating a phase modulation of almost $\pm\pi$ is being applied, which is significantly larger than the required ± 2.41 radians. In Fig. 4.35(c), both modulators are driven and they are adjusted to minimize the residual modulation of the resonance. As seen in the figure, the modulators can be well matched even for this large reciprocal phase modulation, and only a small amount of residual amplitude or frequency modulation is observed.

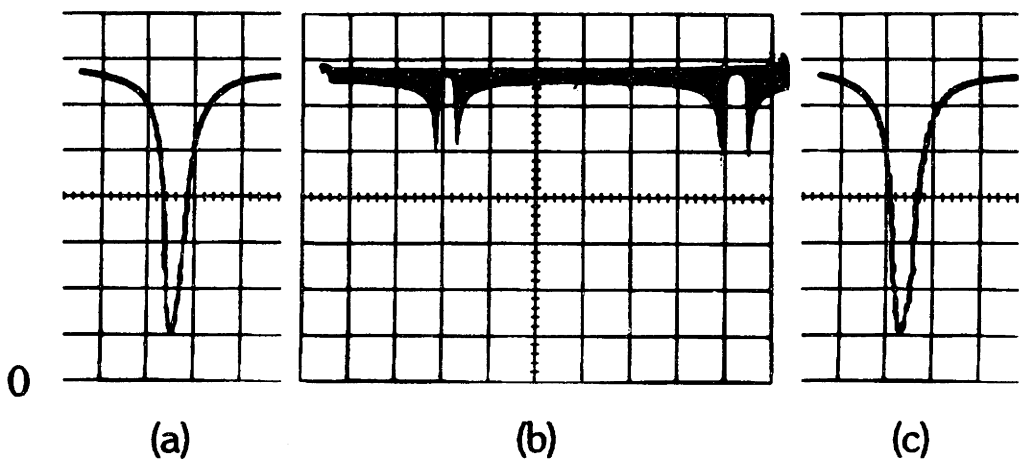

Figure 4.35 The cavity resonance scans (a) without phase modulation, (b) with a single phase modulator and (c) with both phase modulators. Cavity D.

To demonstrate that this cavity modulation is producing a NRPS and not simply modulating the frequency of the cavity, the beatnote between the SBS lasers can be directly observed, using the setup in Fig. 4.36. Note that simply modulating the cavity with a single phase modulator, i.e., applying a NRPS, would put the same frequency modulation on both of the lasers, and would leave the beatnote unchanged. To more easily observe the SBS

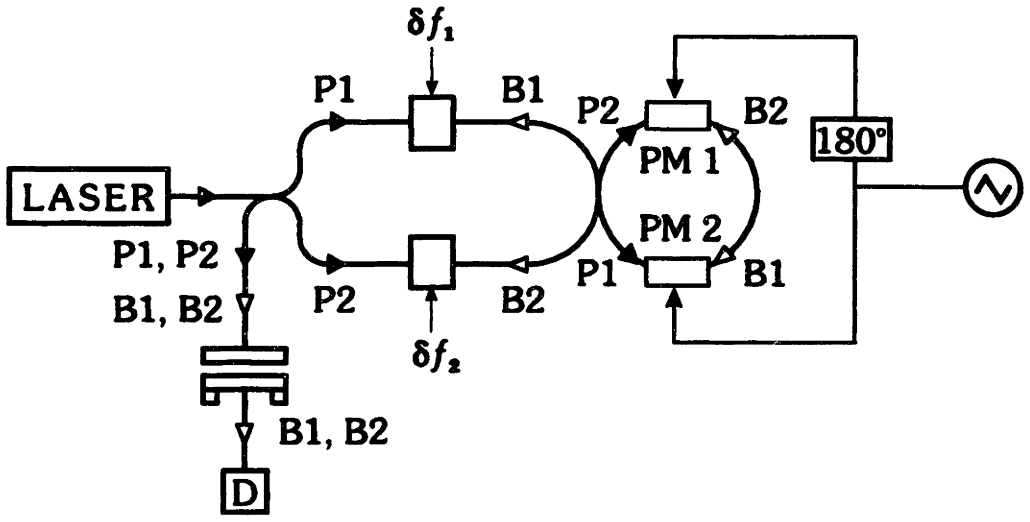

Figure 4.36 Schematic diagram of an SBS fiber RLG with phase shifters for TD-NRS.

beatnote in the absence of rotation, a small frequency difference, around 100 Hz, is introduced using the frequency shifters in the cavity arms, shown in Fig. 4.36. In the absence of NRPS, shown in Fig. 4.37(a), a beat frequency is observed at the applied frequency difference. When a small NRPS is then applied to the cavity, Fig. 4.37(b), frequency modulation of the beat is observed, and as the depth of the NRPS is increased, Fig. 4.37(c), the observed frequency modulation also increases.

4.6.3 TD-NRS for Lock-in Suppression

Lock-in suppression using TD-NRS can be demonstrated using an SBS fiber RLG operated around 633 nm. Similar to the gyroscope at 1.3 μm, a frequency bias of 10 kHz is introduced between the SBS lasers using frequency shifters in the output arms of the cavity, as shown in Fig. 4.36. The rotation signal is recovered by digitizing the output of detector D, using a FFT to find the spectrum of the signal, and measuring the frequency of the beat between the SBS lasers from this spectrum. Note that with the TD-NRS

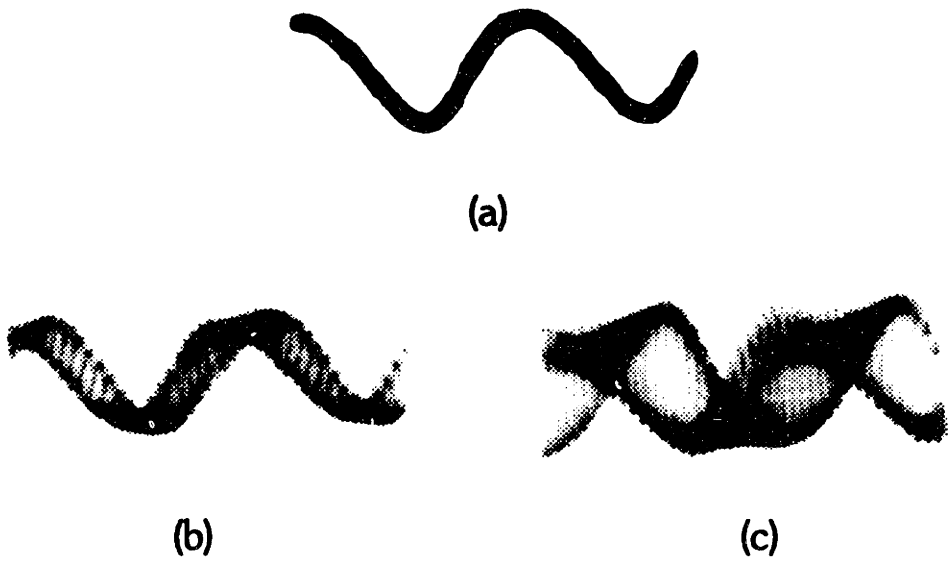

Figure 4.37 Beatnote between SBS lasers with a small frequency bias (a) in the absence of a NRPS, (b) with light NRPS, and (c) with moderate NRPS. Cavity H.

applied, the beatnote at the bias frequency, i.e., 10 kHz, will be suppressed, so the beatnote at one of the sidebands of the suppression frequency, in this case at $f_b = 10$ kHz $\pm$ 35 kHz, must be used.

The effect of TD-NRS will be demonstrated by applying a large rotation to the cavity, which should produce a rotation signal of $\pm$10 kHz. In the absence of the TD-NRS, no rotation signal is observed from the cavity, indicating that the lock-in zone is greater than 10 kHz. However, when the TD-NRS at 33 kHz is quickly turned on, a rotation signal is observed, centered on 43 kHz, as shown in Fig. 4.38(b). The fitted curve over the rotation data demonstrates a $\sim$ 1 kHz residual lock-in zone, thus a reduction of the lock-in zone by at least a factor of 10.

The effect of misadjustment in the depth of the TD-NRS is shown in Fig. 4.38(a) and 4.38(c), which were taken immediately before Fig. 4.38(b). In Fig. 4.38(a), the TD-NRS is initially too small, and a larger residual lock-in range, about 3 kHz, is observed, as compared to Fig. 4.38(b). Similarly, with the modulation depth too large, shown in Fig. 4.38(c), again a larger residual lock-in zone, in this case about 4 kHz, is also observed. Thus, for best suppression, the depth of the TD-NRS modulation must be carefully adjusted.

TD-NRS has also been demonstrated using the lower scattering cavities at 1.3 μm, using a setup similar to Fig. 4.36. In this case, due to the smaller lock-in zone and the narrower linewidth of the cavity, a suppression frequency, f_d, of 10 kHz is used with an external frequency bias, f_b, of 7 kHz. Figure 4.39(b) shows the measured Δf for a cavity mode without TD-NRS, with a lock-in zone of approximately 1.3 kHz. With the TD-NRS applied to the cavity, Fig. 4.39(a), the size of the lock-in zone drops to approximately 350 Hz, a reduction by a factor of almost 4.

It is also important to note that the phase and amplitude of the PZTs must be very precisely aligned. Since the PZTs generate such large phase excursions, even a very small misadjustment in the relative amplitudes of the PZT drives will result in a large, reciprocal modulation of the cavity resonance. For example, with the PZTs driven for complete lock-in suppression, a 1% misadjustment in the amplitude to one of the PZTs results in a peak-to-peak frequency modulation cavity of 150 kHz, twice the linewidth of the cavity. Figure 4.40 shows the result of a slight misadjustment of the PZT drives on the observed SBS beat, using the same setup as Fig. 4.37. In Fig. 4.40(a), a small NRPS is applied to the cavity and the PZT drives are adjusted for best performance, thus, a clean frequency modulation is observed. In Fig. 4.40(b), a small misadjustment is made in the drive amplitude to one of the PZTs, and significant amounts of amplitude modulation

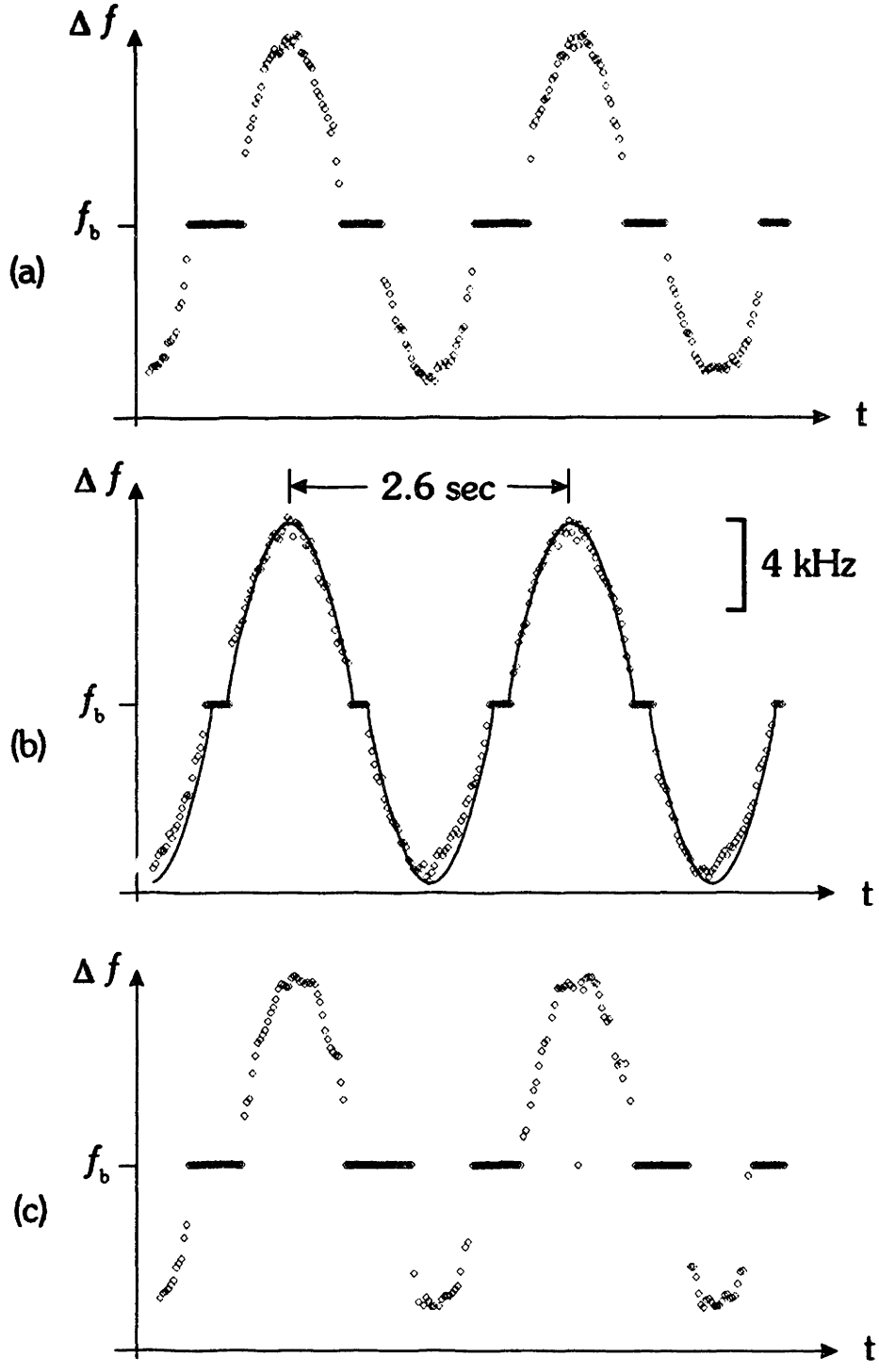

Figure 4.38 Measured rotation from an SBS RLG with (a) too little NRPS, (b) adjusted NRPS, and (c) too much NRPS. Cavity E.

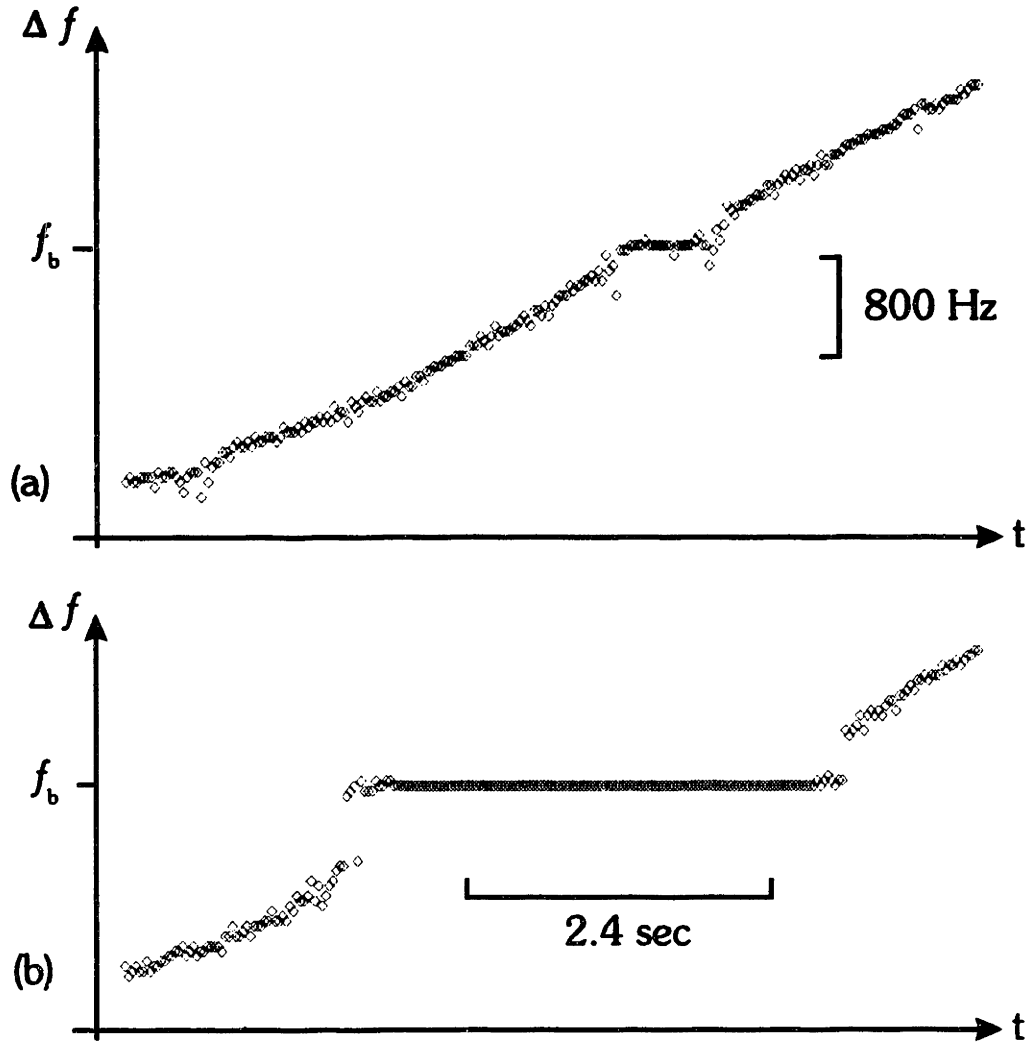

Figure 4.39 IR SBS fiber RLG (a) without TD-NRS and (b) with TD-NRS. Cavity H.

are immediately observed. Thus, the correct adjustment of the drives to the PZTs is very important.

4.6.4 Limitations of Lock-in Suppression

There are several factors which limit the observed lock-in suppression at both 633 nm and 1.3 μm. They include the mislocation of the PZTs, back-scattering from within the modulators, distortions of the modulation drives,

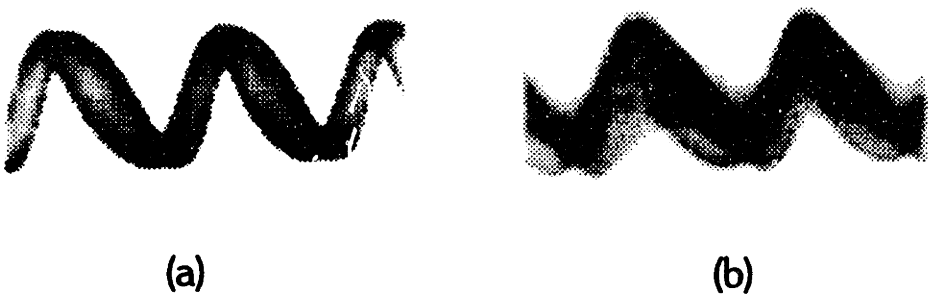

Figure 4.40 Beat note between SBS lasers with a small frequency bias (a) with light dither, and (b) with misadjusted dither. Cavity H.

modulator nonlinearities, residual amplitude modulation from the modulators, and modulation leakage.

As mentioned in Section 4.6.1, for complete suppression of lock-in from backscattering from both sections of the fiber, the modulators must be located exactly $L/2$ apart, where L is the length of the cavity. For example, assuming the backscattering is evenly distributed, a misplacement of 0.15 m in the location of a modulator at 633 nm, or 0.50 m at 1.3 μm, will result in only 90% lock-in zone suppression. In our present setup, the separation between the modulators could only be determined to within ± 0.1 m. However, at 633 nm, we adjusted separation between the modulators ± 0.08 m without improving the suppression performance, indicating that there are other factors limiting the suppression.

Even with perfect modulator placement, lock-in due to backscattering from within the modulators will not be completely suppressed. Qualitatively, the amount of NRPS within the modulators varies from a maximum at the ends, to zero in the middle. Thus, depending of the exact position of the scattering within the modulator, its effect on the lock-in will vary. Further, the addition of the phase modulators to the cavity caused a noticeable increase in the observed backscattering, both at 633 nm and 1.3 μm. Thus,

depending on the exact location of this increased scattering, its effect on the observed residual lock-in could be large.

Modulator nonlinearities, modulator drive distortions, and residual amplitude modulation from the phase shifters can all limit the suppression that can be obtained, by preventing complete elimination of the carrier.

Though the modulation was applied directly to the cavity fiber, some of the modulation could also be coupled, either through the fiber cavity base or through the air, into other parts of the cavity or input arms. Such additional modulations would have the effect of changing the modulation depth in different parts of the fiber cavity. Thus, the backscatter suppression could vary throughout the cavity.

We believe that the suppression performance at 633 nm was limited by modulator placement accuracy, and scattering from within the modulators. The suppression performance at 1.3 μm was limited by the scattering from within the modulators, modulation leakage, and distortions due to the modulators.

In addition, the required NRPS for best suppression of lock-in was observed to vary from mode to mode, and with time for the same mode. Such variations were larger than what could be attributed to modulator variations. These variations have been attributed to changes in the size of the lock-in zone due to backscatter variations. If the size of the lock-in zone is comparable to the TD-NRS frequency, the lock-in causes a reduction in the observed frequency difference between the lasers for a given NRPS, as shown in Eq. (4.25). In this case, this causes a reduction in the frequency excursion for a given modulation depth, thus changing the required modulation depth for complete J_0 suppression.

4.6.5 Suppression Requirements for Navigation Grade Performance

For a practical gyroscope, there are several issues with TD-NRS that must be addressed. First, for navigation grade performance the lock-in zone must be suppressed by a factor of about 10^6, and with TD-NRS, this would require the modulation depths remain constant to within a part in 10^6 of their optimum value. Second, the tolerable distortions, either due to the drive signal asymmetries or modulator nonlinearities would have to be on the same order. Third, the modulator separation would also have to be adjusted to similar accuracy, e.g., on a 10 m cavity to within 10 μm.

Even if the modulators and their drives are stable to within a part in 10^6, variations in the lock-in zone will also cause variations in the apparent depth of the modulation, as previously discussed in Section 4.6.4. For the variation in the apparent modulation depth to be less than the part in 10^6 limit, the separation between the dither frequency and the maximum lock-in range would have to be a factor of 1000, which is impractical for a fiber RLG.

One method to reduce the requirements on the TD-NRS is to use more than one pair of modulators. Since the suppression of the lock-in is multiplicative, by using two, or more, pairs of modulators at different frequencies, the requirements on each individual dither can be greatly reduced. For example, with two TD-NRSs, suppression of only 10^3 is required for each. In addition, residual lock-in due to scattering from within one set of modulators is suppressed by the second pair of modulators. Also, both suppressions would not have to be generated using TD-NRS, but could be a hybrid of TD-NRS and, for example, an optical Kerr effect suppression[63] or a mechanical dither.

The use of multiple frequency modulations, either all using TD-NRS or a hybrid of suppression schemes, however, would require careful consideration

of signal-to-noise issues. With a single suppression, the optical power that used to be in a single sideband is now spread essentially equally among four sidebands. If two dithers are used, sixteen sidebands of approximately equal amplitude are now generated.

4.7 Preliminary SBS RLG Drift Performance

Since bias and bias variations are important errors for the RLG, some preliminary data on bias performance for the $\Delta q = 0$ SBS fiber RLG is presented in this section, even though we have lock-in.

One method for measuring the bias and its variation is to apply a fixed rotation to the RLG, using a precision rotation table, and measuring the corresponding difference frequency, Δf, and the variation in Δf. Although this method is suitable for an RLG with lock-in, unfortunately, we do not have access to such a precision table.

A more accessible method to us is to apply a sinusoidal mechanical rotation to the RLG similar to that used in Fig. 4.11, and examine the peak frequency excursions above and below lock-in. Asymmetry in these excursions would indicate a bias, and symmetric changes would indicate either a scale factor variation or a change in the size of the lock-in zone.

Using the setup previously shown in Fig. 4.10, Δf was observed as a function of time. Figure 4.41 shows Δf for a 12 minute period with the cavity only perturbed by fluctuations in room temperature. As seen in the figure, the measured asymmetry throughout the run was within the 50 Hz observed fluctuations on Δf, which were in part due to noise in the applied rotation. The symmetric changes in Δf were approximately 100 Hz, and were probably due to lock-in variations which have been shown to be very sensitive to cavity perturbations, as discussed in Section 4.3.2.

These preliminary test show that for the $\Delta q = 0$ gyroscope, the bias is not very large, but clearly, more careful measurements need to be carried

out to determine the magnitude and variations of the bias, as well as the sources of such a bias. In the $\Delta q = 0$ configuration, the bias is expected to be very small, primarily influenced by the optical Kerr effect, discussed in Section 4.8.1.

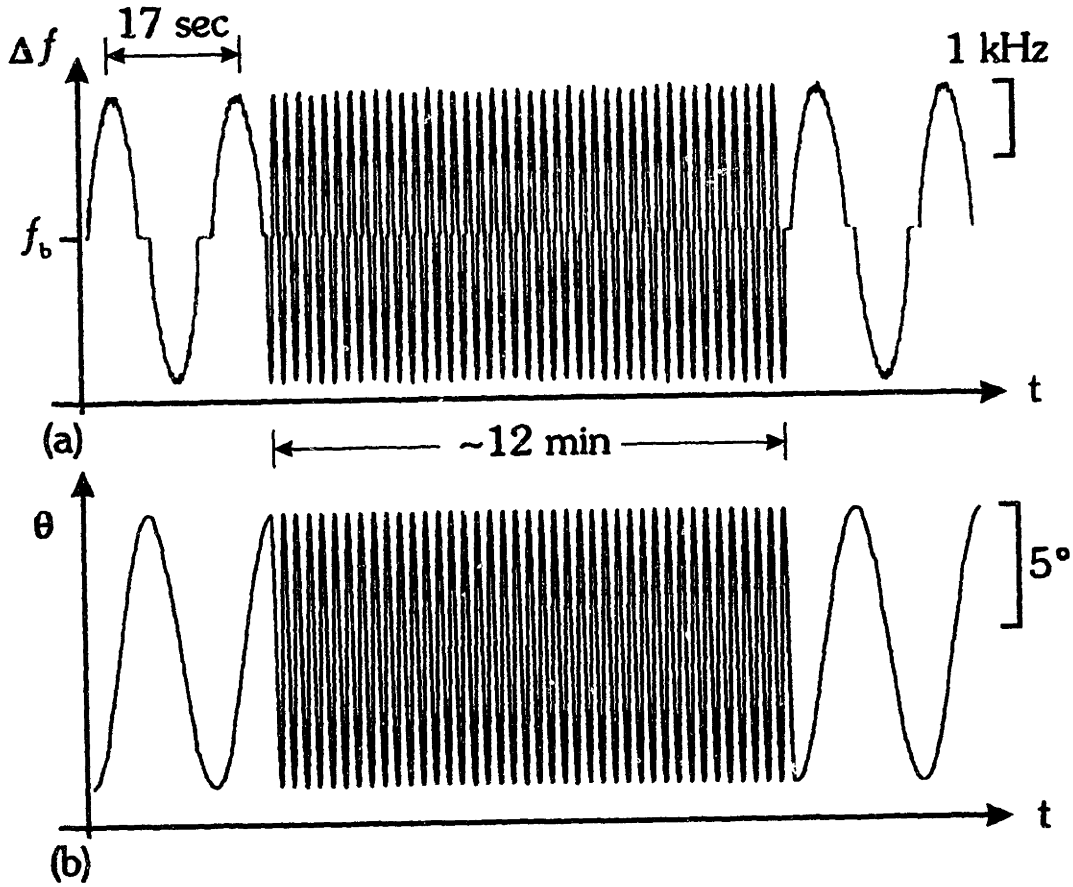

Figure 4.41 SBS RLG output with applied rotation over a 12 minute period. Cavity H.

4.8 Other Error Sources for the SBS RLG

In addition to lock-in, there are a number of other error sources for the $\Delta q = 0$ RLG which must be avoided for proper operation. In this sec-

tion, some of these error sources will be discussed, and possible solutions suggested.[64]

4.8.1 Optical Kerr Effect

One source of offset and drift in the RLG is due to the third order nonlinear optical process, the optical Kerr effect.[65,66] The optical Kerr effect causes an intensity dependent index change for counterpropagating beams. The index change for the CW beam can be written as,

$$\Delta n_{cw} = \beta_o(I_{cw} + 2I_{ccw}) \tag{4.29}$$

where I_{cw} and I_{ccw} are the intensities in the CW and CCW directions, and

$$\beta_o = \frac{48\pi^2\chi^{(3)}}{n^2c} \tag{4.30}$$

Similarly, for the CCW direction, the index change is given by,

$$\Delta n_{ccw} = \beta_o(I_{ccw} + 2I_{cw}) \tag{4.31}$$

Thus, the change in the resonant frequency in the CW direction, δf_{cw}, is given by,

$$\begin{aligned}
\delta f_{cw} &= -f_L \frac{\Delta n_{cw}}{n_{cw}} \\
&= -\frac{qc}{n_{cw}L}\frac{\Delta n_{cw}}{n_{cw}} \\
&= -\frac{qc}{n_{cw}^2 L}\Delta n_{cw} \\
&= -\frac{qc}{n_{cw}^2 L}\beta_o(I_{cw} + 2I_{ccw})
\end{aligned} \tag{4.32}$$

where f_L is optical frequency, q is the longitudinal mode number, and L is the length of the cavity. Similarly, the change in resonant frequency for the CCW direction is given by,

$$\delta f_{ccw} = -\frac{qc}{n_{ccw}^2 L}\beta_o(I_{ccw} + 2I_{cw}) \tag{4.33}$$

Thus, the resulting frequency difference between resonances in the counter-propagating direction of the cavity, Δf_{kerr}, is given by,

$$\Delta f_{kerr} = \delta f_{cw} - \delta f_{ccw} = \frac{qc}{n^2 L}\beta_o(I_{cw} - I_{ccw}) \tag{4.34}$$

The circulating intensities inside the cavity on resonance can be simply related to the output power, W_{cw} and W_{ccw} in the CW and CCW directions, respectively, given by,

$$I_{cw} = \frac{F}{\pi}\frac{W_{cw}}{S} \tag{4.35}$$

and

$$I_{ccw} = \frac{F}{\pi}\frac{W_{ccw}}{S} \tag{4.36}$$

where S is the effective core area of the fiber. Combining Eq. (4.35) and (4.36) with Eq. (4.34) yields,

$$\Delta f_{kerr} = \frac{qcF}{\pi S n^2 L}\beta_o \Delta W = f_L \frac{F}{\pi n S}\beta_o \Delta W \tag{4.37}$$

where $\Delta W = W_{cw} - W_{ccw}$. Evaluating this offset for a cavity with $F = 70$, $n = 1.5$, $S = \pi\,(2.5 \times 10^{-6}\ \text{m})^2$, and $\beta_o = 7.4 \times 10^{-20}$ m/W, yields approximately 28 Hz/μW.

The optical Kerr effect is most easily observed using either a $\Delta q \neq 0$ gyroscope, or a passive resonator gyroscope. In this case, the Kerr effect was measured using both a Δq SBS fiber RLG and a passive resonator gyroscope operated at $\Delta q \neq 0$.

In the Δq SBS fiber RLG, the optical Kerr effect can be measured by alternately reducing the pump powers in the two directions of the cavity, which in turn reduces the corresponding SBS laser powers. Figure 4.42(a) shows amplitude of the beat between two SBS lasers which was used to measure the SBS laser intensity, and Fig. 4.42(b) shows the beat frequency,

Δf. Initially, the intensity of the SBS lasers are approximately matched, and the unperturbed beat frequency is measured. In the second section, the pump laser in the CW direction is attenuated, which reduces the intensity of the SBS laser in the CW direction, causing an increase in Δf. Similarly, the intensity of the SBS laser in the CCW direction is then attenuated, resulting in a reduction in Δf. Finally, when the SBS lasers in the CW and CCW directions are both attenuated, no change in Δf is observed. In this case, the frequency offset was measured to be approximately 7 Hz/μW, which is close to the value predicted by Eq. (4.37) for this cavity, which was overcoupled.

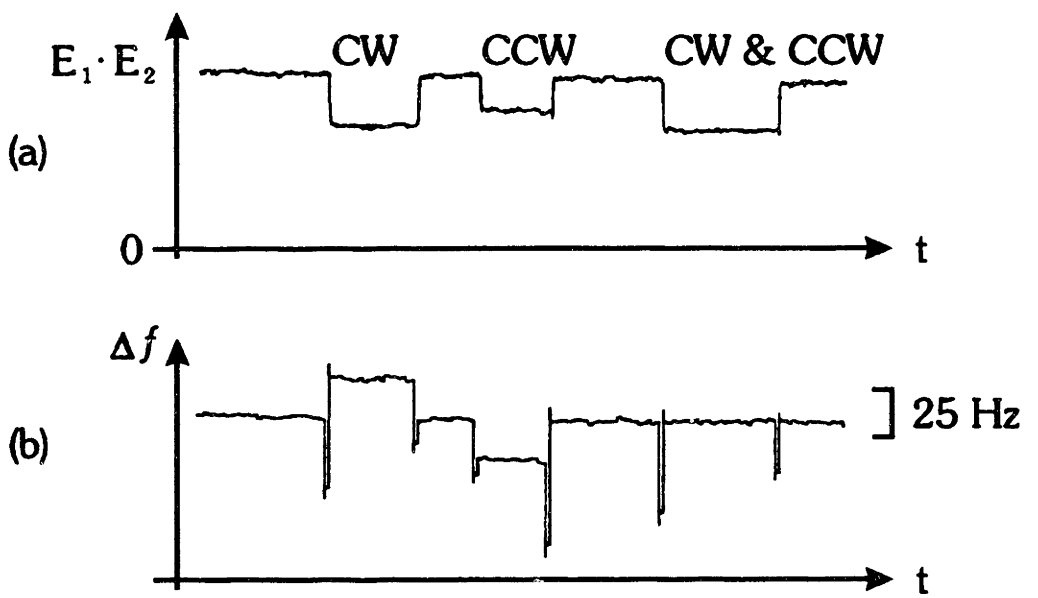

Figure 4.42 Measurement of the optical Kerr effect using a separated mode SBS fiber RLG. Cavity G.

The optical Kerr effect can also be measured in a passive resonator gyroscope. In the passive gyroscope, servos are used to lock both beams to the center of their respective resonances, and the difference frequency between the lasers is used as the gyroscope output. As shown in Fig. 4.43, as the intensity of the beams in the cavity are misbalanced, first by attenuating

the beam in the CW direction, labeled **1**, and then the CCW direction, labeled **2**. As the intensities in the opposite directions of the cavity are attenuated, the frequency difference between the beams also changes. In this case, the optical Kerr effect caused a 25 Hz/μW of input power change in the frequency of the cavity resonance, in good agreement with the value predicted by Eq. (4.37). Further, the sign of the measured Kerr effect is consistent with the observed Sagnac effect in this cavity. In addition, the measurement of the optical Kerr effect using SBS lasers yields the same frequency sensitivity to intensity misbalance.

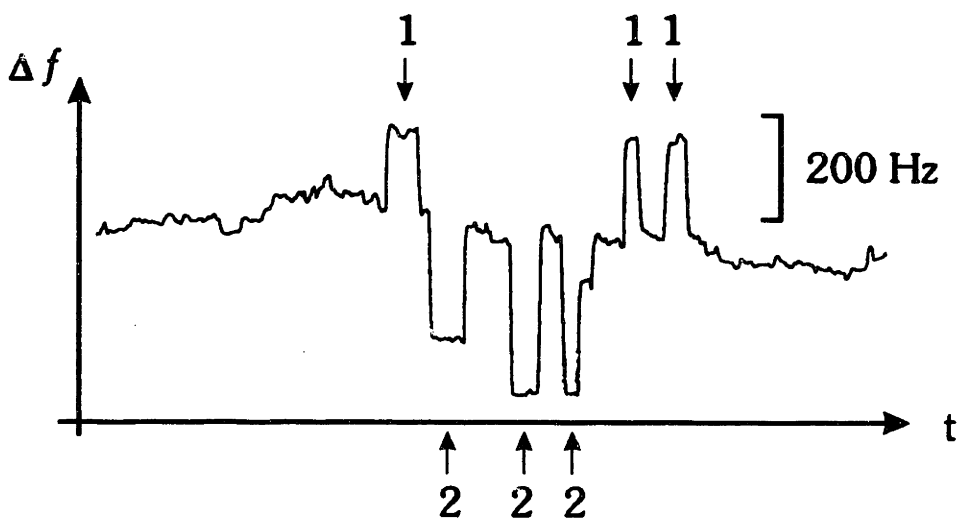

Figure 4.43 Demonstration of the optical Kerr effect in a passive resonator gyroscope. Cavity B.

One method for the elimination of the optical Kerr effect is to use a servo to adjust the relative intensities of the SBS lasers by adjusting their respective pump intensities. Since the absolute intensity of each of the lasers does not have to be controlled, instead of directly measuring the intensity of each SBS laser, the intensities of both the pumps are modulated by the same amount. If there is a difference in the power in the SBS lasers, this power

difference will also be modulated, and the beat frequency between the lasers will have a component at the modulation frequency. The modulation of the beat frequency can be detected using a PSD and used to adjust the relative intensities of the pump lasers. It should be noted that this servo would also have to be fast enough to compensate for intensity changes caused by an applied rotation.

4.8.2 Additional Error Sources

There are a number of smaller error sources for the SBS RLG that may become important as the performance improves. For example, magnetic fields can cause an NRPS, and may require magnetic shielding of the fiber, similar to that used in fiber interferometer gyroscopes. Also, similar to errors observed in interferometer gyroscopes, special winding techniques for the fiber cavity may have to be used to avoid errors due to thermal and stress gradients, i.e., the Shupe effect[68,67], especially for longer cavities. Finally, backscattering can also lead to significant scale factor nonlinearities.[69]

4.9 Experimental Considerations

In this section, some of the details of the various setups and procedures used in this chapter will be presented.

4.9.1 Optical Layout

As with the solitary SBS laser and the common cavity SBS lasers, the optical setup for the SBS fiber RLGs was also a hybrid of bulk-optic and fiber-optic components, as shown schematically in Fig. 4.44, and in the photo in Fig. 4.45. The A/O frequency shifters were driven from very stable frequency synthesizers so that the frequency difference between them, used to bias the SBS beat frequency, was stable to better than 1 Hz, and thus did not significantly contribute to the observed drifts. For Δq operation with a small

frequency difference between the lasers, e.g., 0 to 30 MHz, the difference in the frequencies of the A/O drives can simply be adjusted by this amount, which will require realignment of the A/Os. For large frequency differences, the sign of the frequency shift in one of the two A/Os can be changed by realigning it. In this way, frequency differences between 60 MHz and 120 MHz were reachable with nominally 40 MHz A/Os.

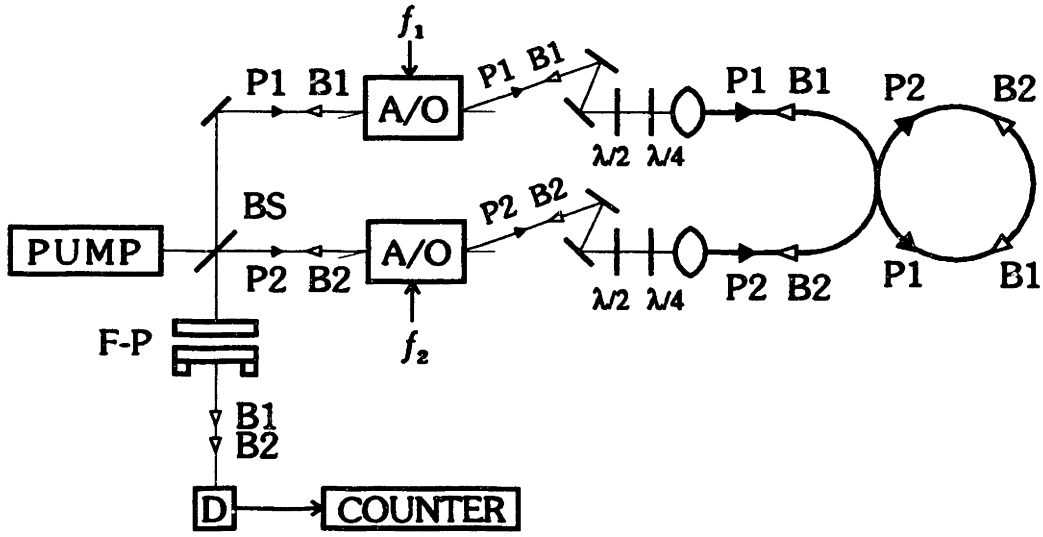

Figure 4.44 Detailed optical setup for an SBS fiber RLG.

Since both pump beams were derived from a single pump laser, only a single servo was needed to lock both beams to cavity resonances, as shown in Fig. 4.46. As previously described, a combination PZT and heater servo was used, as shown in the figure, to extend the length of the data runs. A second servo configuration was used at 1.3 μm, with the "fast" servo feedback to the laser, and the slow feedback to the cavity heater. This arrangement was primarily used to reduce the number of PZTs mounted to the fiber cavity, since there was a noticeable increase in the cavity backscattering with the addition of each PZT.

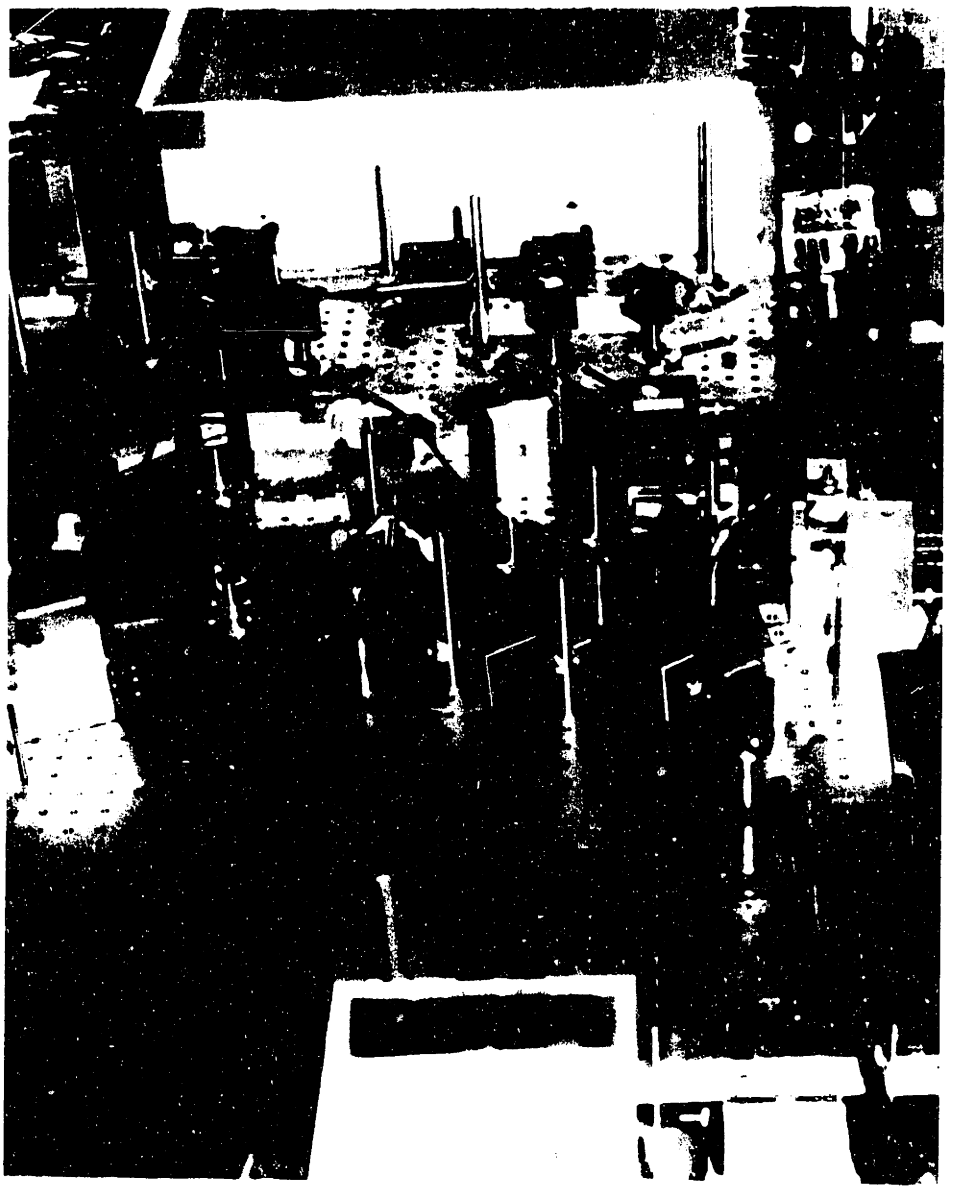

Figure 4.45 Photograph of a typical SBS fiber RLG setup with the pump laser at the bottom and the cavity enclosure at the top.

The choice of modulation frequencies for the RLG is difficult, particularly when optical dither is used. Between the bias frequency, the harmonics of the dither frequency, and the changes in these frequencies as a function of rotation, there are few good choices for the servo modulation frequency. At both 633 nm and 1.3 μm, the servo modulation was changed to be com-

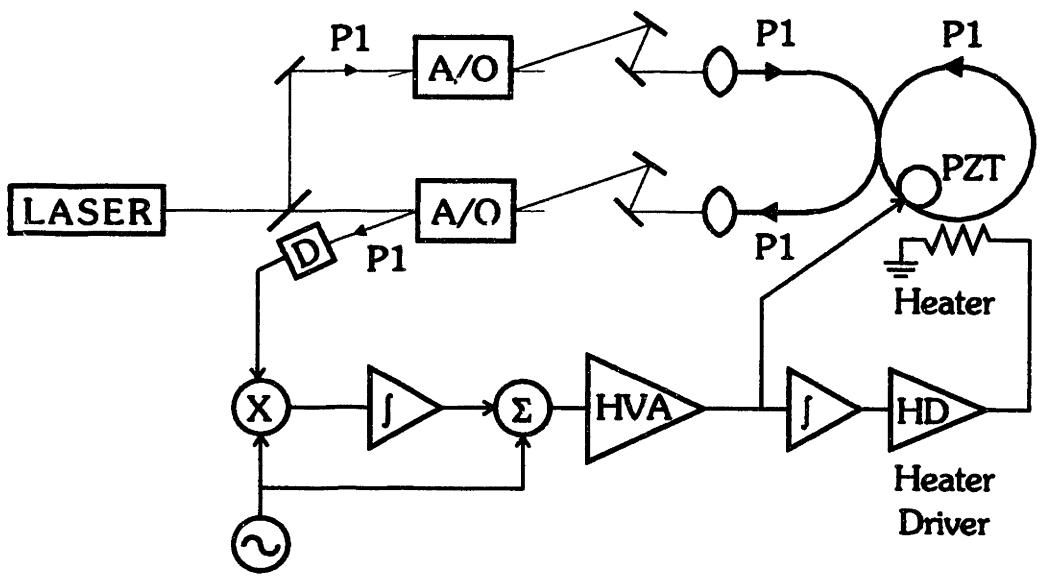

Figure 4.46 Detailed optical setup for SBS RLG with servo.

parable with the cavity linewidth, i.e., 100 kHz for 633 nm and 40 kHz for 1.3 μm, in order to minimize interference.

The rotation table that the fiber cavity was mounted on consisted of a small plate mounted on a precision bearing. The table was driven with a variable speed, DC electric motor which had a disk mounted to its drive shaft. A pin was mounted off-center in this disk, and was connected to the rotation stage with a long copper wire. The restoring force for the table was provided by a stiff spring.

Though this apparatus was used for all the rotation data in this thesis, there were some practical problems with it. First, as the motor made the transition from pulling the rotation table, to being pulled by the table, gear lash in the motor caused a glitch in the rotation. To avoid the glitch, a makeshift brake was installed on the motor, so the motor was continually loaded. While this avoided the gear lash, it also forced the motor to drive

a much larger load than strictly necessary. In addition, the brake tension required frequent readjustment.

Several alternate schemes could be used for the rotation. First, a weak torsion spring can be used to generate a slow sinusoidal rotation, which has the advantage of simplicity and, if driven on resonance, only a very weak drive is required. A second alternative is the use of a high resolution stepper motor, and mounting the cavity directly on the motor shaft. This technique has the advantage of being able to produce a very flexible rotation pattern, however, steps may have to be taken to smooth out any residual "steps" in the rotation. Third, a rotation table could also be used.

In Section 4.5.2, the pump laser **Pump 3** was asymmetrically coupled in to the fiber cavity. One method for achieving this asymmetry was to use a beam splitter that was not exactly 50/50, for example a 60/40 beamsplitter. In this way, the primary pump power in the cavity could be equalized by misadjusting one of the fiber inputs, for example the coupling could be 40% and 60% for the two fiber input couplings for a net coupling of 24% in both arms. **Pump 3**, however, since it is using the beamsplitter from the opposite side, would see a beamsplitter coupling of 40/60, and fiber couplings of 40% and 60% for a net coupling of 16% and 36% for the two arms.

It should also be noted that the extra pump laser, **Pump 3**, does not have to be coupled into the same eigenpolarization as the main pump laser. In this way, the cross coupling between the SBS gain in the two eigenpolarizations can be measured. The dispersion pull with the **B3** SBS gain in the same eigenpolarization as the **B1** and **B2** SBS lasers had a peak of 680 Hz/μW and for the orthogonal eigenpolarization, 150 Hz/μW. This crosstalk was primarily caused by the nonorthogonality of the fiber cavity eigenpolarizations caused by anisotropic loss in the cavity.[35]

4.9.2 Signal Processing

Several details of the signal processing used for counting the SBS beatnote will be discussed here, including processing for $\Delta q = 0$, $\Delta q \neq 0$, and digitization techniques.

Direct counting of the SBS beatnote, both at $\Delta q = 0$ and $\Delta q \neq 0$ was not usually possible, since noise on the beatnote caused the counter to overcount the beat frequency. For $\Delta q = 0$, a large gain stage with very heavy filtering, i.e., an eighth-order low-pass filter, was used to remove most of the noise. In addition, a Schmidt trigger was also used to prevent extra counts from any remaining noise.

A second technique that was used, particularly at $\Delta q \neq 0$, was to lock a phase locked loop (PLL) to the SBS beat. The phase locked loop acted as a very selective narrow band filter, eliminating spurious frequencies due to both pick up and backscattering, and allowing the counter to only see the very clean output of the voltage controlled oscillator (VCO) used in the PLL, or if the VCO was sufficiently stable, the control voltage to the VCO could be directly recorded. This technique was also considered for use at $\Delta q = 0$ when a frequency bias is introduced between the SBS lasers, though it was not implemented.

Digitization of the SBS beats was done with a 12-bit, 100 kHz analog-to-digital converter board, used in an IBM PC type computer. In this case, the maximum throughput for continuous sampling, 85 kHz, was limited by the overhead associated with writing the data to a RAM disk. The length of the run was limited to approximately 1 MB of data, 500 ksamples or about 6 sec at full speed, due to memory limitations. The spectrum of the time domain samples was found using an unwindowed, 2048 point fast Fourier transform, thus about 240 non-overlapping spectra were generated from each data run. The SBS beat frequency was recovered from the spectra using

a very simple peak finding algorithm, and some simple rules for rejecting stationary frequencies, for example, due to pick up or modulations.

4.9.3 TD-NRS

There are several details of the TD-NRS which will be explained in this section, including adjustment of the phase modulations, PZT tuning, and the effects of fast TD-NRS.

The relative phase and amplitude of the phase modulation applied to the cavity had to be extremely well matched for proper gyro operation. For example, a 1% mismatch in the relative phase of the modulations at 633 nm, would result in a 400 kHz residual frequency modulation. Estimates of the residual modulation observed on the resonances indicate the modulation phases were matched to within a few parts in 10^4.

The main effect of a mismatch in amplitude or phase of the modulations was to dramatically increase the residual frequency modulation at the NRPS frequency. Mismatches of over a part in 10^3 would completely extinguish the SBS lasers, thus the modulation phase adjustment was constantly monitored.

The large phase modulations required for TD-NRS were generated using a mechanical resonance of optical fiber driven with a PZT. The fiber was mounted at a single point to a small disk PZT using a very small amount of beeswax, and then a second point on the fiber, a few centimeters away, depending on the frequency required, was mounted to a small weight. Several such modulators are shown in the photograph in Fig. 4.47. Also visible in the photo is the small resistor used as the cavity heater.

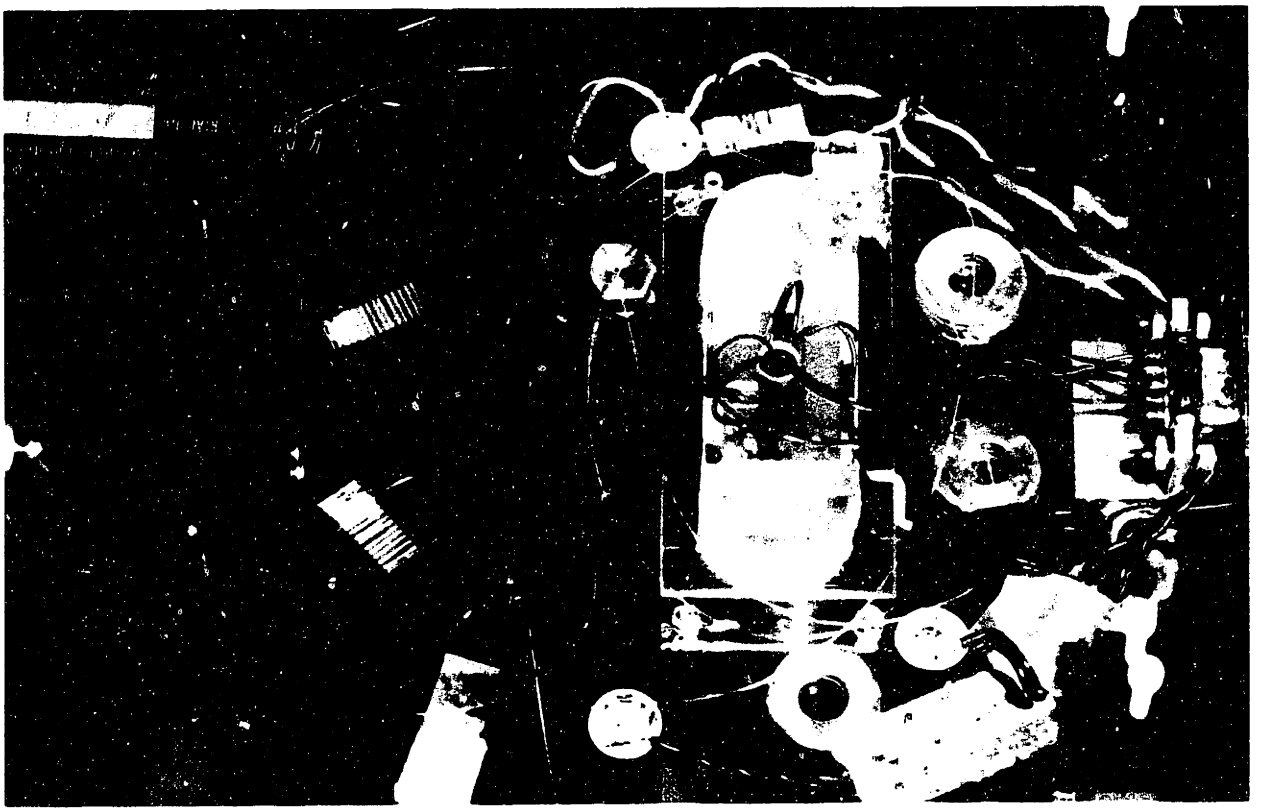

Figure 4.47 Photograph showing several resonant PZT fiber modulators.

The resonance of the fiber was adjusted by changing the length of fiber between the PZT and the weight, and by adjusting the curvature of the fiber between the PZT and the weight. In this way, a mechanical resonance with a Q of up to 10 was generated, allowing PZT drives as low as 20 V peak-to-peak to be used. It should be noted that the choice of PZT material has a significant effect on the Q that can be obtained, as does any foreign material

on the fiber jacket. The exact resonance frequency of the modulator was also quite sensitive to environmental perturbations, and the modulators had to be allowed to "warm-up", by applying the appropriate size modulation for several minutes, before any fine tuning could be done. This technique was demonstrated on at least four different types of fiber and appears to be a convenient method to generate large phase modulations.

One effect of a high modulation rate for TD-NRS is that the effective pump power coupled into the cavity is reduced, due to the frequency modulation of the cavity resonance. Further, since the phase of the modulation is different in opposite directions of the cavity, to eliminate this effect, the pump cannot simply be modulated in phase with cavity modulation. Thus, the maximum TD-NRS rate is limited by the linewidth of the cavity. However, if the effect of the TD-NRS is "undone" by applying a phase modulation in the output arm of the cavity that is 180° out-of-phase with the TD-NRS, this not only increases the beat signal at the detector, but also correctly modulates the pump laser to be matched to the cavity modulation.

Chapter Five

Summary

The goal of this thesis was to study the properties of stimulated Brillouin scattering in optical fibers, and to explore a number of applications, particularly the SBS ring laser gyroscope.

The properties of a solitary SBS laser were first studied. This included measurement of the longitudinal mode structure of the lasers, confirming the homogeneous-like behavior of the SBS gain medium. We also demonstrated the narrow 2 kHz linewidth of the SBS laser by measuring the linewidth of the beatnote between two independent SBS lasers. This linewidth was more than an order of magnitude narrower than the corresponding pump lasers. A number of applications for SBS lasers were also suggested including laser linewidth narrowing, wideband frequency shifting, and sensing of physical phenomena such as temperature and pressure. Several problems of the SBS laser were also studied, including spontaneous modelocking, and backscatter-induced threshold changes.

Using very low threshold cavities, higher order SBS lasers were also observed. Higher order lasing occurs when the primary SBS laser becomes strong enough to act as a pump for a second SBS laser. In our case, primary, secondary and even tertiary SBS lasers were observed. These higher order

SBS lasers have applications for wideband frequency shifting, but they also limit the amount of power that can be efficiently generated by the primary SBS laser.

We have also demonstrated the ability to generate two or more SBS lasers in the same fiber ring cavity, i.e., common cavity SBS lasers. Since these lasers are generated in the same cavity, they have correlated jitters, so the beat between them is very narrow. The short-term linewidth between two such lasers was measured to be approximately 2 Hz, limited primarily by slow, thermally driven dispersion pulls. Further, common cavity lasers have been generated with frequency differences of over 550 MHz, and even at this large spacing, the linewidth was still very narrow.

A number of applications for common cavity SBS fiber lasers have been suggested. For example, since the tuning range of SBS lasers is limited only by the tuning range of the pump lasers and the characteristics of the fiber cavity, common cavity SBS lasers can easily be generated with large frequency differences. The outputs of two such lasers can be combined and detected for use as a microwave, or even millimeter-wave source. In addition, these lasers could also be used for the development of atomic clocks or high precision magnetic field sensors.

One important application of common cavity SBS fiber lasers is for the development of the fiber-optic analog of the He-Ne bulk-optic ring laser gyroscope. Here, we demonstrated the first solid-state fiber ring laser gyroscope based on SBS in optical fibers. The directionality of the SBS gain medium prevents the gain competition that is normally observed in a conventional solid-state gain medium when generating simultaneous, counterpropagating lasers in the same ring cavity.

An important problem for both the bulk-optic and the fiber-optic RLG is the lock-in effect. Lock-in is caused by the coupling of the counterpropagating lasers through backscattering within the cavity. In the bulk-optic

RLG, the effects of lock-in are virtually eliminated by the use of mechanical dither. Mechanical dither is also recommended for the SBS fiber RLG, where the reduced mass of the fiber cavity could simplify the dithering mechanism.

Two optical methods for eliminating, or reducing the effects of lock-in were also demonstrated. In the first technique, the tunability of the SBS gain medium is used to generate the counterpropagating lasers in different longitudinal modes of the cavity, i.e., a Δq gyroscope. In this way, the large frequency bias between the lasers completely eliminates lock-in. However, there are a number of sources of error in this configuration, the largest of which is due to dispersion pulls resulting from pump backscattering. In Section 6.1, two configurations for reducing or eliminating drift in the Δq gyroscope are proposed.

The second method for reducing the effect of lock-in is the use of a time-dependent nonreciprocal phase shift to suppress the coupling between the lasers, i.e., time-dependent nonreciprocal suppression (TD-NRS). With the depth of the TD-NRS properly adjusted, the size of the lock-in effect can be greatly reduced or eliminated. We have demonstrated the reduction of the lock-in zone, in two different fiber cavities, however, there are a number of practical issues with such a scheme which still must be addressed.

In addition to lock-in, there are a number of other problems in the SBS fiber RLG. An additional error source is the nonlinear optical Kerr effect, which causes an index difference between the two directions in the cavity that is proportional to the intensity difference between the two SBS lasers. The frequency offset caused by this effect was measured both for an SBS fiber RLG and a passive resonator gyroscope to be 7 and 25 Hz/μW of input power difference, respectively, in good agreement with the expected values for these resonators. In order to eliminate the errors due to the optical Kerr effect, the intensities in the two directions of the cavity must be kept equal at all times using a servo loop.

There are also a number of smaller potential problems for the fiber RLG including the Faraday effect, and the effects of thermal and stress gradients along the cavity, i.e., the Shupe effect, which may become important as the performance of this RLG improves.

In Chapter 6, several suggestions for extensions to this work will be presented.

Chapter Six

Future Work

In this chapter, several promising extensions of the work presented in this thesis will be outlined for future study. These extensions fall into three general categories, ring laser gyroscope studies, common cavity SBS laser applications, and basic cavity studies.

6.1 Ring Laser Gyroscope Studies

There are several techniques for the elimination of lock-in that need to be investigated, including the use of mechanical dither.

6.1.1 A Mechanically Dithered SBS RLG

Mechanical dither has been very successful in the bulk-optic RLG, and it also is well suited for use with the SBS fiber RLG. Though the size of the backscattering, hence the lock-in zone, in a typical fiber cavity is larger than that of a bulk-optic cavity, the lower mass of the fiber cavity should allow a similar dither technology to be used. Such a mechanically dithered cavity would allow the careful study of biases, offsets, and scale factor nonlinearities in the gyroscope.

6.1.2 Multi-Frequency RLG

One method for avoiding the effects of lock-in is to generate the counterpropagating lasers in different longitudinal modes of the fiber cavity, as demonstrated in Section 4.5. However, there were a number of additional error sources for such a configuration, most importantly, large bias variations due to dispersion pulls and thermal drifts, that would prevent its use as a navigation grade gyroscope.

However, the directionality and tunability of the SBS gain medium allow more than two SBS lasers to be generated in the same ring cavity. By using additional SBS lasers, it may be possible to remove most, if not all, of these bias variations. One possible configuration is shown in Fig. 6.1, using four SBS lasers, two in the CW direction, and two in the CCW direction (the corresponding pump lasers are not shown in the figure).

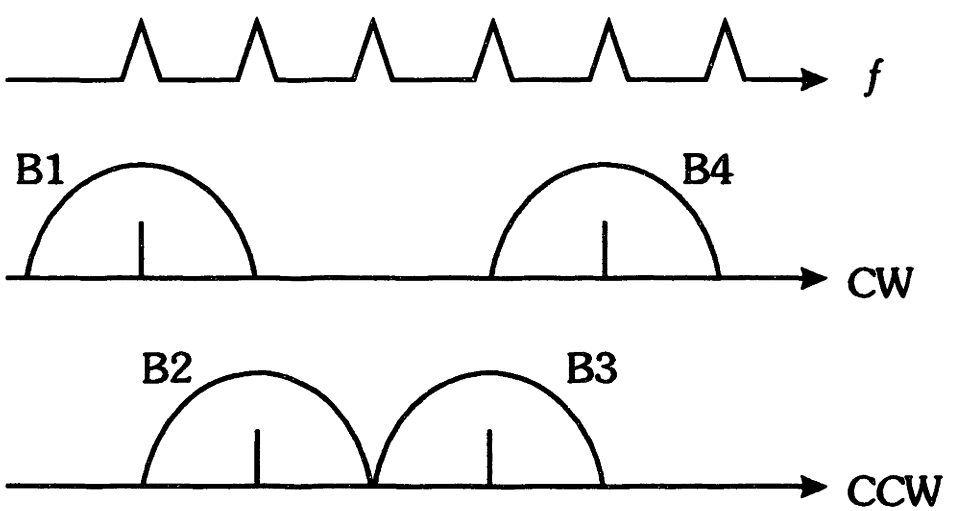

Figure 6.1 An example of an SBS multi-frequency gyroscope using four lasers.

In this configuration, two beatnotes are present at a frequency equal to the cavity FSR, one due to the beat between **B1** and **B2**, and the other due

to the beat between **B3** and **B4**. However, in the presence of rotation, the sign of the Sagnac effect is different for the **B1**–**B2** and the **B3**–**B4** beats, so the difference frequency between these beats is simply twice the Δf due to the Sagnac effect. Hence, by measuring the frequency difference between the beatnotes, the frequency bias between the lasers does not have to be explicitly measured and removed. This technique also has the important property that drifts due to temperature are completely eliminated, and drifts due to pump backscattering may also be reduced or eliminated.

Finally, it may also be possible to generate each pair of copropagating lasers in a different cavity eigenpolarization. In this way, if the eigenpolarizations are orthogonal, or nearly orthogonal, the dispersion pulls due to pump backscattering will be greatly reduced, or eliminated.

6.1.3 Switched Mode RLG

In the $\Delta q = 0$ RLG, both the counterpropagating lasers are generated in the same longitudinal mode of the cavity. In this case, the offset and drifts are good, but lock-in is a problem. On the other hand, in the $\Delta q \neq 0$ RLG, the lasers are generated in different longitudinal modes of the cavity. In this case, lock-in is completely eliminated but large bias variations are observed.

One technique for avoiding lock-in while still using the same longitudinal modes of the cavity is to generate the SBS lasers at $\Delta q = 1$, for example, and to periodically switch their directions, as shown in Fig. 6.2. Initially, **B1** is generated in the CCW direction of the cavity and **B2** is generated in CW direction, but after some time, the directions of the two lasers are switched, by switching the directions of their respective pump lasers (not shown in the figure). Thus, **B1′** will be in the CW direction and **B2′** in the CCW direction. In this way, the difference between the beat frequency in the two modes of operation is simply twice Δf due to the Sagnac effect, and, as long as the bias variations are slow compared with the switching time, they are automatically subtracted out.

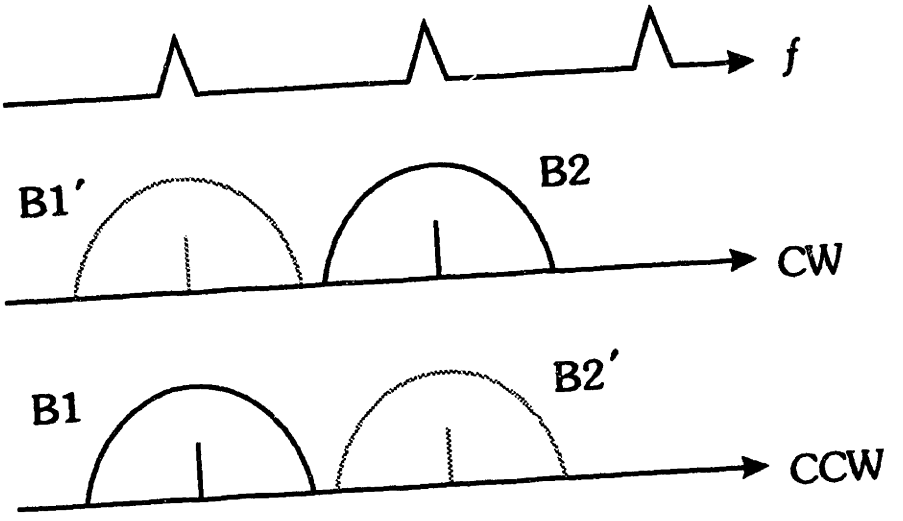

Figure 6.2 An example of a switched mode SBS fiber RLG.

However, there are a number of issues with this technique which must be addressed, including the choice of switching speeds and the effect of the phase discontinuities due to switching.

6.2 Common Cavity Applications

Several common cavity SBS fiber ring lasers applications were suggested in Section 3.2, and in this section, three of these applications are highlighted as future research topics.

6.2.1 Atomic Clock

A very interesting application of common cavity SBS lasers is for the development of simple atomic clocks based on the stimulated Raman effect, as discussed Section 3.2.4. Both the fiber cavities and tunable diode lasers for such a clock are available if rubidium, at 780 nm, or cesium, at 852 nm are used. Such a clock would have a number of important advantages including small size, low weight, long lifetime, low power, and low cost.

Another area of interest to our group is the possibility of a mm-wave clock. Since the observed linewidths in a typical atomic clock are transit-time limited, the use of a mm-wave transition could yield better fractional stability. In addition, by using a stimulated Raman transition, the need for a mm-wave cavity would be eliminated.

6.2.2 Magnetic Field Sensors

Another potential application of two-photon spectroscopy is for magnetic field sensing. In this case, the magnetic field is measured using the Zeeman splitting of the lower levels of the stimulated Raman transition. This technique has applications for measuring both very strong magnetic fields, and also for measuring very weak fields with high precision.

6.2.3 Spectroscopic Sensors

Yet another potential application of two-photon spectroscopy is for quasi-distributed, evanescent wave sensors. By using cladding stripped fibers, the evanescent field of the light inside the fiber can be allowed to interact with the surrounding environment, for example, for use as a gas sensor. Such sensors have a number of advantages including low cost, the ability to have long separations between sensors, and high sensitivity.

6.3 Basic Cavity Studies

In this section, two important properties of the fiber cavity are proposed for future study. The first is a detailed study of the sources of backscattering in a fiber cavity, and the second is a study of the cavity eigenpolarizations.

6.3.1 Backscatter Studies

Backscattering from within the fiber cavity has been shown to cause problems in the SBS fiber RLG, in common cavity SBS laser applications, and even in solitary SBS lasers. In addition, since the specific contributions to the total backscattering have not been individually measured, it is difficult to predict the effects of different perturbations to the cavity.

Therefore, a careful measurement of the size and location of the backscattering inside a fiber cavity could provide valuable information about the choice of optical fiber, the construction of the coupler, and the effects of perturbations to the optical fiber. For example, if a significant amount of the backscattering is due to fiber inhomogeneities, prescreening of the fiber before manufacture of the coupler may be able to significantly improve cavity backscattering. Similarly, if a significant portion of the backscattering is due to external perturbations, such as PZTs mounted on the fiber, these perturbations could be studied further and minimized.

6.3.2 Fiber Cavity Eigenpolarizations

The orthogonality of the cavity eigenpolarization has a significant impact on many SBS laser applications. Thus, a careful evaluation of eigenpolarization orthogonality and the variations in the orthogonality with perturbations for non-polarization maintaining, polarization maintaining, and also polarizing fiber cavities could provide valuable information about the choice of fiber for SBS applications and the effects of cavity perturbations.

References

1. L. Brillouin, "Diffusion de la lumiére et des rayons par un corp transparent homogéne," Ann. Phys. **17**, 88 (1922).
2. R.Y. Chiao, C.H. Townes and B.P. Stoicheff, "Stimulated Brillouin scattering and coherent generation of intense hypersonic waves," Physics Review Letters **12**, 592 (1964).
3. E.P. Ippen and R.H. Stolen, "Stimulated Brillouin scattering in optical fibers," Applied Physics Letters **21**, 539-540 (1972).
4. K.O. Hill, B.S. Kawasaki and D.C. Johnson, "cw Brillouin laser," Applied Physics Letters **28**, 608-609 (1976).
5. Donald R. Ponikvar and Shaoul Ezekiel, "Stabilized single-frequency stimulated Brillouin fiber ring laser," Optics Letters **6**, 398-400 (1981).
6. L.F. Stokes, M. Chodorow and H.J. Shaw, "All-fiber stimulated Brillouin ring laser with submilliwatt pump threshold," Optics Letters **7**, 509-511 (1982).
7. B.S. Kawasaki, D.C. Johnson, Y. Fujii and K.O. Hill, "Bandwidth-limited operation of a mode-locked Brillouin parametric oscillator," Applied Physics Letters **32**, 429-431 (1978).
8. N.A. Olsson and J.P. van der Ziel, "Cancellation of fiber loss by semiconductor laser pumped Brillouin amplification at 1.5 μm," Applied Physics Letters **48**, 1329-1330 (1986).
9. N.A. Olsson and J.P. van der Ziel, "Characteristics of a Semiconductor Laser Pumped Brillouin Amplifier with Electronically Controlled Bandwidth," Journal of Lightwave Technology **LT-5**, 147-152 (1987).
10. Toshio Kurashima, Tsuneo Horiguchi and Mitsuhiro Tateda, "Distributed-temperature sensing using stimulated Brillouin scattering in optical silica fibers," Optics Letters **15**, 1038-1040 (1990).
11. M. Ohashi, N. Shibata and K. Shiraki, "Fibre Diameter Estimation Based on Guided Acoustic Wave Brillouin Scattering," Electronics Letters **28**, 900-902 (1992).

12. Kazuyuki Shiraki and Masaharu Ohashi, "Sound Velocity Measurement Based on Guided Acoustic-Wave Brillouin Scattering," IEEE Photonics Technology Letters **4**, 1177-1180 (1992).

13. A.M. Scott and K.D. Ridley, "A Review of Brillouin-Enhanced Four-Wave Mixing," IEEE Journal of Quantum Electronics **25**, 438-459 (1989).

14. P. Bayvel and I.P. Giles, "Frequency Generation by Four Wave Mixing in All-Fibre Single-Mode Ring Resonator," Electronics Letters **25**, 1178-1180 (1989).

15. D. Culverhouse, K. Kalli and D.A. Jackson, "Stimulated Brillouin Scattering Ring Resonator Laser for SBS Gain Studies and Microwave Generation," Electronics Letters **27**, 2033-2035 (1991).

16. M.G. Prentiss, J.L. Davis and S. Ezekiel, "Closed Loop, High Sensitivity Fiberoptic Gyroscope," in *Fiber Optic Sensors*, S. Ezekiel and H.J. Arditty, Ed., 297-301, Springer–Verlag, Berlin, (1982).

17. S. Ezekiel and S.R. Balsamo, "Passive ring resonator laser gyroscope," Applied Physics Letters **30**, 478-480 (1977).

18. G.A. Sanders, M.G. Prentiss and S. Ezekiel, "Passive ring resonator method for sensitive inertial rotation measurements in geophysics and relativity," Optics Letters **7**, 569-571 (1981).

19. F. Zarinetchi and S. Ezekiel, "Observation of lock-in behaviour in a passive resonator gyroscope," Optics Letters **11**, 401-403 (1986).

20. P.J. Thomas, H.M. van Driel and G.I.A. Stegeman, "Possibility of using an optical fiber Brillouin ring laser for inertial sensing," Applied Optics **19**, 1906-1908 (1980).

21. L.F. Stokes, M. Chodorow and H.J. Shaw, "All-single-mode fiber resonator," Optics Letters **7**, 288-290 (1982).

22. R. Dahlgreen and O. Laznicka, "Ultra-High Finesse Polarization-Maintaining Fiber Resonator," SPIE Fiber Optic and Laser Sensors VII, **1169**, 382-387 (1989).

23. S.P. Smith, F. Zarinetchi and S. Ezekiel, "Fiberoptic Ring Laser Gyroscope," Proceedings of the OFS '89, post deadline paper, Paris, France (1989).

24. F. Zarinetchi, S.P. Smith and S. Ezekiel, "Stimulated Brillouin fiber-optic laser gyroscope," Optics Letters **16**, 229-231 (1991).

25. S.P. Smith, F. Zarinetchi and S. Ezekiel, "Narrow-linewidth stimulated Brillouin fiber laser and applications," Optics Letters **16**, 393-395 (1991).

26. R. Kadiwar and I.P. Giles, "Optical Fibre Brillouin Ring Laser Gyroscope," Electronics Letters **25**, 1729-1732 (1989).

27. W. Bernard, G. Giester, T. Quast and M. Raab, "Fundamentals of a Fiber Integrated Brillouin Ring Laser Gyro," DGON, Stuttgart, Germany (1991).

28. S. Huang, K. Toyama, P.-A. Nicati, L. Thévenaz, B.Y. Kim and H.J. Shaw, "Brillouin fiber optic gyro with push-pull phase modulator and synthetic heterodyne detection," SPIE Fiber Optic and Laser Sensors X, **1795**, 48-59 (1992).

29. Peter W. Milonni and Joseph H. Eberly, *Lasers*, John Wiley & Sons, Inc., New York, (1988).

30. Govind P. Agrawal, *Nonlinear Fiber Optics*, Academic Press, Inc., Boston, (1989).

31. D. Heiman, D.S. Hamilton and R.W. Hellwarth, "Brillouin scattering measurements on optical glasses," Physical Review B **19**, 6583-6592 (1979).

32. P. Bayvel and I.P. Giles, "Linewidth Narrowing in Semiconductor Laser Pumped All-Fibre Brillouin Ring Laser," Electronics Letters **25**, 260-262 (1989).

33. Toshio Kurashima, Tsuneo Horiguchi and Mitsuhiro Tateda, "Thermal effects on the Brillouin frequency shift in jacketed optical silica fibers," Applied Optics **29**, 2219-2222 (1990).

34. Z.K. Ioannidis, R. Kadiwar and I.P. Giles, "Polarization mode coupling in highly birefringent optical-fiber ring resonators," Optics Letters **14**, 520-522 (1989).

35. Bruce A. Ferguson and Chin-Lin Chen, "Polarization-effect controllability in recirculating delay-line systems," Applied Optics **31**, 6427-6436 (1992).

36. M. Prentiss, B. Peuse and S. Ezekiel, "Interaction of phase modulated laser fields with resonant systems," Research Laboratory of Electronics Progress Report 123, Massachusetts Institute of Technology, Cambridge, MA (1981).

37. I. Bar-Joseph, A. Dienes, A.A. Friesem, E. Lichtman, R.G. Waarts and H.H. Yaffe, "Spontaneous Mode Locking of Single and Multi Mode Pumped SBS Fiber Lasers," Optics Communications **59**, 296-298 (1986).

38. A.L. Schawlow and C.H. Townes, "Infrared and Optical Masers," Physical Review **112**, 1940-1949 (1958).

39. P.R. Hemmer, S. Ezekiel and C.C. Leiby, Jr., "Stabilization of a microwave oscillator using a resonance Raman transition in a sodium beam," Optics Letters **8**, 440-442 (1983).

40. S.P. Smith, F. Zarinetchi and S. Ezekiel, "Stimulated Brillouin Scattering Fiber Lasers for Novel Fiber Sensor Applications," Proceedings of the OFS '92, Monterey, CA (1992).

41. G. Sagnac, "L'éther luminex démontré par l'effet du vent relatiff d'éther dans un interférométre en rotation uniforme," C.R. Acad. Sci. **95**, 708-710 (1913).

42. E.J. Post and Asim Yildiz, "Cavity Resonances in Accelerated Systems," Physical Review Letters **15**, 177-178 (1965).

43. E.J. Post, "Sagnac Effect," Reviews of Modern Physics **39**, 475-493 (1967).

44. V. Vali and R.W. Shorthill, "Fiber ring interferometer," Applied Optics **15**, 1099-1100 (1976).

45. A.A. Michelson, "The Effect of the Earth's Rotation on the Velocity of Light," The Astrophysical Journal **61**, 137-145 (1929).

46. W. Burns, ed., *Optical Fiber Rotation Sensors*, Academic Press, Inc., New York, (1993).

47. Adolph H. Rosenthal, "Regenerative Circulatory Multiple-Beam Interferometry for the Study of Light-Propagation Effects," Journal of the Optical Society of America **52**, 1143-1148 (1962).

48. W.M. Macek and T.M. Davis, Jr., "Rotation Rate Sensing with Traveling-Wave Ring Lasers," Applied Physics Letters **2**, 67-68 (1963).

49. Frederick Aronowitz, "The Laser Gyro," in *Laser Applications, Volume 1*, 133-200, Academic Press, Inc., New York, (1971).

50. W.W. Chow, J. Gea-Banacloche, L.M. Pedrotti, V.E. Sanders, W. Schleich and M.O. Scully, "The ring laser gyro," Reviews of Modern Physics **57**, 61-104 (1985).

51. F. Aronowitz and R.J. Collins, "Mode Coupling due to backscattering in a He-Ne traveling-wave ring laser," Applied Physics Letters **9**, 55-58 (1966).

52. Frederick Aronowitz, "Lock-In and Intensity-Phase Interaction in the Ring Laser," Journal of Applied Physics **5**, 130-141 (1970).

53. Hermann A. Haus, Hermann Statz and Irl W. Smith, "Frequency Locking Modes in a Ring Laser," IEEE Journal of Quantum Electronics **QE-21**, 78-85 (1985).

54. R. Adler, "A study of locking phenomena in oscillators," Proceedings of the IRE **34**, 351-357 (1946).

55. Joseph E. Killpatrick, "The Laser Gyro," IEEE Spectrum **4**, 44-55 (1967).

56. J.E. Killpatrick, "Laser Angular Rate Sensor," U.S. Patent, 3,373,650 (1968).

57. J.J. Roland and J.M. Lamarre, "Periodic Faraday Bias and Lock-In Phenomena in a Laser Gyro," Applied Optics **12**, 1460-1467 (1973).

58. Michael L. Dennis, Jean-Claude M. Diels and Ming Lai, "Femtosecond ring dye laser: a potential new laser gyro," Optics Letters **16**, 529-531 (1991).

59. Ming Lai, Jean-Claude Diels and Michael L. Dennis, "Nonreciprocal measurements in femtosecond ring lasers," Optics Letters **17**, 1535-1537 (1992).

60. William R. Christian and Mark J. Rosker, "Picosecond pulsed diode ring-laser gyroscope," Optics Letters **16**, 1587-1589 (1991).

61. H.A.H. Boot, P.G.R. King and R.B.R. Shersby-Harvie, "Ring-Laser Bias Using Reciprocal Optical Components," Electronics Letters **5**, 347-348 (1969).

62. H. Sabert and R. Ulrich, "Spatial hole burning in Nd^{3+}-fiber suppressed by push-pull phase modulation," Applied Physics Letters **58**, 2323-2325 (1991).

63. Koichi Takiguchi and Kazuo Hotate, "Removal of Lock-in Phenomenon in Optical Passive Ring-Resonator Gyros by Using Optical Kerr Effect in Fiber Resonator," IEEE Photonics Technology Letters **4**, 810-812 (1992).

64. W.R. Bennett, Jr., S.F. Jacobs, J.T. Latourette, and P. Rabinowitz, "Dispersion Characteristics and Frequency Stabilization," Applied Physics Letters **5**, 56 (1964).

65. S. Ezekiel and J.L. Davis, "Intensity Dependent Nonreciprocal Phase Shift in a Fiberoptic Gyroscope," in *Fiber Optic Sensors*, S. Ezekiel and H.J. Arditty, Ed., 332-336, Springer–Verlag, Berlin, (1982).

66. S. Ezekiel, J.L. Davis and R.W. Hellwarth, "Observation of intensity-induced nonreciprocity in a fiber-optic gyroscope," Optics Letters **7**, 457-459 (1982).

67. D.M. Shupe, "Fiber resonator gyroscope: sensitivity and thermal nonreciprocity," Applied Optics **20**, 286 (1981).

68. D.M. Shupe, "Thermally induced nonreciprocity in the fiberoptic interferometer," Applied Optics **19**, 654 (1980).

69. Raymond Carroll and James E. Potter, "Backscatter and the Resonant Fiber-Optic Gyro Scale Factor," Journal of Lightwave Technology **7**, 1895-1900 (1989).